Discharge Characteristics of Embankment-Shaped Weirs

GEOLOGICAL SURVEY WATER-SUPPLY PAPER 1617-A

Prepared in cooperation with the Georgia Institute of Technology

Discharge Characteristics of Embankment-Shaped Weirs

By CARL E. KINDSVATER

STUDIES OF FLOW OF WATER OVER WEIRS AND DAMS

GEOLOGICAL SURVEY WATER-SUPPLY PAPER 1617–A

Prepared in cooperation with the Georgia Institute of Technology

UNITED STATES GOVERNMENT PRINTING OFFICE, WASHINGTON : 1964

UNITED STATES DEPARTMENT OF THE INTERIOR

STEWART L. UDALL, *Secretary*

GEOLOGICAL SURVEY

Thomas B. Nolan, *Director*

For sale by the Superintendent of Documents, U.S. Government Printing Office
Washington, D.C., 20402

CONTENTS

ILLUSTRATIONS

TABLES

STUDIES OF FLOW OF WATER OVER DAMS AND WEIRS

DISCHARGE CHARACTERISTICS OF EMBANKMENT-SHAPED WEIRS

By CARL E. KINDSVATER*

ABSTRACT

An embankment-shaped weir is an embankment overtopped by flood waters. Among the engineering problems frequently resulting from this occurrence is the need to compute the peak discharge from postflood field observations. The research described in this report was concerned with the theoretical and experimental bases for the computation procedure.

The research had two main objectives. One was to determine the relationship between embankment form and roughness and some of the more important discharge characteristics. The second was to define, theoretically and experimentally, the relationship between free-flow discharge and the boundary layer on the roadway. The first objective was accomplished with the experimental determination of coefficients of discharge and other significant flow characteristics for a variety of boundary and flow conditions. The second objective was accomplished with the development and experimental verification of a discharge equation which involved the boundary-layer displacement thickness. This phase of the research included a general investigation of boundary-layer growth on the roadway.

It is concluded that both free- and submerged-flow discharge are virtually independent of the influence of embankment shape and relative height. The influence of boundary resistance is appreciable only for smaller heads. The most practical solution for discharge is one which is based on the simple weir equation and experimentally determined coefficients. A completely analytical equation of discharge is impractical.

The report contains the results of 936 experiments on the discharge characteristics of 17 different models, plus 106 boundary-layer velocity traverses on 4 different models. The data are summarized in both graphical and tabular form.

INTRODUCTION

PURPOSE

The subject of this report is the highway embankment, which becomes a weir when it is overtopped by flood waters. Several problems which result from this occurrence are of interest to hydraulic engineers as well as highway engineers. One of these is the problem of destructive erosion. Another is the backwater which results from the obstruction of the flood channel. Still another is the problem of determining the magnitude of the flood discharge. The last-named problem is the one which especially concerns the Geological Survey.

*Regents Professor of Civil Engineering, Georgia Institute of Technology, Atlanta, Ga.; consultant to the U.S. Geological Survey.

The Geological Survey's interest in the hydraulics of embankments is related to one of the so-called indirect methods of discharge determination. Indirect methods involve the use of computation procedures in lieu of discharge or velocity-area measurements. One such method is based on the computation of the discharge capacity of spillways and weirs. The highway embankment belongs in this category because it is a form of broad-crested weir.

The common ingredients in all indirect methods of discharge determination are postflood field measurements and observations. Thus, the accuracy of the discharge determination depends on the accuracy and sufficiency of the field data as well as the computation procedure. As it pertains to the work of the Geological Survey, this investigation was concerned primarily with the principles involved in the computation procedure. The primary objective was an understanding of the mechanics of the flow over some typical highway embankments. A natural consequence of the investigation was the development of equations and coefficients which can be used to compute the discharge for a wide range of embankment forms and flow conditions.

HISTORY OF THE INVESTIGATION

The first of a series of related research projects on the hydraulics of embankments was begun at the Georgia Institute of Technology in 1947. On that occasion the Institute cooperated with the Georgia State Highway Department in a brief, exploratory study of a 1:6-scale model of a typical two-lane highway embankment. Laboratory tests were performed by R. L. Chapman, a State Highway Department engineer. From the results of the investigation, preliminary conclusions were drawn regarding the nature and scope of the problem.

Tests on a rebuilt version of the 1:6-scale model were made in 1948 by C. J. Chi and H. R. Henry, graduate students in the School of Civil Engineering. A major contribution of this investigation was a comprehensive record of water-surface profiles, velocity measurements, and photographs required to describe the external flow characteristics.

In 1949, tests on a 1:12-scale model were made by H. Y. Lu, another graduate student. The purpose of his investigation was to explore the scale effect related to the formation of the boundary layer on the surface of the model. The kind of data recorded was similar to that obtained from the previous tests on a 1:6-scale models. The investigation was terminated before completion.

After a lapse of several years, embankment research was reactivated in 1954 by Sigurdsson.[1] In addition to summarizing and reanalyzing

[1] Sigurdsson, Gunnar, 1956, Discharge characteristics of an embankment shaped weir: Georgia Inst. Technology, Master's degree thesis, 83 p., 38 figs.

the results of the previous investigations, Sigurdsson made additional tests on a 1 : 9-scale model. The purpose of his tests was to explore more critically the boundary-layer influence on free-flow discharge characteristics.

Subsequently, from 1956 to 1958, two more laboratory studies of the 1 : 9-scale model were made. One of these, by Davidian,[2] was especially concerned with the relationship between the free-flow coefficient of discharge and the boundary layer on the roadway. The other, by Prawel,[3] was principally concerned with the influence of changes in boundary form on significant flow characteristics. Finally, in 1959, some tests on the influence of surface roughness and some verification tests were made by W. W. Emmett.

For most of the work described above, one embankment form was used as the basis of design for all the models. In one of the recent investigations, the basic form was systematically varied in order to determine the separate influence of some of the more critical geometric characteristics. For most of the tests, the model surfaces were essentially smooth. For some tests, however, the model surfaces were artificially roughened. The test procedure, scope and kind of recorded data, and experimental techniques varied with the objectives of the individual investigators.

ACKNOWLEDGMENTS

The laboratory investigations were performed in the Hydraulics Laboratory, School of Civil Engineering, Georgia Institute of Technology, Atlanta, Ga. The experimental data which are used in this report were obtained primarily from the investigations during 1948 and 1956–59. All of the data accumulated since 1947, whether used herein or not, contributed to the experience and understanding upon which the conclusions are based.

The principal investigators were Chapman, Chi, Henry, Lu, Sigurdsson, Prawel, Davidian, and Emmett. Chapman's work on the initial, exploratory study was contributed by the Georgia State Highway Department. Chi, Henry, and Lu were graduate research assistants employed by the Institute. Sigurdsson's work was supported by the American Society of Civil Engineers through its J. Waldo Smith Hydraulic Fellowship. Prawel's research was partly supported by the Geological Survey. Emmett's work was supported by the Geological Survey and the Institute. For the purpose of preparing this report, the author was employed as a consultant by the Geological Survey.

[2] Davidian, Jacob, 1959, Influence of the boundary layer on embankment-shaped weirs: Georgia Inst. Technology, Master's degree thesis, 97 p., 38 figs.

[3] Prawel, S. P., Jr., 1959, Discharge characteristics of an embankment-shaped weir: Georgia Inst. Technology, Master's degree thesis, 58 p., 38 figs.

Homer Bates, Laboratory Technician in the School of Civil Engineering, constructed special instruments and assisted in the construction of the models. A complete photographic record of the 1948 tests was made by the author with the assistance of Chi. Most of the data used in the report were computed from original laboratory data by Emmett, who also assisted in the preparation of illustrations. John Shen, Geological Survey, and E. R. Holley, Jr., graduate student, assisted with the computations. All the work was done under the direction of the author.

Three Master's degree theses (Sigurdsson, 1956; Davidian, 1959; Prawel, 1959) have been based on parts of the investigation. A summary of certain results was contained in a previous publication (Kindsvater, 1957).

REVIEW OF THE LITERATURE

A paper by Yarnell and Nagler (1930) was the only research publication on embankment hydraulics available to the investigators. The research described in that paper was concerned primarily with railroad embankments. The basic embankment was flattopped, with a short, flat berm on both the upstream and downstream sides. The embankment slopes were covered with grouted gravel, and the top surface contained timber ties embedded in gravel ballast. The test data consisted of information needed to compute discharge coefficients for both free and submerged flow. Water-surface levels were measured with staff gages, and the discharge was measured with a full-width thin-plate weir. The results of a few tests made without rails on the ties have been used widely to describe the flow over highway embankments.

Because the highway embankment is classified as a form of broad-crested weir, the literature in this field is pertinent. A compilation and analysis of the most important information on broad-crested weirs is contained in a report by Tracy (1957). Most of the published work on the subject is concerned with the experimental determination of the discharge coefficient for smooth, level weirs. Very little is known about the influence of the boundary layer on the crest, separation at the upstream edge of the crest, boundary roughness, or variations in boundary form.

DESCRIPTION AND ANALYSIS OF THE PROBLEM

NATURE OF THE PROBLEM

Theoretical analyses of the embankment-shaped weir are complicated by a combination of effects related to boundary resistance and boundary form. Experimental studies are complicated by the occurrence of several significantly different flow patterns. Both analysis

and experiment are complicated by characteristic difficulties associated with free-surface phenomena.

Typical flow patterns for an embankment-shaped weir involve boundary-layer growth under conditions of acceleration and separation, nonhydrostatic pressure distribution due to curvilinearity, and an unstable transition between a boundary flow and a separation flow on the downstream slope. It is evident that a general analytical solution for discharge is impossible. Nevertheless, existing theory can be used to explain some of the different flow regimes. Experiment, guided by dimensional reasoning, must be depended upon to fix the limits of the flow regimes and evaluate the coefficients needed for practical solutions.

FLOW PATTERNS

An important contribution of the 1948 tests was a classification of the different flow patterns which characterize the flow of water over highway embankments. Doubtless the most significant classification is that which distinguishes between free and submerged flow. For the low-tailwater condition known as free flow, critical-flow control occurs on the roadway and the discharge is determined by the upstream head. At higher tailwater levels, when the depth of flow over the roadway is everywhere greater than the critical depth, the discharge is controlled by the capacity of the tailwater channel as well as the head. Under conditions of tailwater control, the flow is said to be submerged. With a rising tailwater level, the change from free flow to submerged flow occurs rather abruptly. The flow pattern antecedent to the change is described as incipient submergence.

Free flow is subclassified into plunging flow and surface flow. Plunging flow occurs when the jet plunges under the tailwater surface, producing a submerged hydraulic jump on the downstream slope. Surface flow occurs when the jet separates from the roadway surface at the downstream shoulder and "rides" over the tailwater surface. Whereas free flow can be either a plunging or a surface flow, submerged flow is always a surface flow.

The free-flow transition range is the range of tailwater levels within which a given discharge can produce either a plunging flow or a surface flow, depending on the antecedent conditions. Thus, if the tailwater is initially low and the flow plunging, this pattern persists as the tailwater level rises until it reaches the upper limit of the transition range, whereupon the plunging flow changes abruptly to a surface flow. However, if the tailwater is initially high and the flow is a surface flow, this pattern persists as the tailwater drops until it reaches the lower limit of the transition range, whereupon the flow pattern changes abruptly to plunging flow. The stability or persistence of

the flow patterns within the transition range is related to the inertia of the large, horizontal-axis rollers which occur on the downstream side of the embankment.

The tailwater-level limits of the transition range were recorded for all the models investigated. In addition to their general significance in the description of the characteristic flow pattern, the transition-range data are also significant in determining the safety of the structure against destructive erosion. This conclusion is based on the observation that surface flows are doubtless less erosive than plunging flows. Although the safety of flooded highway embankments was not a primary objective of the investigation, this information is believed to provide an important contribution to erosion prevention and control.

Figure 1 shows water-surface profiles for typical tests on the 1:6-scale model. Attention is called to the fact that the profiles are plotted to a distorted scale. Thus, vertical dimensions are shown 2.5 times larger than equivalent horizontal dimensions. For 3 different discharges (3.01, 14.7, and 25.0 cfs per ft in the prototype), the profiles illustrate the major flow-pattern classifications described above. Only 1 of the 2 possible flow patterns is shown at each of the free-flow transition limits. Profile *a* is a typical example of submerged flow, whereas *e* is an example of free, plunging flow at a tailwater level considerably below the lower limit of the transition range. Characteristic standing-wave patterns mark incipient submergence and the upper limit of the transition range. The theoretical value of the critical depth and its intercept on each of the free-flow profiles is shown on the figure. It is apparent that the depth at the crown line is very nearly equal to the theoretical critical depth for all discharges.

Figure 2 shows photographs of the three intermediate classifications of flow illustrated on figure 1. The discharge shown in figure 2 is 20.4 cfs per ft in the prototype.

Figures 3 and 4 show closeup photographs of the flow in the vicinity of the downstream shoulder for the conditions illustrated in figure 1*B*. The discharge is constant at 14.7 cfs per ft (prototype). The photographs shown in figure 3 represent a rising-tailwater sequence, beginning with a free, plunging flow. Figure 4 shows a falling-tailwater sequence, beginning with submerged flow. In all of the photogaphs, the flow is from left to right. The streaks shown in some of the photographs were made with an injection of potassium permanganate solution.

Attention is called to the similarity between figures 3*B* and 4*D*, 3*C* and 4*C*, and 3*D* and 4*B*. It is observed that the flow patterns which

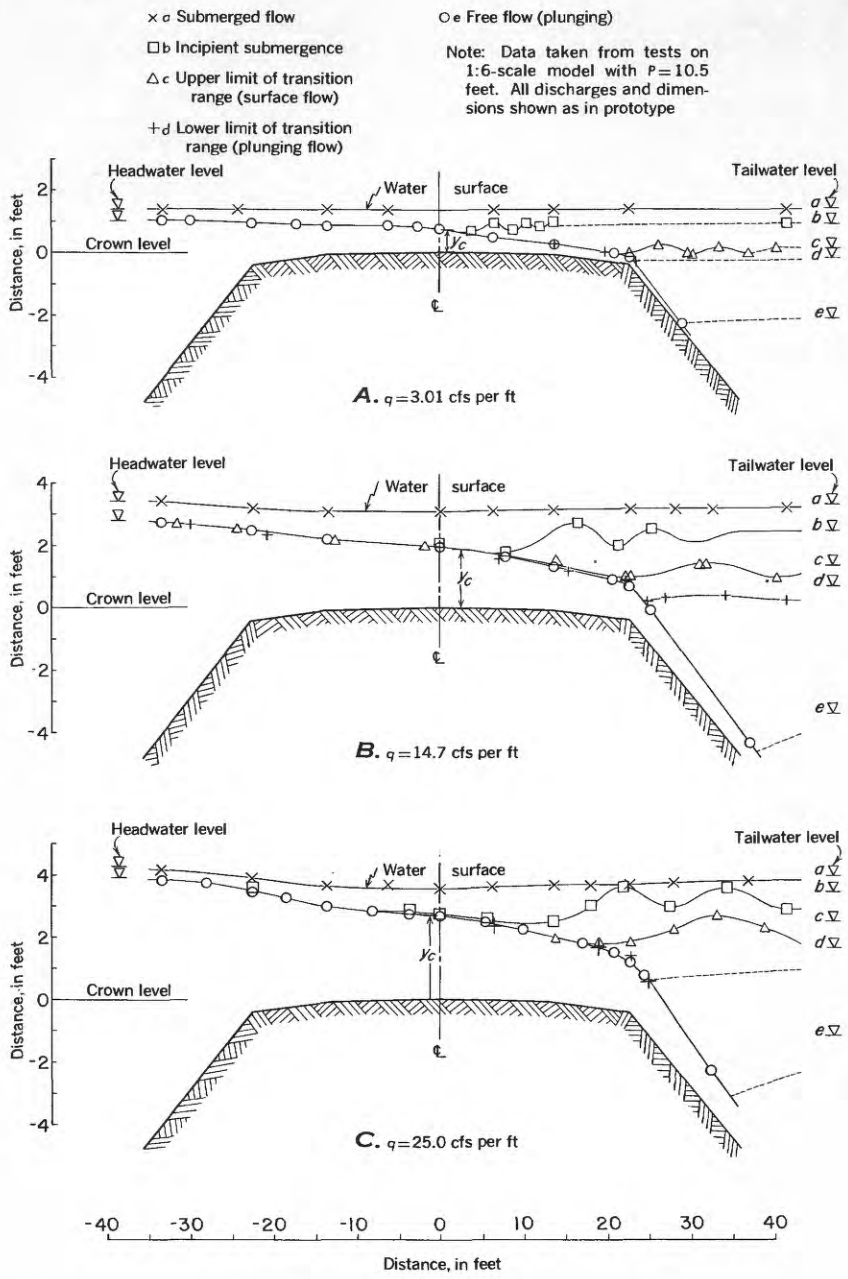

FIGURE 1.—Typical water-surface profiles in 1:6-scale model.

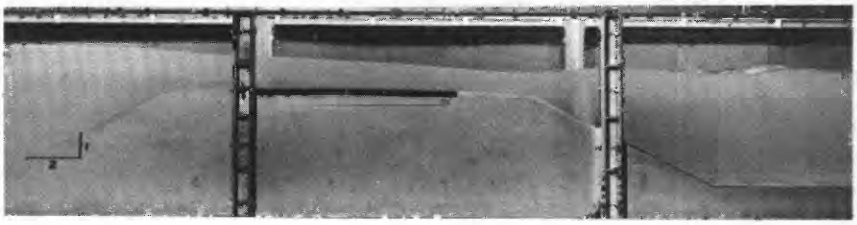

A. Free, surface flow at the upper limit of the transition range

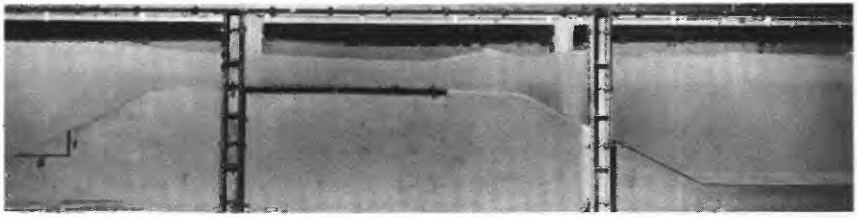

B. Surface flow, incipient submergence

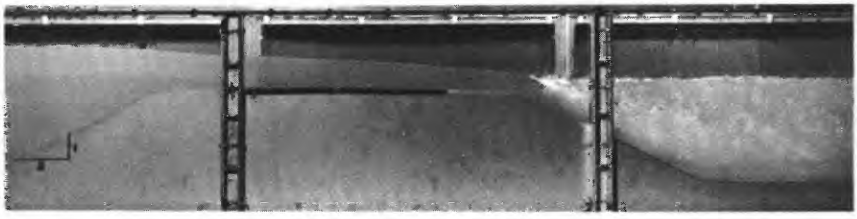

C. Free, plunging flow at the lower limit of the transition range

FIGURE 2.—Three significant flow patterns in the 1:6-scale model. The discharge is equivalent to 20.4 cfs per ft in the prototype.

appear to be almost identical in surface and streak-line configuration actually correspond to a difference in tailwater elevation of approximately 1.5 ft in the prototype. This difference is the difference in tailwater levels at the upper and lower limits of the free-flow transition range for this discharge.

NOMENCLATURE

The principal variables needed to describe the flow of water over a highway embankment are shown in figure 5. The selection of the variables is based on the following assumptions: The cross section is symmetrical about the vertical centerline; the embankment surface, shoulder surface, and each half of the pavement surface are planes; the crown line is horizontal, straight, and perpendicular to the flow;

the channel bottoms upstream and downstream from the embankment are horizontal, plane, smooth surfaces, and both are at the same elevation. Under these conditions, the variables needed to describe the embankment are the total height of the embankment (P), the width of the shoulder (L_s), the width of the pavement (L_p), the total width of the roadway, including the pavement and two shoulders (L), the embankment slope (S_e), the shoulder slope (S_s), and the pavement cross slope (S_p).

The variables needed to describe the one-dimensional flow characteristics are the discharge per foot of length of embankment (q), the average velocity in a channel section upstream from the embankment (V_1), the piezometric head of the upstream water surface measured with respect to the level of the crown line (h), the average total energy head referred to the crown level (H_1), the depth of flow at the crown line (y_0), and the piezometric head of the downstream water surface referred to the crown level (t).

In addition to the variables shown on figure 5, quantities needed to describe the flow over an embankment include the absolute roughness of the boundary surfaces (k), the specific weight of the fluid (γ), the density of the fluid (ρ), and the dynamic viscosity of the fluid (μ).

DIMENSIONAL ANALYSIS

Because some of the quantities defined above are not independent, they can be excluded from a general expression of the discharge function. For example, L, V_1, and H_1 can be excluded because their meanings can be described in terms of two or more of the other variables listed. An expression which includes the minimum number of independent variables required to describe the one-dimensional discharge characteristics is

$$f(P, L_s, L_p, S_e, S_s, S_p, q, h, t, k, \gamma, \rho, \mu)=0. \tag{1}$$

From this array, 10 independent ratios can be formed, as follows:

$$f\left(\frac{h}{P}, \frac{L_s}{L_p}, S_e, S_s, S_p, \frac{k}{h}, \frac{h}{L_p}, \frac{t}{h}, \frac{q}{h\sqrt{(\gamma h)/\rho}}, \frac{q\rho}{\mu}\right)=0. \tag{2}$$

The next to the last ratio in equation 2 is equivalent to a coefficient of discharge, C_1, and the last ratio is the Reynolds number, $\mathbf{R}$. Selecting the coefficient of discharge as the dependent ratio,

$$C_1=f\left(\frac{h}{P}, \frac{L_s}{L_p}, S_e, S_s, S_p, \frac{k}{h}, \frac{h}{L_p}, \frac{t}{h}, \mathbf{R}\right). \tag{3}$$

In the experimental investigation, L_s/L_p and S_e were constants. Consequently, for the purposes of this report, both ratios can be omitted from the functional relation for the coefficient of discharge.

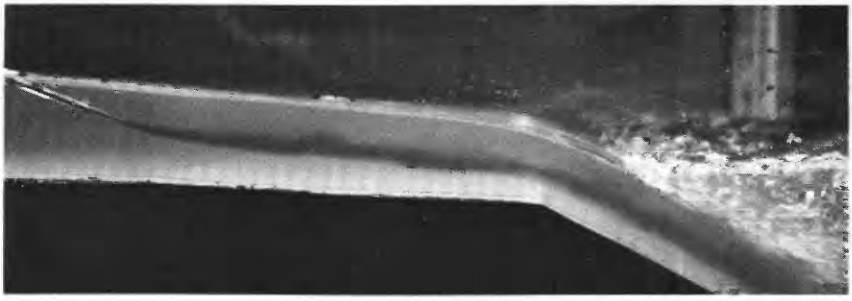

A. Free, plunging flow

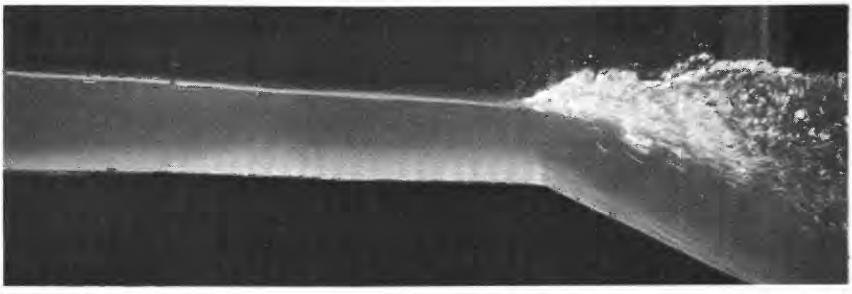

B. Free, plunging flow at the upper limit of the transition range

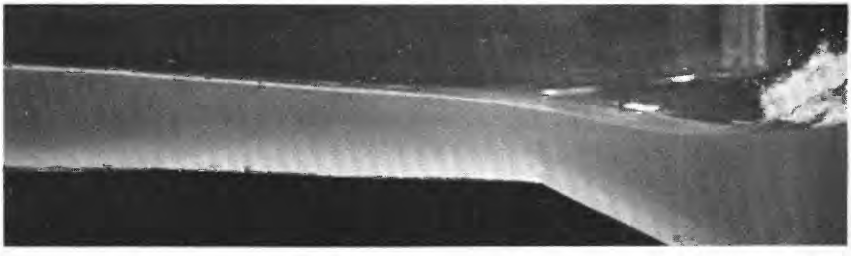

C. Upper limit of the transition range, changing from plunging to surface flow

FIGURE 3.—Changing flow pattern with rising tailwater. The discharge shown here in the 1:6-scale model is equivalent to 14.7 cfs per ft in the prototype.

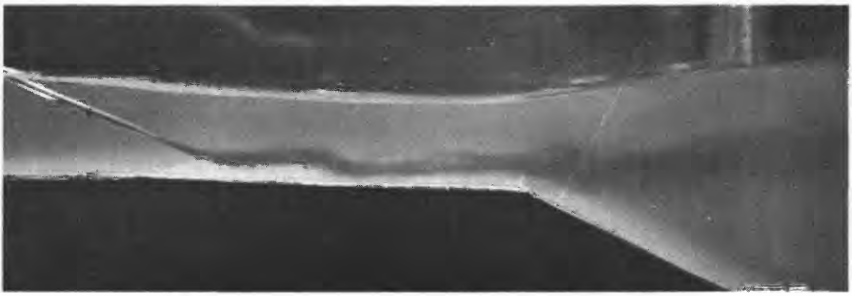

D. Free, surface flow at the upper limit of the transition range

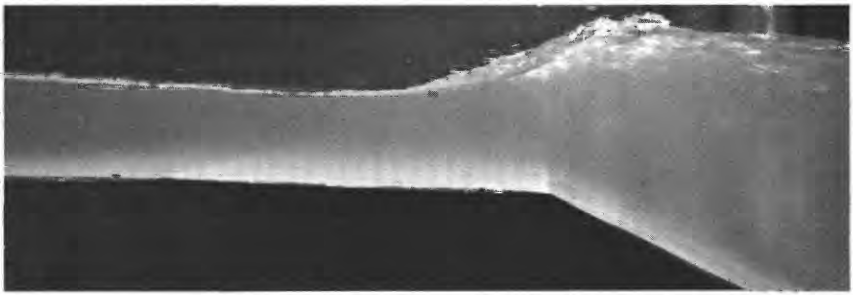

E. Free, surface flow between the upper limit and incipient submergence

F. Surface flow, incipient submergence

690-195 O - 64 - 3

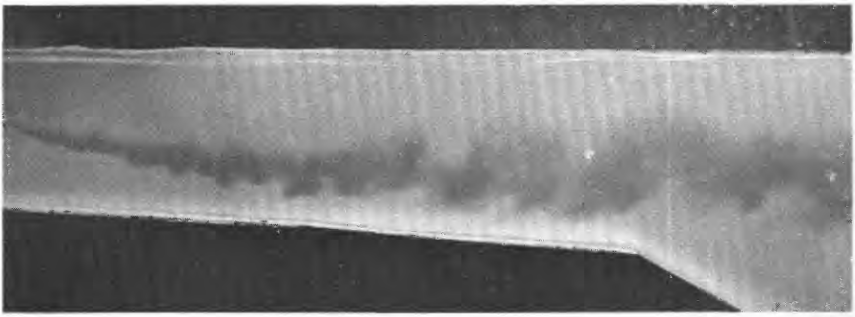

A. Submerged, surface flow

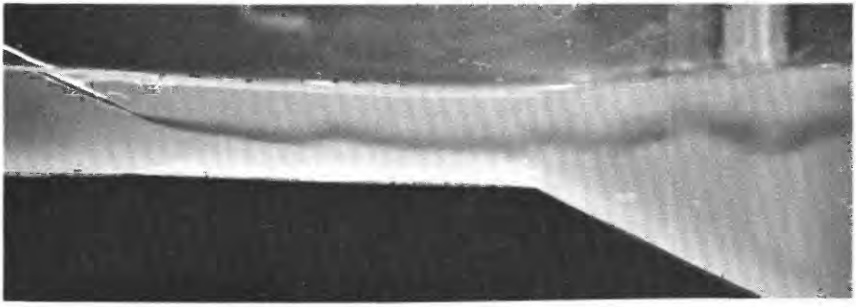

B. Free, surface flow at the lower limit of the transition range

C. Lower limit of the transition range, changing from surface flow to plunging flow

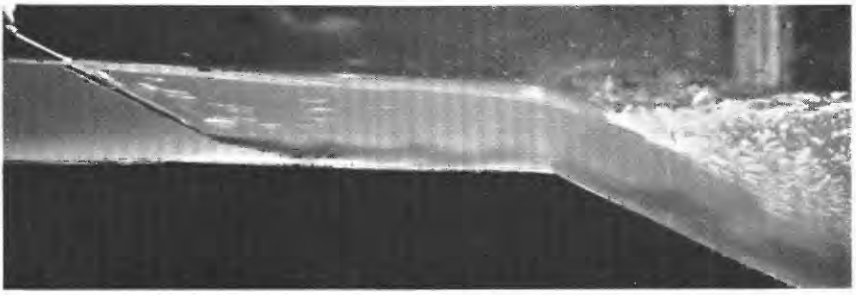

D. Free, plunging flow at the lower limit of the transition range

FIGURE 4.—Changing flow pattern with falling tailwater. The discharge shown here in the 1:6-scale model is equivalent to 14.7 cfs per ft in the prototype.

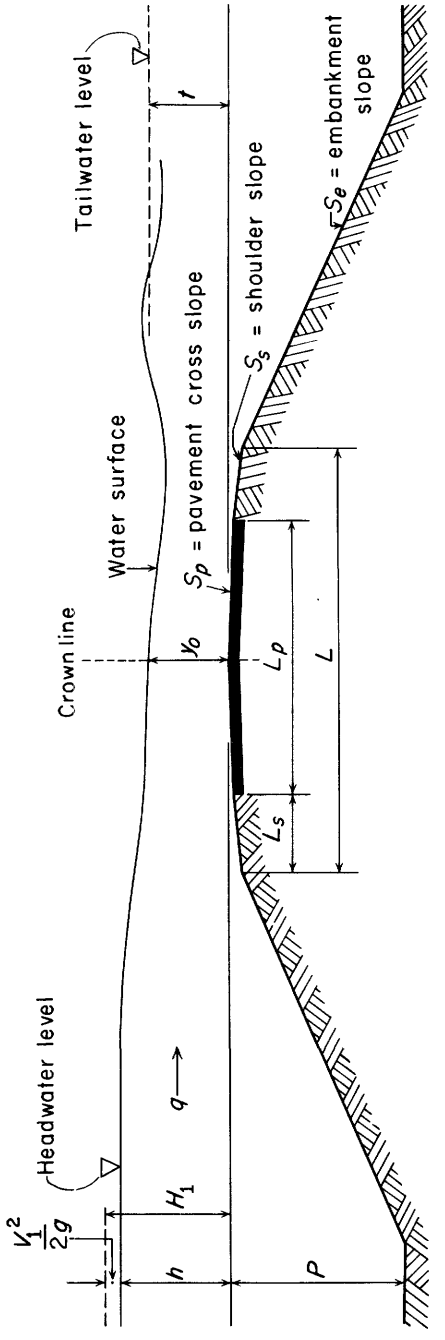

FIGURE 5.—Principal variables needed to describe flow over an embankment.

Furthermore, for convenience, L can be substituted for L_p in the h/L_p ratio. Thus, the scope of the investigation is represented by the expression

$$C_2=f\left(\frac{h}{P}, S_s, S_p, \frac{k}{h}, \frac{h}{L}, \frac{t}{h}, \mathbf{R}\right). \tag{4}$$

FREE-FLOW DISCHARGE EQUATIONS

For free flow, discharge control occurs at a critical-flow section on the roadway. This means that a unique relationship exists between the discharge and the head on the embankment. Consequently, a one-dimensional discharge equation can be derived from a simple energy analysis.

The discharge equation for a so-called ideal fluid is based on the assumption of potential flow (no boundary resistance, no energy losses), with uniform velocity distribution and hydrostatic pressure distribution in the approach channel and on the roadway. From the one-dimensional energy and continuity equations for the reach between a section at the crown line and a section in the channel immediately upstream from the embankment, the free discharge of an ideal fluid is

$$q_i=y_o\sqrt{2g(H_1-y_o)}, \tag{5}$$

in which y_o is the depth of flow at the crown line. From the additional assumption that y_o is equal to the critical depth for the discharge q_i, and from the fact that the critical depth is theoretically equal to two-thirds the total head,

$$q_i=\frac{2}{3}\sqrt{\frac{2}{3}g}\,H_1^{\frac{3}{2}}. \tag{6}$$

Because the conditions assumed in the derivation of equation 6 are never actually satisfied, the discharge equation for an ideal flow must be adjusted to the flow of a real fluid. Thus, in the following equation,

$$q=C_3\frac{2}{3}\sqrt{\frac{2}{3}g}\,H_1^{\frac{3}{2}}, \tag{7}$$

q is the true discharge of a real fluid, and C_3 is an experimentally determined coefficient which accounts for the inaccuracies inherent in equation 6.

It is customary in American engineering practice to use a coefficient C which combines the coefficient of discharge and the constants, in-

cluding g, in equation 7. Thus, the equation of discharge in its simplest form is

$$q=CH_1^{\frac{3}{2}}, \tag{8}$$

in which C has the dimensions of $\sqrt{g}$. The obvious practical advantages of the simple equation have been weighed against the fact that C is a dimensional qauntity. The decision to use equation 8 as the basic equation of discharge for this investigation is a concession to the convenience of the practicing American engineer. Those who insist that the coefficient of discharge must be nondimensional will be compelled to divide C by a constant involving $\sqrt{g}$.

The independent variables which govern C are the same as those which govern C_2 in the general functional expression for the coefficient of discharge. Therefore, from equation 4,

$$C=f\left(\frac{h}{p}, S_s, S_p, \frac{k}{h}, \frac{h}{L}, \frac{t}{h}, \mathbf{R}\right). \tag{9}$$

For free flow, t/h is significant only as it defines the condition of incipient submergence.

From equation 6, a simple equation for the discharge of an ideal fluid is

$$q_i=\frac{2}{3}\sqrt{\frac{2}{3}(32.2)}\,H_1^{\frac{3}{2}}=3.09\,H_1^{\frac{3}{2}}, \tag{10}$$

and the coefficient 3.09 can be described as the ideal value of C in equation 8.

EFFECT OF BOUNDARY RESISTANCE

Two equations for free-flow discharge have been described. One, illustrated by equation 6, is sometimes called a theoretical or ideal equation, because certain real-fluid characteristics were ignored in its derivation. The second, illustrated by equation 7, is a simple modification of equation 6 which depends on the experimental evaluation of a coefficient of discharge for real-fluid flows. To the second can be added the result of the dimensional analysis, which provides a means of correlating the variables which govern the coefficient of discharge. Still lacking is a completely analytical equation of discharge for real fluids.

An analytical equation must contain terms capable of describing the influence of boundary characteristics and real-fluid characteristics which were ignored in the development of equation 6. Of these, the most important for free-flow discharge conditions are the effects of

boundary resistance. These effects are incorporated symbolically in an equation which begins, as did equation 6, with the one-dimensional equations of energy and continuity.

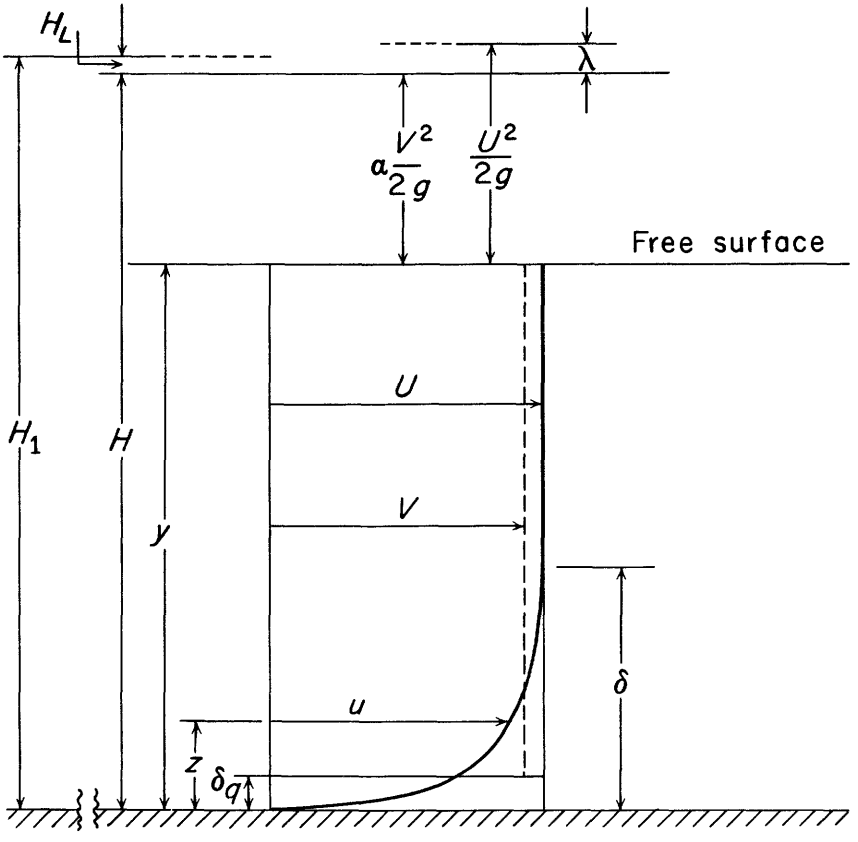

FIGURE 6.—Partially established boundary-layer flow.

In figure 6 the flow at a typical section on the roadway is represented as a partially established boundary-layer flow. In the figure, V is the average velocity in the section; U is the uniform velocity in the potential flow outside the boundary layer; λ is the difference between $U^2/(2g)$ and the true average velocity head, $\alpha V^2/(2g)$; H_1 is the total head at the upstream measuring section (referred to the local level of the boundary); H is the true total head at the roadway section; and H_L is the head loss between the upstream section and the roadway section. Because the flow is uniform (the velocity vectors are everywhere straight and parallel), y in figure 6 is both the depth of flow and the true piezometric head referred to the boundary. The boundary-layer thickness, δ, is represented as the nominal distance

from the boundary to the point where the velocity, u, is equal to U. Also shown on figure 6 is δ_q, the boundary-layer displacement thickness, which is defined in the equation

$$q=yU-\delta_q U=(y-\delta_q)U, \tag{11}$$

in which q is the true discharge, yU is the potential discharge, and $\delta_q U$ is the discharge decrement due to the boundary layer.

From figure 6 and the preceding definitions, a one-dimensional energy equation is

$$H=H_1-H_L=y+\frac{U^2}{2g}-\lambda, \tag{12}$$

and from the simultaneous solution of equations 11 and 12,

$$q=(y-\delta_q)\sqrt{2g(H_1-H_L-y+\lambda)}. \tag{13}$$

If it is assumed that the roadway section is located at the crown line, then $y=y_o$ (see fig. 5) and, without special identification, δ_q and λ are the crown-line values of the boundary-layer quantities. It follows that the counterpart of equation 5 is

$$q=(y_o-\delta_q)\sqrt{2g(H_1-H_L-y_o+\lambda)}, \tag{14}$$

in which H_L is now defined as the head loss between the measuring section and the crown line.

When the measuring section is a considerable distance from the roadway, H_L must be evaluated in order to determine the net head on the embankment. Actually, H_L can only be estimated, for it depends on the resistance characteristics of the upstream channel as well as the embankment. On the other hand, if the measuring section is located close to the embankment, as it was for the model tests described herein, H_L is very small. At this point it is convenient to assume that H_L is negligible. Consequently, from equation 14,

$$q=(y_o-\delta_q)\sqrt{2g(H_1-y_o+\lambda)}. \tag{15}$$

In the derivation of equation 6 from equation 5 it was assumed that the depth at the crown line is equal to the critical depth. With this assumption and the assumption that the critical depth is again equal to two-thirds the total head, y_o can be eliminated from equation 15, whence

$$q=\left(\frac{2}{3}H_1-\delta_q\right)\sqrt{2g\left(\frac{H_1}{3}+\lambda\right)}. \tag{16}$$

Simplifying,

$$q=\frac{2}{3}\sqrt{\frac{2}{3}g}\left(H_1-\frac{3}{2}\delta_q\right)(H_1+3\lambda)^{\frac{1}{2}}. \tag{17}$$

Expanding, and discarding terms which are negligible when δ_q and λ are small relative to H_1,

$$q=3.09\left[H_1^{\frac{3}{2}}-\frac{3}{2}H_1^{\frac{1}{2}}(\delta_q-\lambda)\right], \tag{18}$$

or,

$$q=3.09\,H_1^{\frac{3}{2}}\left[1-\frac{3}{2}\left(\frac{\delta_q-\lambda}{H_1}\right)\right]. \tag{19}$$

Therefore, from equations 8 and 19,

$$C=3.09\left[1-\frac{3}{2}\left(\frac{\delta_q-\lambda}{H_1}\right)\right]. \tag{20}$$

From equation 10, the quantity $3.09\ H_1^{\frac{3}{2}}$ in equation 19 is equal to q_i, the discharge of an ideal fluid. Thus, the quantity in brackets in the last two equations is a measure of the total influence of boundary resistance.

The quantity in brackets in equations 19 and 20 involves the relative magnitude of the quantities δ_q and λ. It is significant to recall that δ_q is a measure of the influence of boundary resistance on the continuity equation, and λ is a measure of the influence of boundary resistance on the energy equation. The usefulness of equations 19 and 20 depends on the determination of a means of evaluating δ_q and λ.

It should be emphasized that the preceding development involves several assumptions which must be verified or delimited by experiment. For example, the equations are misleading when (for large values of h/L) form effects are dominant in comparison with the effects of boundary resistance. Similarly, it is obviously wrong to neglect H_L under some circumstances. The determination of the real significance of such qualifications is an important objective of the experimental investigation.

SUBMERGED FLOW

Equations of discharge for free flow have been derived on the basis of a simple energy analysis. The analysis was made possible because critical-flow control occurs on the roadway when the flow is free. When the flow is submerged, however, the discharge capacity of the

downstream channel is a primary control. Thus, for submerged flow, the discharge depends on the tailwater level as well as the head.

Complications introduced by the influence of the tailwater make it impractical to derive an independent equation for submerged flow. The most expedient alternative is an empirical solution based on experiment and the free-flow discharge equation.

In the general functional relationship for the coefficient of discharge (eq 4), a single ratio (t/h) distinguishes submerged flow from free flow. This observation leads to the conclusion that the effect of submergence can be expressed in terms of C_{free} and t/h, as in

$$C_{subm}=f\left[C_{free}, \frac{t}{h}\right]. \tag{21}$$

Frequently it leads to another conclusion, namely,

$$\frac{C_{subm}}{C_{free}}=f\left(\frac{t}{h}\right), \tag{22}$$

which is difficult to justify physically as well as mathematically. Actually, of course, the coefficient of discharge for submerged flow should be expected to be independently related to all the ratios listed in equation 4. In other words, there is no basis for believing that all ratios must have the same significance in both free and submerged flow. Thus, empirical solutions based on equation 22 are adequate as well as convenient only to the extent that C_{free} is constant over the full range of conditions considered. When C_{free} is not constant, application of equation 22 results in a vague definition of the conditions which govern the value of C_{free} to be used as a reference parameter for C_{subm}.

For purposes of reducing and analyzing the experimental data, the simple equation of discharge, with C defined as in equations 8 and 9, is used for both free and submerged flow.

LABORATORY INVESTIGATION

EXPERIMENTAL EQUIPMENT

GENERAL ARRANGEMENT

The equipment used for all the tests made after 1954 was essentially the same. Embankment models were located in an existing flume. Water is supplied to the flume from the laboratory's constant-head system. A gate valve in the supply line is used to regulate the discharge, and a hinged tailgate in the flume is used to regulate the tailwater level. The maximum discharge used in the tests was about 6 cfs (q=2 cfs per ft in the model, corresponding to 54 cfs per ft in the prototype). Figure 7 shows the general arrangement of the experimental equipment.

690-195 O - 64 - 4

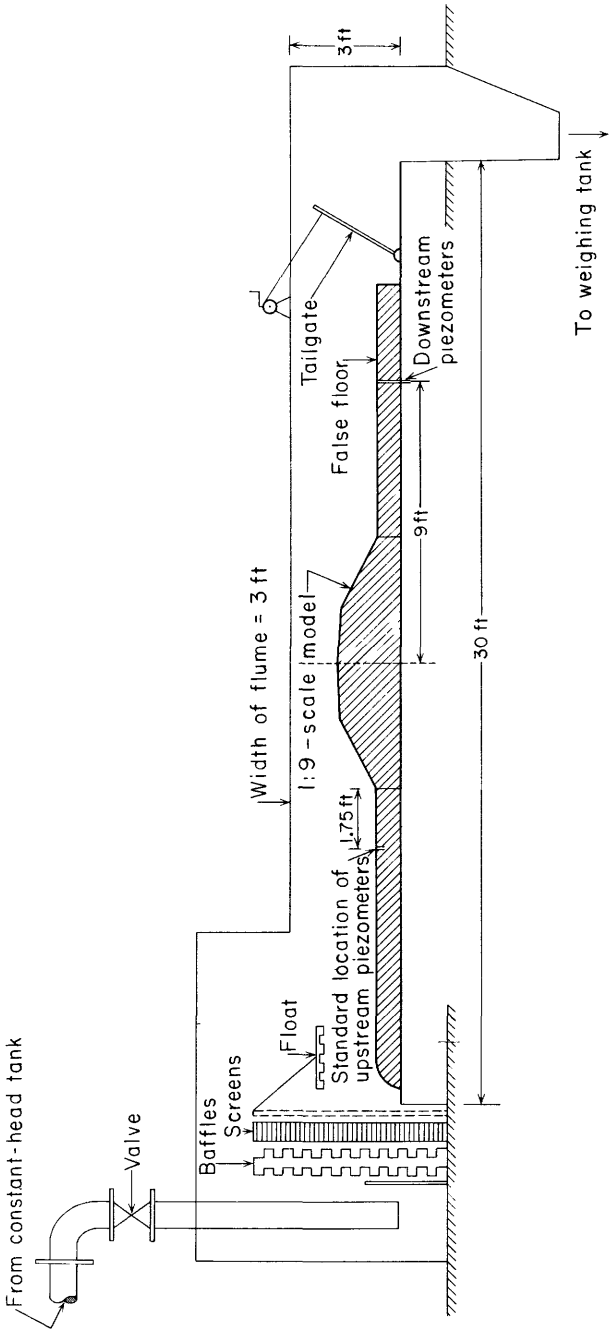

FIGURE 7.—Arrangement of experimental equipment.

FLUME

The flume is 3 feet wide, 3 feet deep, and about 30 feet long. The average inside width at the position of the embankment is 3.010 feet. The flume is constructed of steel, with three 5-foot-long glass panels on each side. Adjustable rails on the top of the flume walls provide a level track for instrument carriages. The bottom-hinged steel tailgate is operated with a winch, which is mounted on the top of the flume. Figure 8 is a photograph of the test section of the flume with a model installed.

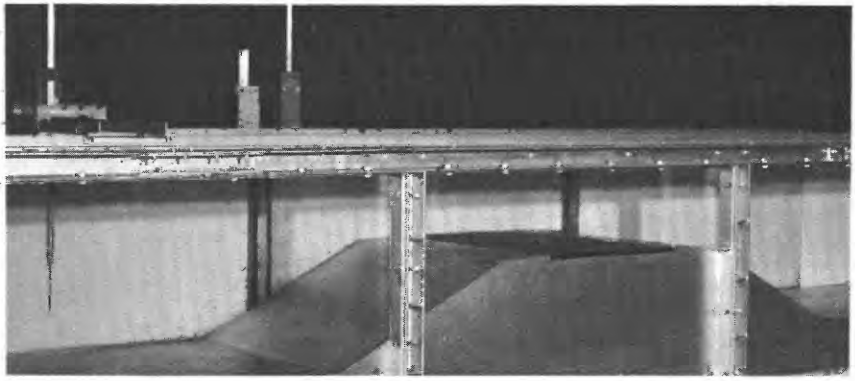

FIGURE 8.—View of 1:9-scale model embankment in test flume.

Water enters the flume from a 12-inch pipe, which discharges vertically into the deep forebay section of the flume. Baffles required to produce a uniform flow upstream from the models consist of chain-link wire fencing at the inlet, a low weir, 2 corrugated-metal cribs, 2 expanded-metal screens, and a surface float.

EMBANKMENT MODELS

The basic structure for all models was a framework of exterior-grade plywood and aluminum angles. The pavement and shoulder surfaces were made of ¼-inch aluminum plate, and the embankment and berm surfaces were made of ¾-inch plywood. False floors both upstream and downstream from the embankment model were used to vary the height of the embankment. The downstream floor was made of plywood; the upstream floor was made of aluminum plate.

When the original 1:9-scale model was built in 1954, sharp lines marked the intersections of the embankment, shoulder, and pavement surfaces. The crown line was marked by the intersection of the separate plates which comprised the two lanes of the pavement. Subsequent use and repeated polishing of the metal plates resulted in a slight rounding of the intersections. However, comparisons of similar tests

made at different times during the period from 1954 to 1959 showed no effects which could be attributed specifically to the rounding. It is significant that the model with slightly rounded surface intersections is doubtless a better representation of the prototype than a model built in strict accordance with the design specifications.

Variations in the slopes of the pavement and shoulder surfaces were accomplished by placing metal shims between the surface plates and the supporting angles. For model K, a piece of 16-gage sheet metal was rolled to form a smooth transition between the upstream embankment and the shoulder. A ⅛-inch bronze rod was fastened to the downstream edge of the downstream shoulder for model L. For model M, berms were built on a framework of wood and covered with plywood.

Figure 9 shows details and dimensions of the basic embankment design (model A). Figure 10 shows special details of models K, L, and M. A photograph of a typical 1:9-scale model in the flume is shown in figure 8.

For models A through M, all exposed model surfaces were smooth. Aluminum surfaces were polished, and they were kept waxed to prevent pitting by corrosion. Plywood surfaces were sanded and painted.

For models AA, AB, AC, and KA the embankment surfaces were made rough. Two methods were used. For models AA and KA, a piece of new 14- by 18-mesh bronze window screen was stretched taut over the entire surface of the model. The diameter of the wire from which the screen was made was 0.011 inch.

For models AB and AC the roughness elements consisted of No. 9 lead birdshot. The shot was 0.080 inch in diameter and very nearly spherical. The distribution density on the model was approximately 75 shot per square inch. The birdshot was attached to the model surfaces with varnish. Two coats of varnish were brushed on the surfaces and allowed to become tacky, then the birdshot was sprinkled on the surfaces. The varnish was allowed to dry at least 48 hours, then a thin coat of varnish was sprayed on and allowed to dry at least 24 hours. For model AB the birdshot was applied to the embankment slopes and shoulder surfaces only. For model AC it was applied to the entire model surface. Figure 11 shows a photograph of model AC and a closeup of the birdshot-roughened surface.

DISCHARGE MEASUREMENTS

The discharge for all the tests was determined from measurements made with the laboratory's semiautomatic weighing system. Flow from the downstream end of the flume drops directly into the weighing tank, which is located on the floor below the flume. The weighing sys-

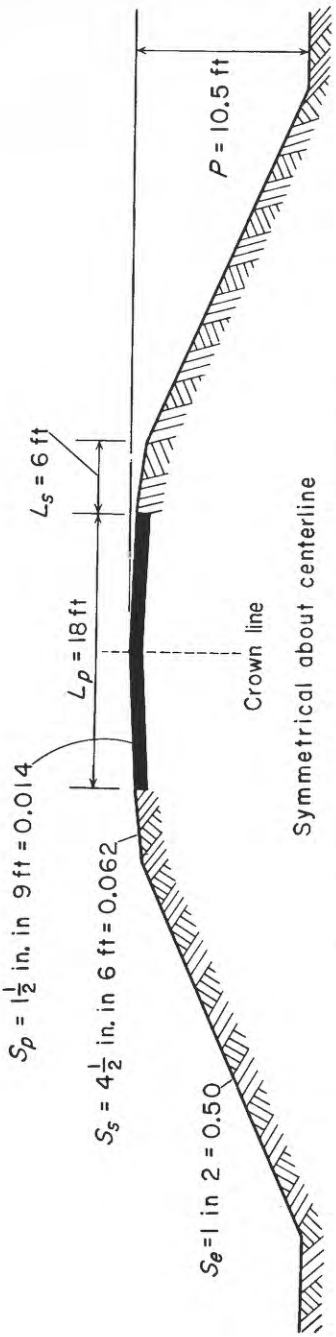

FIGURE 9.—Basic embankment design. All dimensions as in prototype.

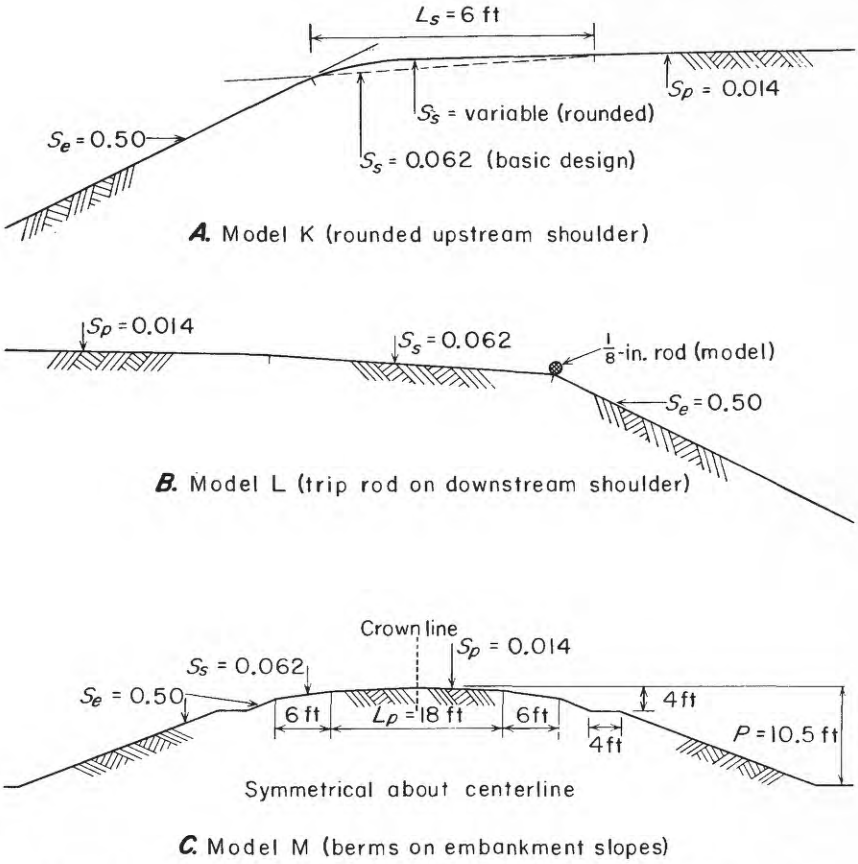

FIGURE 10.—Special design variations (models K, L, and M). All dimensions as in prototype.

tem includes automatic controls to move the diversion car, to open and close the tank valve, and to start and stop an electric time-interval clock. The overall accuracy of the equipment is believed to be such that discharge measurements are accurate within ½ of 1 percent. Figure 12 shows the downstream end of the test flume (upper floor) and the weighing-tank apparatus (lower floor).

PIEZOMETRIC-HEAD AND PROFILE MEASUREMENTS

Headwater and tailwater piezometric levels were generally measured with hook gages mounted over stilling wells connected to pairs of floor piezometers. Some measurements were made with a precise manometer. An engineer's transit and a special light-weight target rod were used to zero the hook gages. The average of several readings

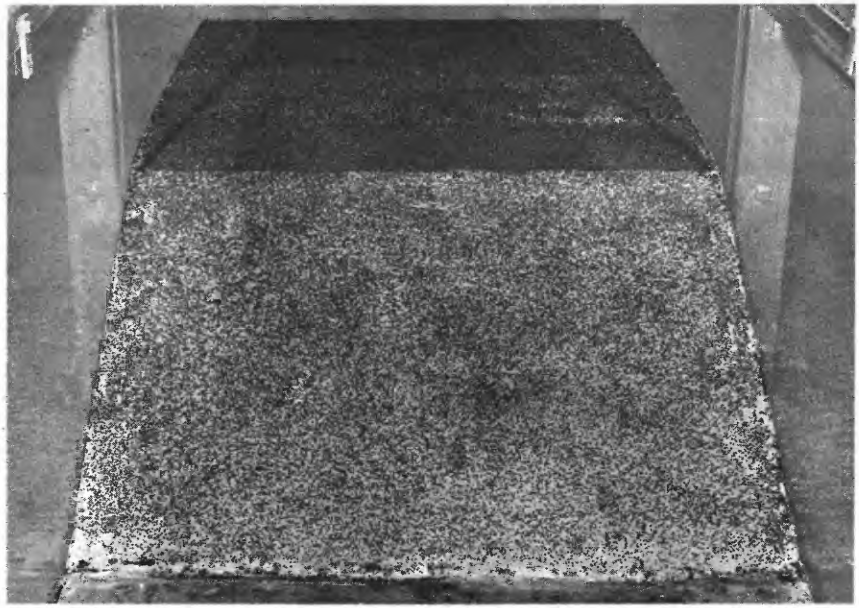

A. Looking downstream at model

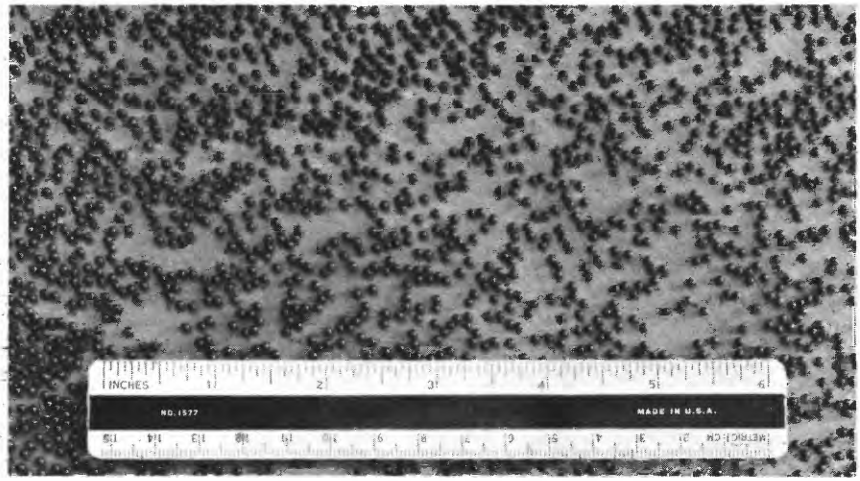

B. Closeup of birdshot roughness

FIGURE 11.—Model AC with birdshot roughness.

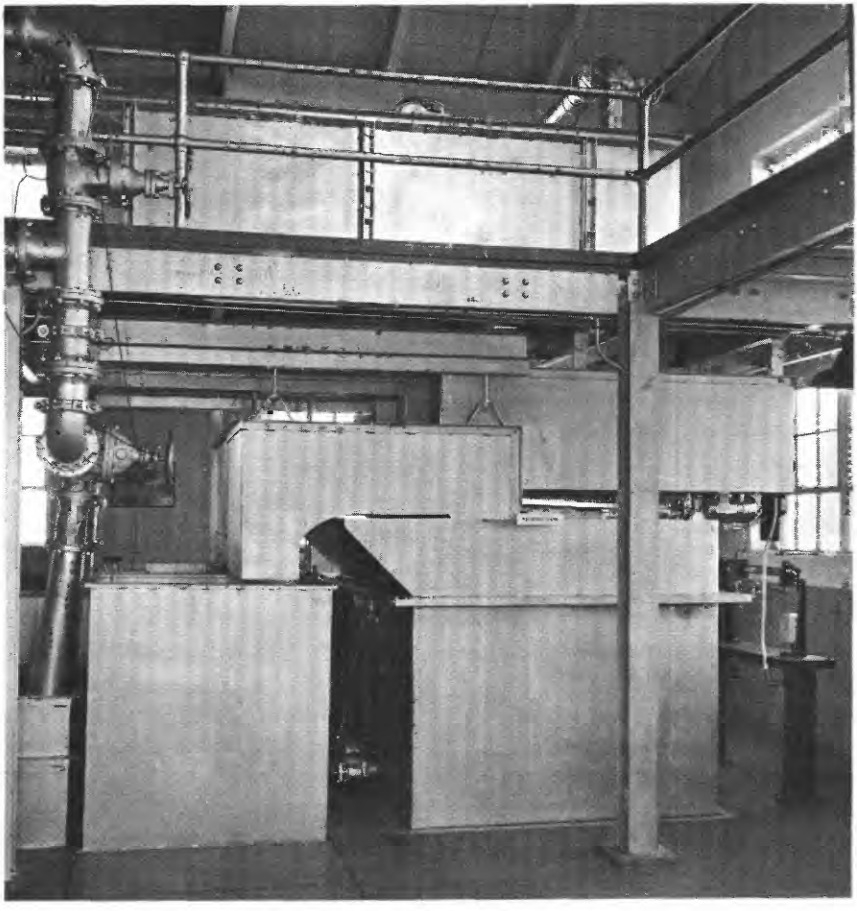

FIGURE 12.—Weighing-tank system for discharge measurements.

on the crown line was used to establish the reference level for gage zero.

Piezometers for most of the headwater measurements were located in the aluminum false floor, 1.75 feet (corresponding to 15.8 feet in the prototype) upstream from the intersection of the false floor and the embankment slope. For some tests, piezometers located farther upstream were used, but the measurements were subsequently adjusted, if necessary, to correspond with measurements made at the standard location.

Stilling wells were made of transparent plastic pipe. They were attached to the side of the flume and located close to the crown line to avoid any influence of laboratory-floor deflection. Headwater and tailwater levels are believed to be accurate within 0.001 foot.

Water-surface profiles and the depth of flow at the crown line were measured with a point gage mounted on a movable carriage (fig. 13). The headwater level, as determined by the hook gage, was used to zero

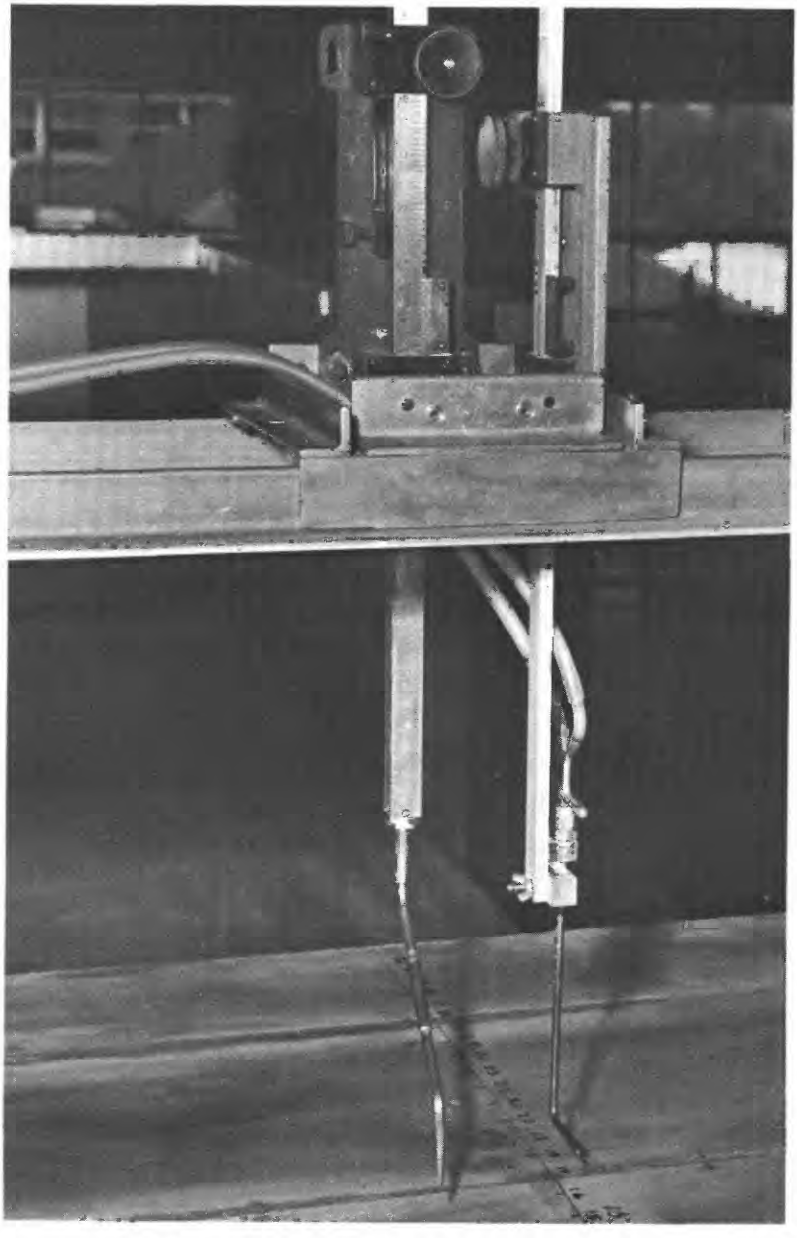

FIGURE 13.—Point gage (left) and pitot-static tube (right).

690-195 O - 64 - 5

the point gage. Longitudinal stationing for the point-gage measurements was obtained from a steel tape located adjacent to the carriage rail on the top of the flume. The accuracy of point-gage measurements depends on the instability of the water surface, but it is believed that the measurements were accurate within 0.002 foot.

VELOCITY MEASURMENTS

Equipment required especially for boundary-layer measurements consisted principally of velocity-measuring instruments and precision manometers. Velocities outside the boundary layer were measured with a pitot-static tube. This tube, shown on the right in figure 13, has an outside diameter of $\frac{3}{16}$ inch. Its stagnation and static openings are so located that the coefficient of the tube is very nearly 1.0. The tube was fastened to the staff of a hook gage, which was mounted on a movable carriage. A scale on the top rail of the flume, indexed to the carriage, and a scale on the hook-gage staff provided for accurate determination of the position of the pitot-static tube relative to the model. A pivoted connection between the gage staff and the tube permitted the tip leg of the tube to be adjusted so that it was always parallel to the flow at the point of measurement.

The air-water manometer used with the pitot-static tube is shown in figure 14. The manometer is of the zero-displacement type, with backlighted stainless-steel needles in glass tubes for accurate positioning of the menisci. Differential heads can be measured accurately within 0.001 foot with this manometer.

The stagnation tube used for boundary-layer velocity measurements is shown in figure 15. The tip of this tube was made from a 22-gage (0.028-inch outside diameter) stainless-steel hypodermic needle. The vertical leg is a brass tube, $\frac{1}{8}$ inch in outside diameter, backed up with a streamlined brass bar. The stagnation tube is mounted on a hook-gage staff, and a dial-type displacement gage is attached to the staff to provide for the accurate determination of the position of the tube. The smallest division on the dial scale is 0.001 inch. The stagnation-tube staff was provided with a pivot mount, in order that velocity traverses could be taken on sections which were perpendicular to the boundary at all stations.

The gage zero for the stagnation-tube displacement gage was determined at each measuring station by setting the dial scale to read zero when the bottom of the tube was placed against the surface of the model without bearing any of the weight of the tube assembly. The bottom of the tube was accurately located in this position by means of a horizontal light beam focused through the glass wall of the flume from a position opposite the observer and at an elevation just above the surface. Thus, the tube could be positioned very sensitively by

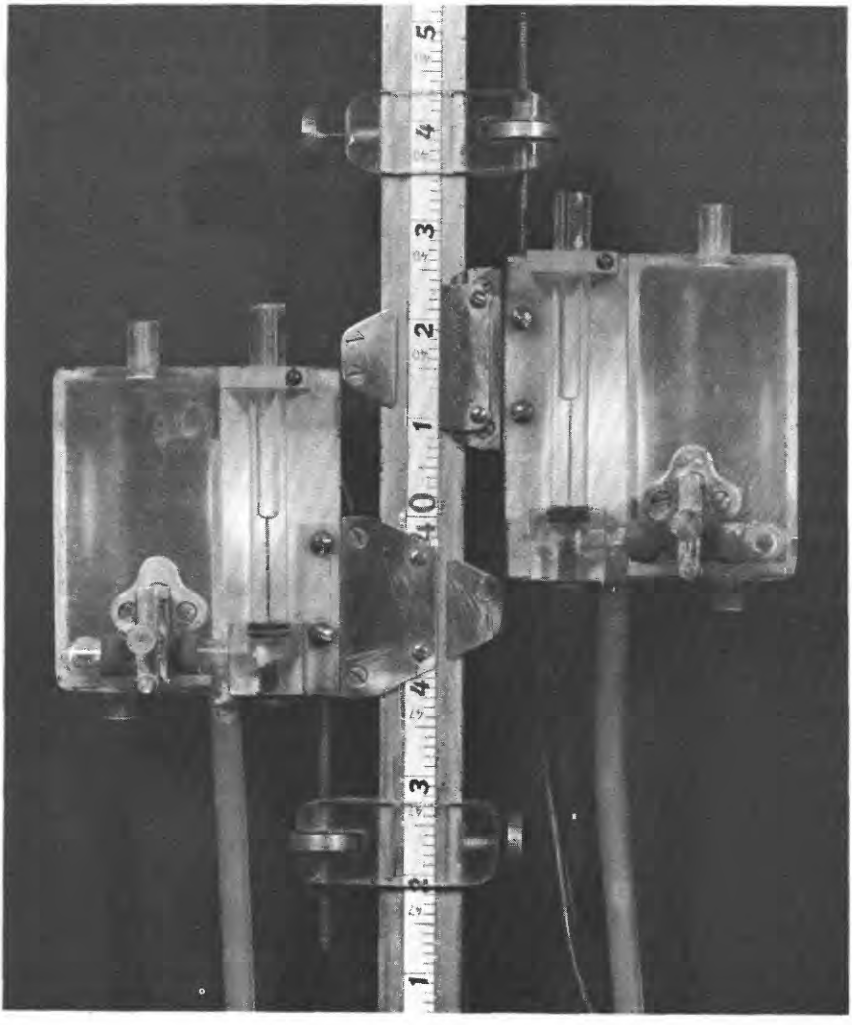

FIGURE 14.—Manometer for the pitot-static tube.

lowering it until no light could be seen between the bottom of the tube and the surface of the model.

The manometer used for the stagnation-tube measurements is shown in figure 16. The manometer is essentially a zero-displacement point gage. It consists of a black-lighted needle in a small glass tube, mounted on a frame which utilizes a vernier caliper for level determinations. Piezometric levels can be measured accurately within 0.001 inch with the manometer.

The zero reading for velocity determinations with the stagnation tube was determined by comparison with the differential-head reading

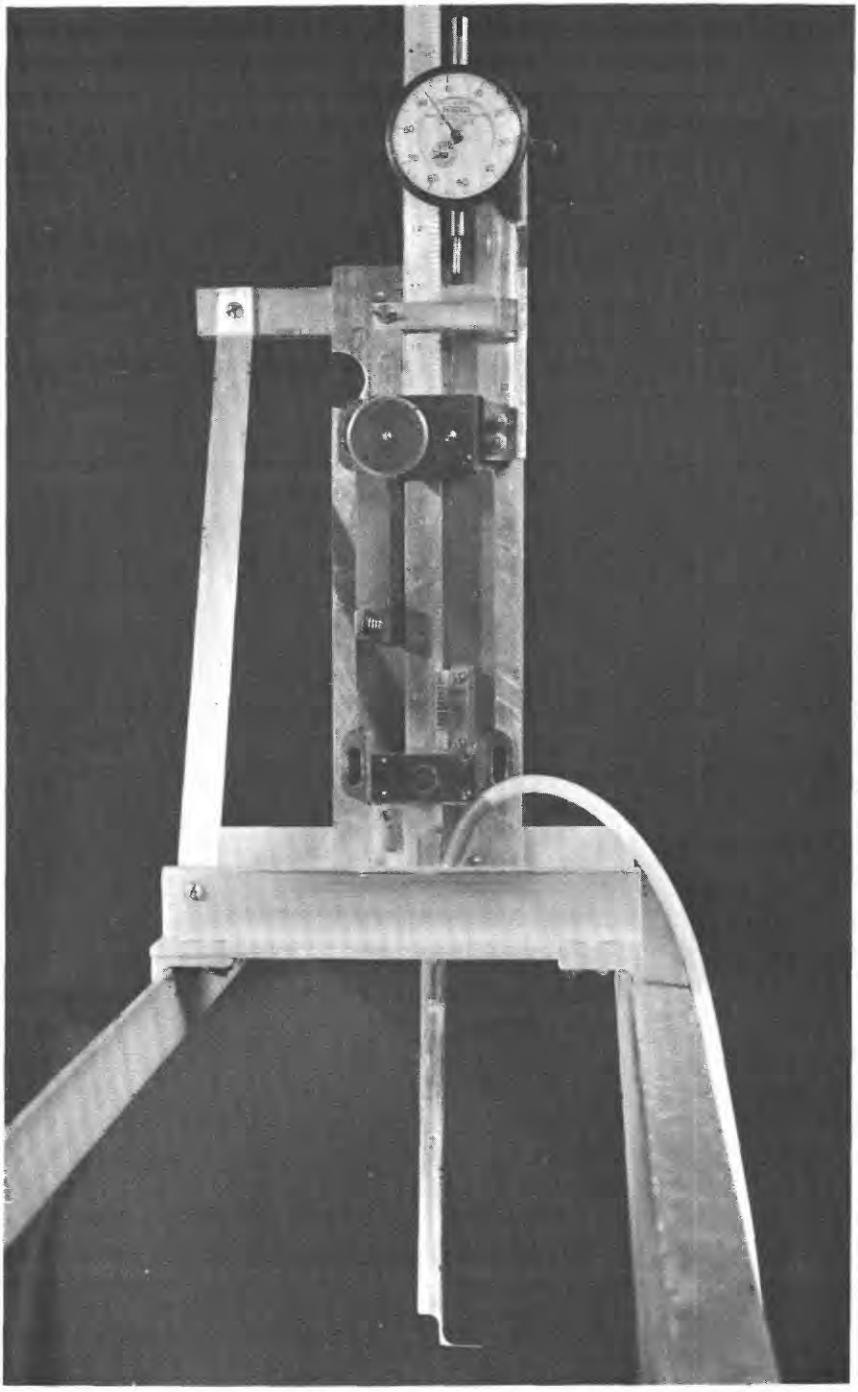

FIGURE 15.—Stagnation tube for boundary-layer velocity measurements.

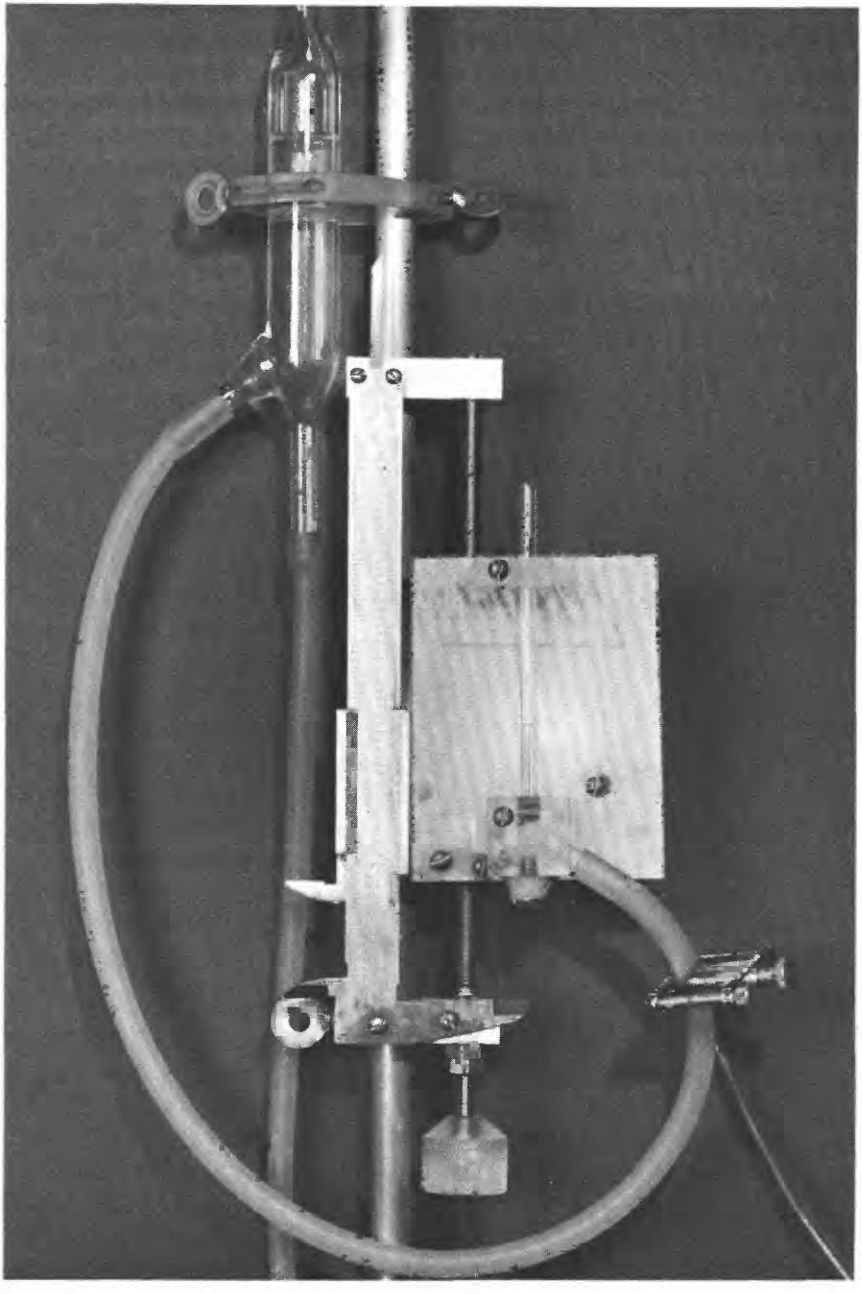

FIGURE 16.—Manometer for the stagnation tube.

obtained with the pitot-static tube in a uniform-flow zone outside the boundary layer at the same station. Thus, the absolute accuracy of the stagnation-tube velocity measurements depends on the accuracy of the pitot-static tube measurements.

SCOPE OF EMBANKMENT-DESIGN VARIATIONS

Scale-model tests were made on 17 variations of the basic embankment design. Data used in the report were obtained from tests made by Prawel, Davidian, and Emmett. Included in these tests, which were made after 1956, are duplications of test conditions investigated before 1956.

The scope of the design variations involved in the tests is given in table 1. All models described in table 1 were built to a scale of 1:9. The corresponding unit-discharge (q) scale is 1:27. Model A is the basic design, which is shown in prototype dimensions in figure 9. The design for model A was suggested by the Georgia State Highway Department in 1947. At that time it was typical of designs being used for secondary asphaltic-pavement two-lane highways. It is believed that subsequent changes in design standards, at least as they concern hydraulic characteristics, are adequately represented by the design variations described in table 1.

Models A–1 through A–4 are different versions of the basic design. Each model represents a minor reconstruction or refurbishing which followed tests on some of the design variations. The purpose of models B, C, and D was to demonstrate the influence of h/P by comparison with model A. Thus, models otherwise identical with model A were tested with a full range of heads and with values of P equal to one-fourth, one-half, and three-fourths of the value of P for the basic design.

To demonstrate the influence of pavement cross slope (S_p), models otherwise identical with model A were tested with 4 different values of S_p, 2 larger and 2 smaller than S_p for the basic design. Similarly, the influence of shoulder slope (S_s) was demonstrated with two models. For one of these, S_s was equal to S_p for model A. For the other, S_s was somewhat larger than S_s for the basic design.

Model K was built especially for tests concerned with the influence of the boundary layer. It involved a rounded intersection between the upstream embankment slope and shoulder. Model L was identical with the basic design except for a tripwire located on the downstream edge of the downstream shoulder. The purpose of this variation is described subsequently. Model M was designed to simulate the influence of the berm on both slopes of the embankment tested by Yarnell and Nagler (1930). Otherwise, model M was identical with

TABLE 1.—Summary of designs tested, 1:9-scale models

[Asterisk (*) indicates that shape detail differs from basic design]

Model	Investigator	Height, P (feet)		Pavement cross slope, S_P		Shoulder slope, S_S		Surface roughness	Remarks
		Prototype	Model	Inches: feet [1]	Nondimensional	Inches: feet [1]	Nondimensional		
A–1	Davidian	10.5	1.17	1.5:9	0.014	4.5:6	0.062	Smooth	Basic design.
A–2	Prawel	10.5	1.17	1.5:9	.014	4.5:6	.062	do	Do.
A–3	do	10.5	1.17	1.5:9	.014	4.5:6	.062	do	Do.
A–4	Emmett	10.5	1.17	1.5:9	.014	4.5:6	.062	do	Do.
B	Prawel	*7.88	*.875	1.5:9	.014	4.5:6	.062	do	Effect of P.
C	do	*5.25	*.583	1.5:9	.014	4.5:6	.062	do	Do.
D	do	*2.62	*.292	1.5:9	.014	4.5:6	.062	do	Do.
E	do	10.5	1.17	*0:9	*.000	4.5:6	.062	do	Effect of S_P.
F	do	10.5	1.17	*.9:9	*.008	4.5:6	.062	do	Do.
G	do	10.5	1.17	*2.2:9	*.020	4.5:6	.062	do	Do.
H	do	10.5	1.17	*2.8:9	*.026	4.5:6	.062	do	Do.
I	do	10.5	1.17	1.5:9	.014	*1.0:6	*.014	do	Effect of S_S.
J	do	10.5	1.17	1.5:9	.014	*5.7:6	*.079	do	Do.
K–1	Davidian	10.5	1.17	1.5:9	.014			do	[2]
K–2	Prawel	10.5	1.17	1.5:9	.014			do	[2]
L	do	10.5	1.17	1.5:9	.014	4.5:6	.062	do	[3]
M	do	10.5	1.17	1.5:9	.014	4.5:6	.062	do	[4]
AA–1	Davidian	10.5	1.17	1.5:9	.014	4.5:6	.062	Window screen (all surfaces).	
AA–2	Emmett	10.5	1.17	1.5:9	.014	4.5:6	.062	do	
AB	do	10.5	1.17	1.5:9	.014	4.5:6	.062	Birdshot (except on pavement).	
AC	do	10.5	1.17	1.5:9	.014	4.5:6	.062	Birdshot (all surfaces).	
KA	Davidian	10.5	1.17	1.5:9	.014			Window screen (all surfaces).	[2]

[1] Dimensions given in prototype units (see fig. 9).
[2] Rounded transition between upstream embankment and shoulder surfaces. (See fig. 10A.)
[3] Trip wire on downstream edge of downstream shoulder. (See fig. 10B.)
[4] Berm on embankment slopes. (See fig. 10C.)

model A. Details of design for models K, L, and M are shown on figure 10.

The remaining four design variations shown in table 1 were intended to demonstrate the influence of surface roughness on the discharge characteristics of an embankment. These models involve 3 kinds of roughness on model design A and 1 on model design K.

SIGNIFICANCE OF ROUGHNESS VARIATIONS

Only four different degrees or patterns of surface roughness (including "smooth") were involved in all the model variations described in table 1. Furthermore, the simple k/h ratio used to represent relative roughness in equation 10 is inadequate to describe the roughness variations tested. Nevertheless, the tests made with rough-surfaced models are expected to result in a general understanding of the influence of roughness on the coefficient of discharge and other important flow characteristics.

Model A, the basis of comparison for all other designs, included smooth surfaces on all parts of the embankment and roadway. In terms of the prototype, the characteristics revealed by this model are

believed to simulate reasonably accurately the characteristics of a smooth, paved roadway in good repair.

Models AA and KA were rough-surfaced models. The roughness consisted of wire screen, a type of roughness used previously by Bauer (1954) in a related investigation. Uniform-flow tests made by Bauer, using a slightly different kind of screen, indicated that the effective roughness could be compared with rough concrete in the prototype.

Models AB and AC featured a relatively large, granular-type roughness, consisting of birdshot cemented to the surface in a random pattern (see fig. 11). This variety of roughness is believed to simulate a reasonable maximum prototype roughness. For model AC the birdshot was applied to the entire model surface. For model AB the birdshot was applied only to the embankment slopes and shoulders. Model AB should give an indication of the influence of rough shoulders bordering a smooth pavement.

Roughness investigations for open-channel flows are usually complicated by the fact that the depth of flow varies with the discharge. Therefore, a ratio like k/h or k/y, unlike the corresponding relative-roughness ratio used for pipe flow, varies with discharge as well as roughness. Also, because the Reynolds number for the mean flow is $\mathbf{R}=Vy/\nu=q/\nu$, values of $\mathbf{R}$ for the prototype are in a higher range than values of $\mathbf{R}$ in the model for corresponding values of geometric ratios such as h/P and h/L. Furthermore, the nature of prototype roughness, especially embankment and shoulder roughness, is extremely variable and very difficult to simulate in the laboratory. It is believed that a comprehensive investigation of the influence of roughness will require, in addition to small-scale model tests, a carefully controlled program of tests on full-scale models or prototypes.

INFLUENCE OF EMBANKMENT FORM AND ROUGHNESS

OBJECTIVE

The laboratory investigations had two main objectives. One was the experimental determination of the relationship between embankment form and roughness and some of the more important discharge characteristics. The second was the theoretical and experimental definition of the relationship between free-flow discharge and the boundary layer on the roadway. The first objective is discussed in this part of the report.

The data needed to accomplish the first objective are mostly those needed to define the coefficient of discharge and the characteristic flow patterns for free and submerged flow. The analysis is empirical, but it is guided by the results of the dimensional analysis. A summary of the results of the tests described in this part of the report is given in table 3 in the section "Experimental Data."

ANALYSIS OF RESULTS

COEFFICIENT OF DISCHARGE FOR FREE FLOW

Tests made to determine the coefficient of discharge for free flow involved the measurement of the head and discharge. The discharge coefficient, C, was computed from equation 8, wherein H_1 is the total head referred to the crown line (see fig. 5),

$$H_1=h+\frac{V_1^2}{2g}=h+\frac{q^2}{2g(P+h)^2}, \tag{23}$$

and q is the total measured discharge divided by the width of the flume at the crown line,

$$q=\frac{Q}{B}. \tag{24}$$

Figures 17, 18, and 19 show the coefficient of discharge for all the designs tested. In these figures, values of C are plotted as a function of both h and h/L, where h is the piezometric head (as measured in the model) and L is the total width of pavement and two shoulders. The two abscissa scales are independently significant. Thus, h is a scale of reference for the influence of boundary resistance and "scale effect," because h is directly proportional to the Reynolds number. On the other hand, h/L is a scale of reference for form effects, including the effect of curvilinear flow at the control section.

Figure 17 shows the coefficient of discharge for the basic design,

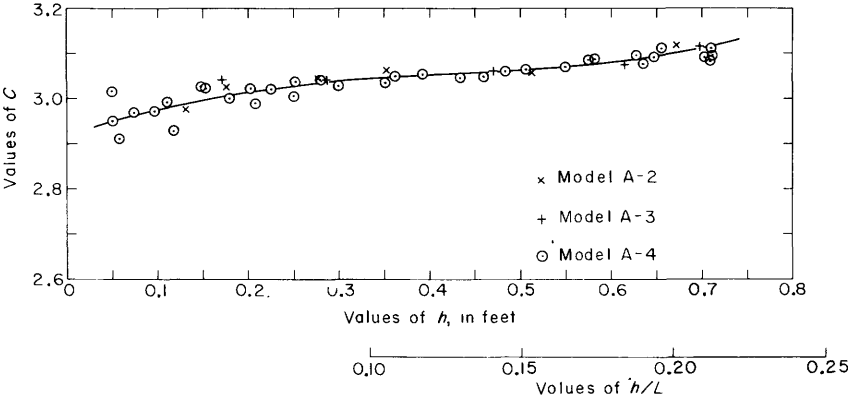

FIGURE 17.—Coefficient of discharge for free flow; basic design, model A.

model A. The curve, visually fitted to the plotted points, shows an initial trend for C to increase with h and approach asymptotically the ideal value (3.09). When h exceeds about 0.5 feet, however, the curve

inflects, and C begins to increase more rapidly, eventually exceeding 3.09. As implied by the overlapping scales of h and h/L, the inflection in the C curve is believed to be related to the gradual change from dominant boundary-resistance influence to dominant boundary-form influences.

Figure 18 shows the coefficient of discharge for all the smooth-surfaced models. The several parts of the figure show, by comparison with the basic design (model A), the independent effects of h/P, S_p, and S_s, as well as the special features represented by models K, L, and M.

Figure 18A shows the effect of P and, indirectly, the influence of h/P. The figure shows the results of tests made with models B, C, and D, as well as the curve for model A from figure 17. Considering the probable experimental error, which can be expected to increase as P decreases (the result of waves and surges in the approach channel), figure 18A shows no distinct, systematic relationship between C and P. Consequently, because the tests cover approximately the same range of h values for each of the four P values represented, it is concluded that C is virtually independent of h/P.

Figure 18B shows the influence of pavement cross slope on the coefficient of discharge for free flow. The results of tests on models A, E, F, G, and H show a poorly defined but systematic relationship between C and S_p. However, the average deviation from the model A curve is less than 1 percent for all models except model H, for which S_p was nearly twice the value specified for the basic design. Thus, for purposes of practical application, the correlation between C and S_p is believed to be insignificant.

Figure 18C shows the influence of shoulder slope, S_s, based on the results of tests on models I, J, and K–2, as well as model A. Model K–2 is included because it simulates the prototype condition of a rounded or variable-slope shoulder which is tangent to both the embankment slope and the pavement. The results of the tests shown on figure 18C are somewhat contradictory, because the maximum consistent deviation from the model A curve is shown by the model which most nearly resembles the basic design. Again, however, the average deviation from the model A curve is not more than 1 percent for any of the design variations represented. Thus, for practical purposes, C is believed to be independent of S_s.

In view of the results shown on figures 18 (A, B, C), it is not surprising to find that the special design variations represented by models L (tripwire on downstream shoulder) and M (berm on both embankment slopes) have an insignificant influence on the coefficient of discharge for free flow. This conclusion is substantiated by the test results shown on figure 18D.

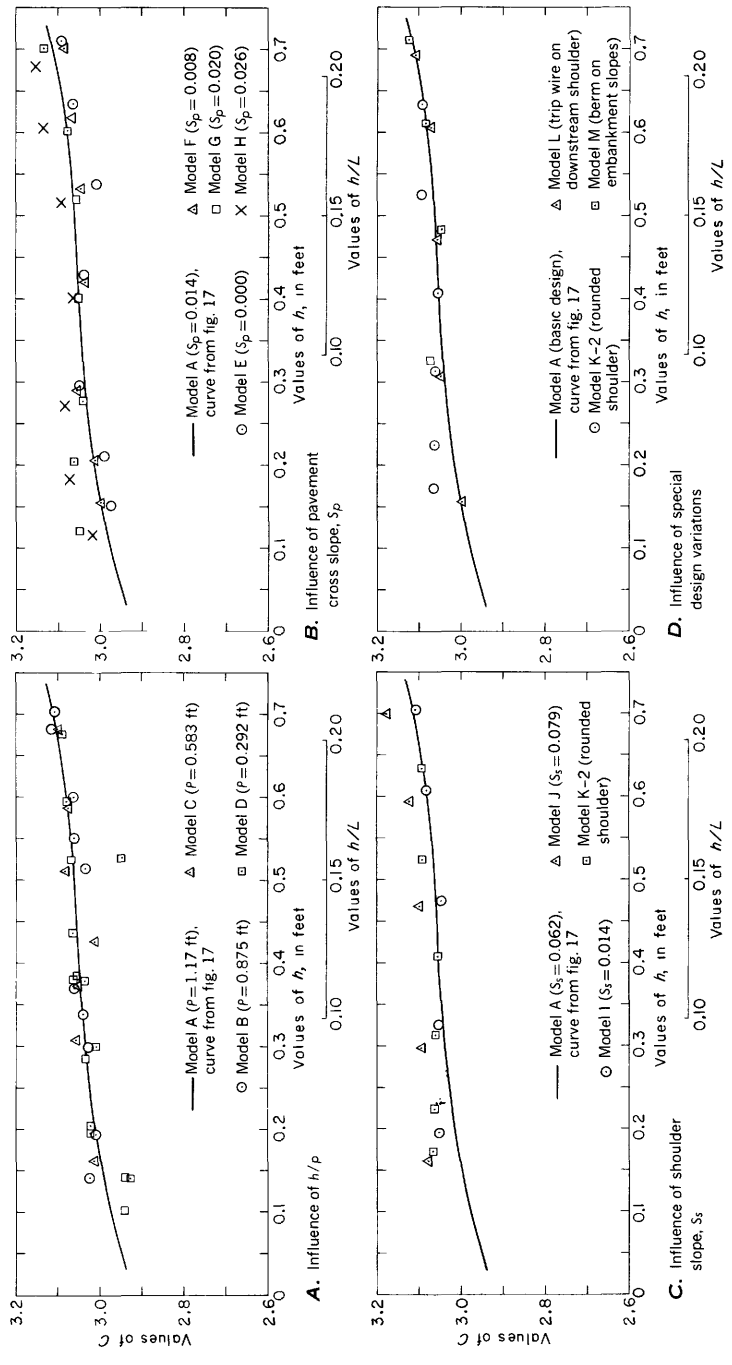

FIGURE 18.—Coefficient of discharge for free flow; smooth-surfaced models.

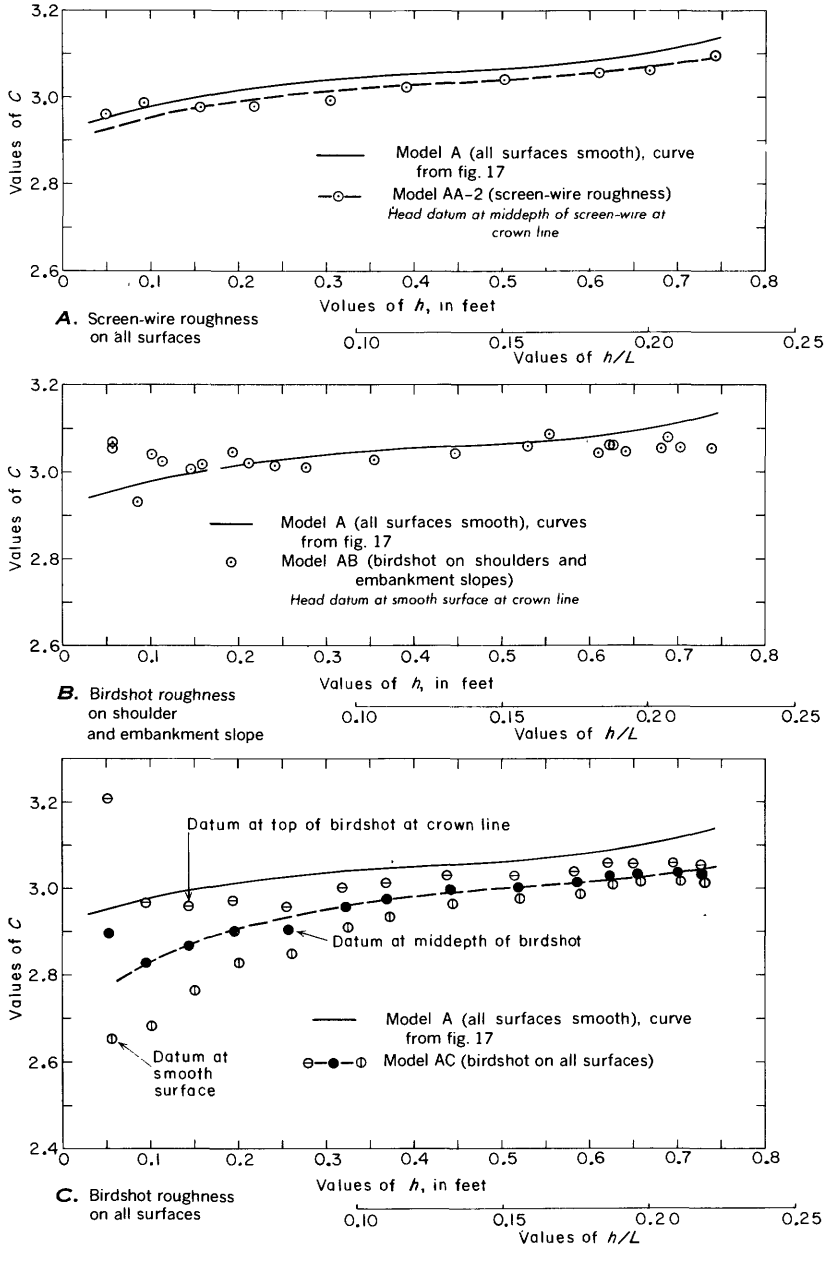

FIGURE 19.—Coefficient of discharge for free flow; rough-surfaced models.

Figure 19 shows the influence of roughness on the coefficient of discharge. As in figure 18, the curve for model A is used as a basis for comparison. Figure 19*A* shows that screen-wire roughness over the entire model surface (model AA–2) causes the coefficients to be consistently about 1 percent lower than the coefficients for model A. It is noted in the figure that C is computed on the basis of the assumption that the head datum is at the level of the middepth of the screen wire at the crown line. Alternate assumptions might have placed the datum at the level of the top of the screen or at the level of the smooth surface of the model. As the thickness of the screen fabric is approximately 0.002 foot, the maximum difference in heads computed on the basis of the different assumptions would have been only 0.002 foot. Thus, the corresponding difference in computed values of C would have been negligible except at very small values of h. The question of head datum relative to screen-wire thickness is obviously meaningless in terms of the prototype.

Figure 19*B* shows the influence of a relatively large, granular-type (birdshot) roughness on the shoulders and embankment slopes. Because the pavement was smooth, as in model A, the head datum was the level of the smooth model surface at the crown line. The coefficient of discharge for model AB appears to differ very little from that for the basic design.

Figure 19*C* shows the results of tests on model AC, with birdshot roughness on all model surfaces. The results are presented in a form which shows the influence of alternate assumptions regarding the datum for head computations. In this instance, because the diameter of the birdshot was nearly 0.007 foot, the effect of the alternative assumptions on computed values of C is appreciable. A dashed curve is drawn through the points which correspond to the datum at middepth of the birdshot.

COEFFICIENT OF DISCHARGE FOR SUBMERGED FLOW

In the previous discussion of submerged flow (p. 18), it was emphasized that the coefficient of discharge for submerged flow is independently related to all the variables involved in free flow, plus the submergence ratio, t/h. It was concluded that C for submerged-flow tests, like C for free-flow tests, should be computed from equation 8.

Figure 20 shows C plotted as a function of t/h for models A–2, B, C, and D. Different symbols are used to identify the plotted points which correspond to different constant values of P. It is apparent from the figure that the relationship between C and t/h is independently correlated with P. For purposes of application to the prototype, the P variable in figure 20 should be expressed as a non-

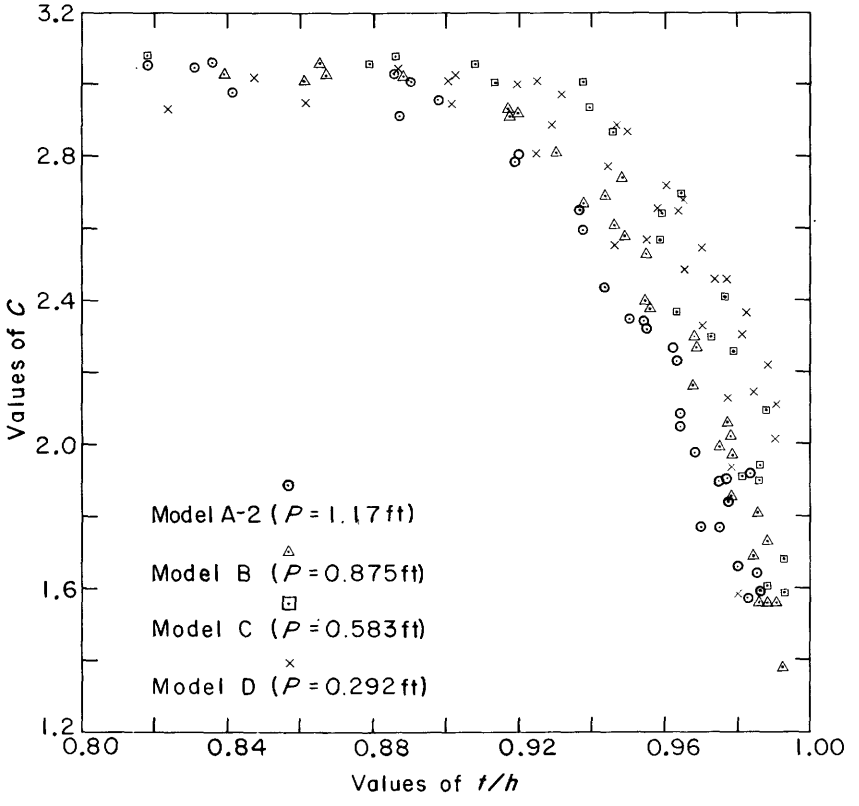

FIGURE 20.—Coefficient of discharge for submerged flow; influence of h/P, with t/h as the submergence ratio.

dimensional ratio. Unfortunately, however, the most likely parameter for this purpose, h, varies independently with q and t/h. Therefore, the ratio h/P is incapable of defining a single family of curves on a figure such as figure 20. The problem was conveniently resolved by changing the definition of the submergence ratio. Thus, when the submergence ratio is defined as t/H_1 instead of t/h, the effect of P is virtually eliminated. This conclusion is substantiated by a comparison of figures 20 and 21.

Figure 21 shows a considerable scatter of plotted points but no systematic correlation with P. In general, points showing the maximum deviation from the average curve represent tests made with larger values of h/P. It is significant that waves and surges in the approach channel cause increasing difficulties and errors of measurement as h/P increases. Subsequent demonstrations of the sensitivity of C_{subm} to small irregularities on the roadway are more reason

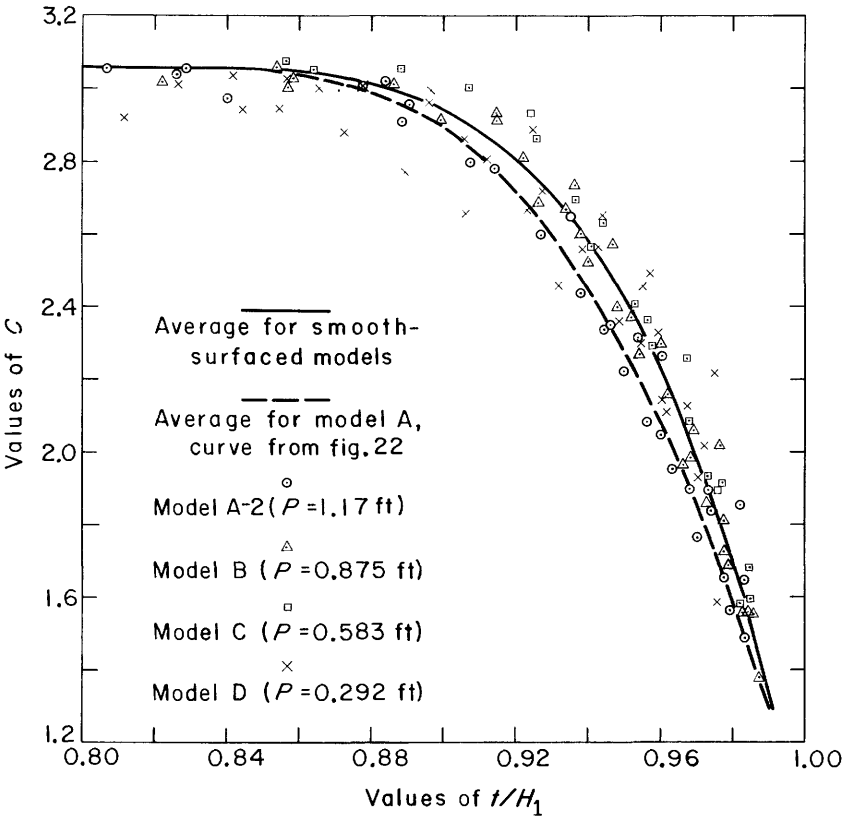

FIGURE 21.—Coefficient of discharge for submerged flow; influence of h/P, with t/H_1 as the submergence ratio.

to accept the scatter of points in figure 21 as evidence of normal experimental error.

The data shown on figures 20 and 21 represent the same tests and, therefore, the same range of discharges as were used for the free-flow coefficients shown on figure 18*A*. In figure 18*A*, as for all free-flow tests, the coefficient is clearly related to h (or q). It seems reasonable to expect that the rate of flow will be similarly involved in the relationship between C_{subm} and t/H_1. This conclusion is readily tested on the basis of the data shown on figure 22. Here, for two versions of model A, different rates of flow are identified with different symbols. The obvious conclusion to be drawn from figure 22 is that the effect of q is insignificant.

For purposes of comparison with other model designs, an average curve for model A is fitted to the data shown on figure 22. It is observed that the plotted points do not deviate from the curve by an

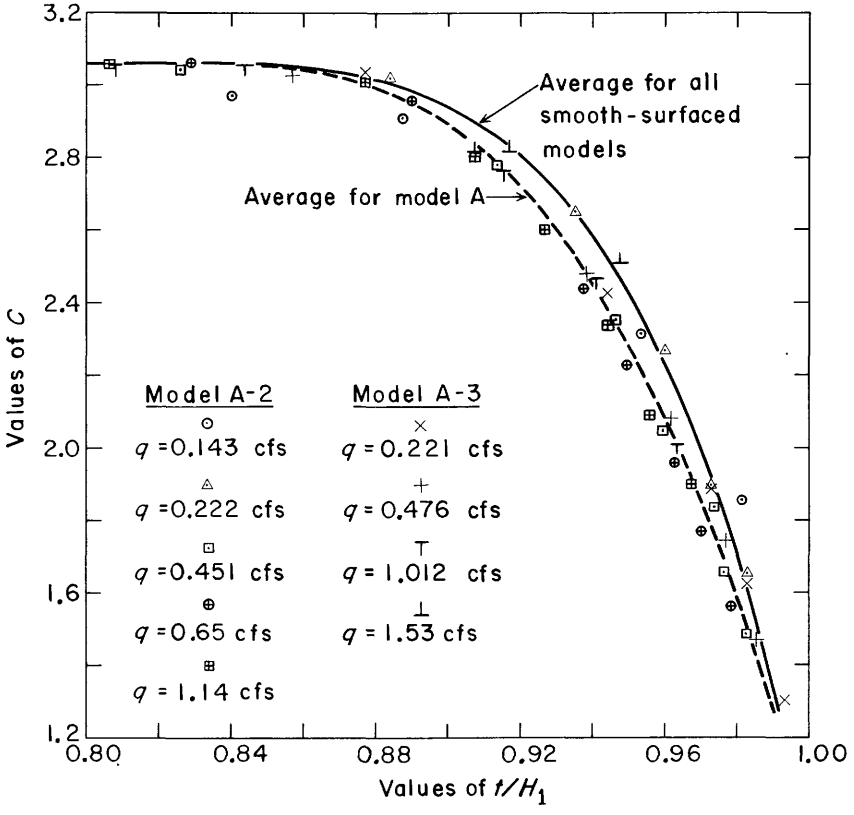

FIGURE 22.—Coefficient of discharge for submerged flow; basic design, model A.

amount in excess of the probable experimental accuracy. Some uncertainty may exist, however, regarding the value of C represented by the incipient-submergence end of the curve. Here, at least, it might be expected that the previously observed influence of q on C_{free} would require consideration.

It is recalled that the variation of C_{free} with h shown on figures 17, 18, and 19 is related to the influence of boundary resistance at low heads and to the influence of boundary-form effects (principally flow curvature) at higher heads. Characteristics related to heads smaller than 0.5 foot are seldom likely to be significant in terms of the prototype. Furthermore, when t/H_1 is 0.84 or over, as it is when incipient submergence occurs, flow at the control section is very nearly uniform (see fig. 2 B), and, regardless of the head, flow curvature is not likely to have a significant influence on C. Thus, in figure 22 and all subsequent plots of C versus t/H_1, the value of C_{free} used to define the incipient-submergence end of the average curves is the value at the

point of inflection on the corresponding curve in figures 17, 18, and 19. The average curve for model A is shown on figure 21 as well as figures 22 through 28. Also shown on those figures is an average curve for all smooth-surfaced models (A through M).

Figure 23 shows the results of submerged-flow tests made with models A, E, F, G, and H, all with different values of S_p. The plotted points are remarkably close to the average curve for smooth-surfaced models. They show no significant correlation with S_p.

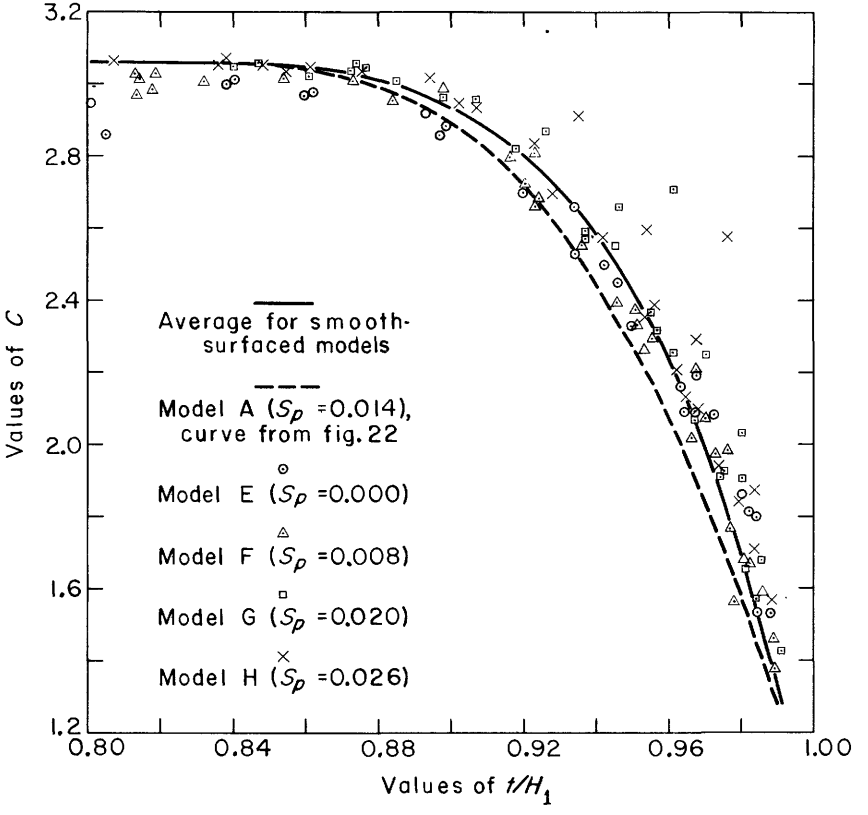

FIGURE 23.—Coefficient of discharge for submerged flow; influence of pavement cross slope, S_p.

Figure 24 shows the influence of shoulder slope, S_s, based on tests made with models A, I, J, and K–2. Points representing model I deviate considerably from the average curve. However, the value of S_s used in this model is smaller than that ordinarily used in practice. Considerable scatter characterizes the results of tests made with the rounded-shoulder model (K–2). The average of the scattered points agrees reasonably well with the average curve for all smooth-surfaced

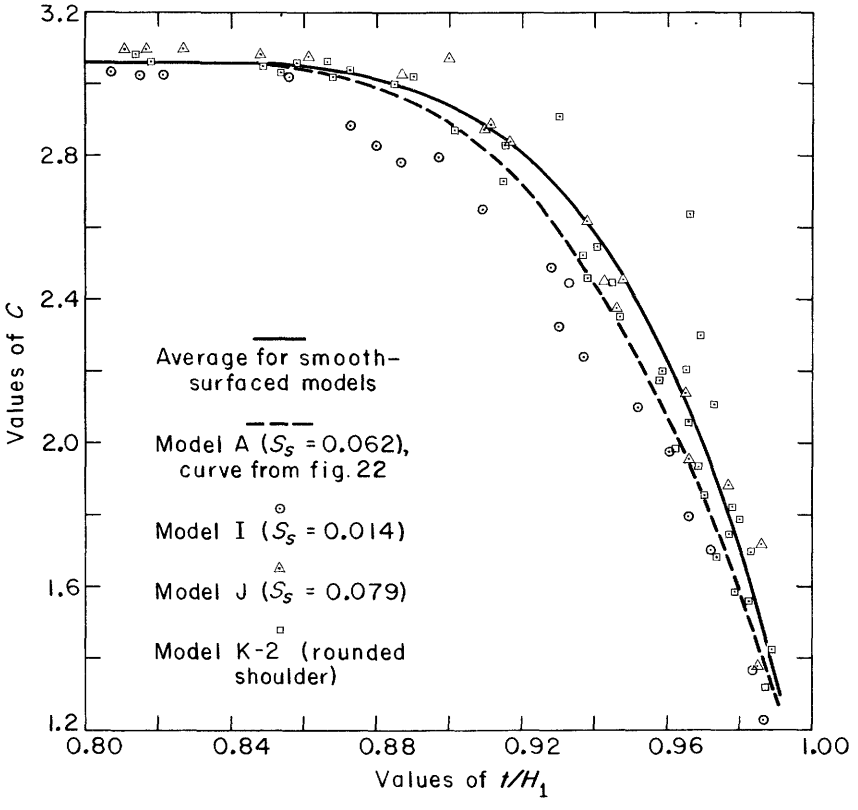

FIGURE 24.—Coefficient of discharge for submerged flow; influence of shoulder slope, S_s.

models. The magnitude of the scatter is believed to be consistent with the experimental accuracy to be expected.

The influence of the special design variations, models K–2, L, and M, is shown in figure 25. Maximum deviation from the average curve is shown by models K–2 (discussed above in connection with fig. 24) and L. The results of tests on model L, with a tripwire on the downstream shoulder (see fig. 10 *B*), are particularly significant. These results lead to the conclusion that the influence of small obstructions on the downstream side of the roadway, particularly at the downstream end of the shoulder, is greater than the influence of any of the major geometric parameters previously considered.

Figures 26, 27, and 28 show the influence of surface roughness on the submerged-flow discharge coefficient for models AA–2, AB, and AC. As in the preceding figures, the curve for model A and the average curve for smooth-surfaced models is shown for comparison.

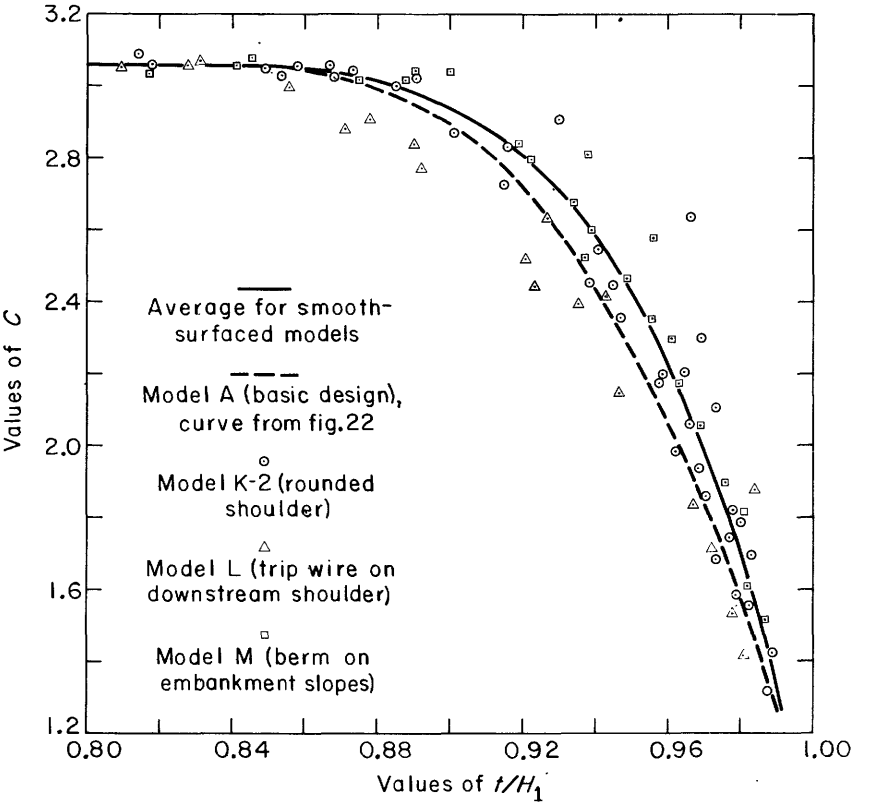

FIGURE 25.—Coefficient of discharge for submerged flow; influence of special design variations.

It is apparent that the effect of roughness is to decrease the coefficient of discharge and to cause the inception of submergence at lower values of t/H_1. It is also apparent, from comparison of figures 27 and 28, that roughness on the shoulders and embankment slopes is nearly as effective as roughness distributed uniformly over all surfaces of the model. Because the birdshot roughness used for models AB and AC is believed to simulate a maximum prototype roughness, the curve showing the results of tests on model AC, figure 28, is believed to represent a reasonable maximum influence of roughness on C_{subm}. The points showing considerable scatter on this figure correspond to small discharges and small heads and consequently large relative errors in computed values of C and t/H_1.

INCIPIENT SUBMERGENCE

The transition from free flow to submerged flow has been described as incipient submergence. In the laboratory test procedure, the tail-

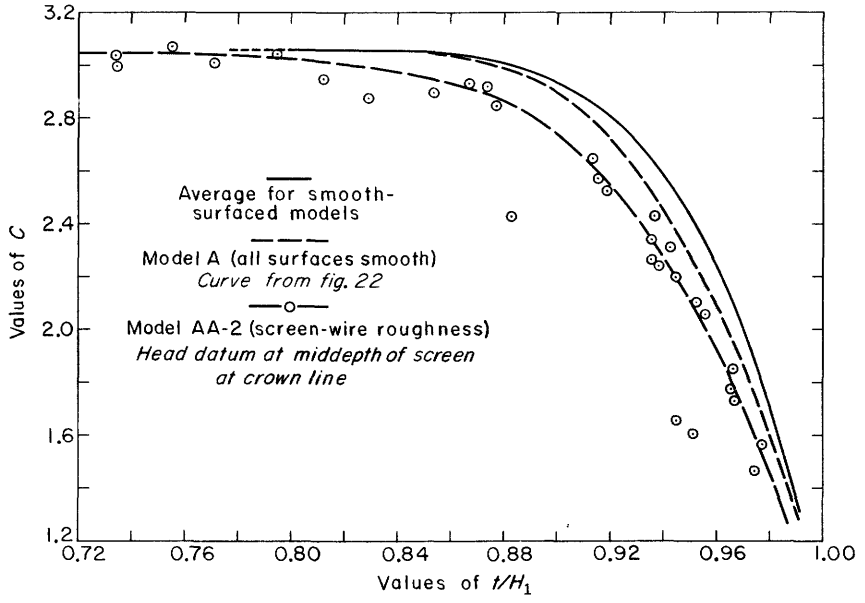

FIGURE 26.—Coefficient of discharge for submerged flow; influence of screen-wire roughness on all surfaces.

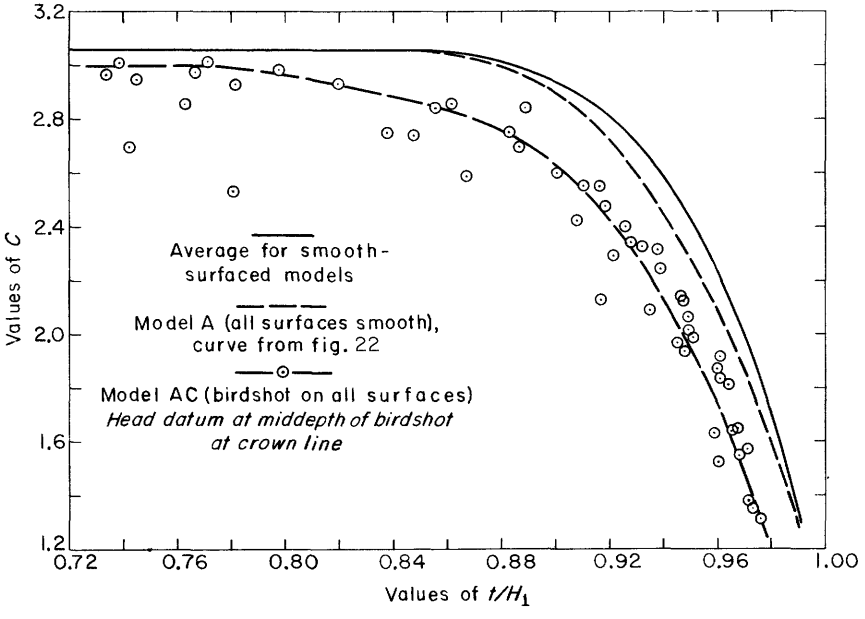

FIGURE 27.—Coefficient of discharge for submerged flow; influence of birdshot roughness on shoulders and embankment slopes.

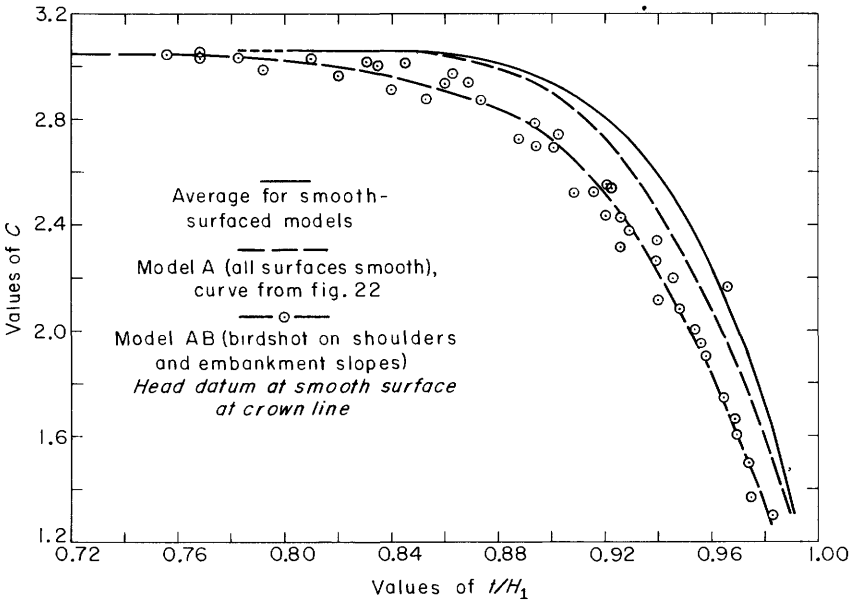

FIGURE 28.—Coefficient of discharge for submerged flow; influence of birdshot roughness on all surfaces.

water level corresponding to incipient submergence for a given discharge was determined by gradually raising the tailwater and observing the tailwater level at which the headwater began to rise. The results of tests made to define the incipient-submergence tailwater level for the full range of model discharge are shown in the upper half of figures 29 through 37, The average curves for model A are shown for comparison on figures 32 through 37.

Figures 29 and 30 show a comparison of alternative dependent-variable (ordinate) scales used to define incipient submergence. The variables used are the tailwater ratios t/h (fig. 29) and t/H_1 (fig. 30), and the tests used for the comparison are those involving different values of P (models A, B, C, and D). Neither ratio shows a significant correlation with P, but the scatter of test points is somewhat smaller when t/H_1 is used. Furthermore, because t/H_1 was used in the presentation of C_{subm} data (figs. 21 through 28), it is used in subsequent figures showing incipient-submergence and transition-range characteristics.

The overlapping abscissa scales used for figures 29 through 37 are h and h/L. It has been explained that the two scales are independently significant, because h is a scale of reference for the boundary-layer influence and h/L is a scale of reference for form influence. The test results shown on figure 30 indicate that incipient submerg-

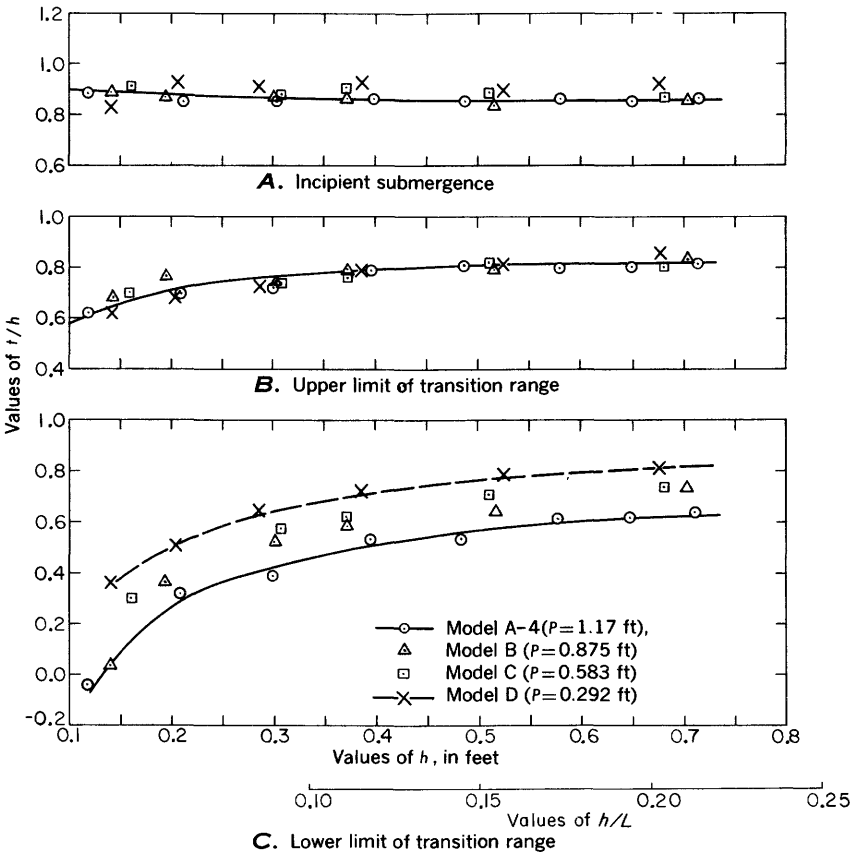

FIGURE 29.—Incipient submergence and free-flow transition range; influence of h/P, with t/h as the submergence ratio.

ence occurs at $t/H_1=0.84$ when h is greater than about 0.4 feet. Somewhat higher values of t/H_1 are indicated for lower values of h. It is reasonable to believe that the increase in t/H_1 is related to the influence of boundary resistance.

Figure 31 shows the results of tests on three versions of the basic design. The average curves obtained from the figure are shown as the characteristics of model A in the subsequent figures in this series.

Figs. 32, 33, and 34 show the results of tests involving different values of S_p (fig. 32) and S_s (fig. 33) and the special design variations represented by models K–2, L, and M (fig. 34). From these figures it is apparent that none of the design variations causes an appreciable change in the incipient-submergence characteristics of the smooth-surfaced models. All the data show remarkably good agreement with the results of tests on the basic design. A little scatter of test points

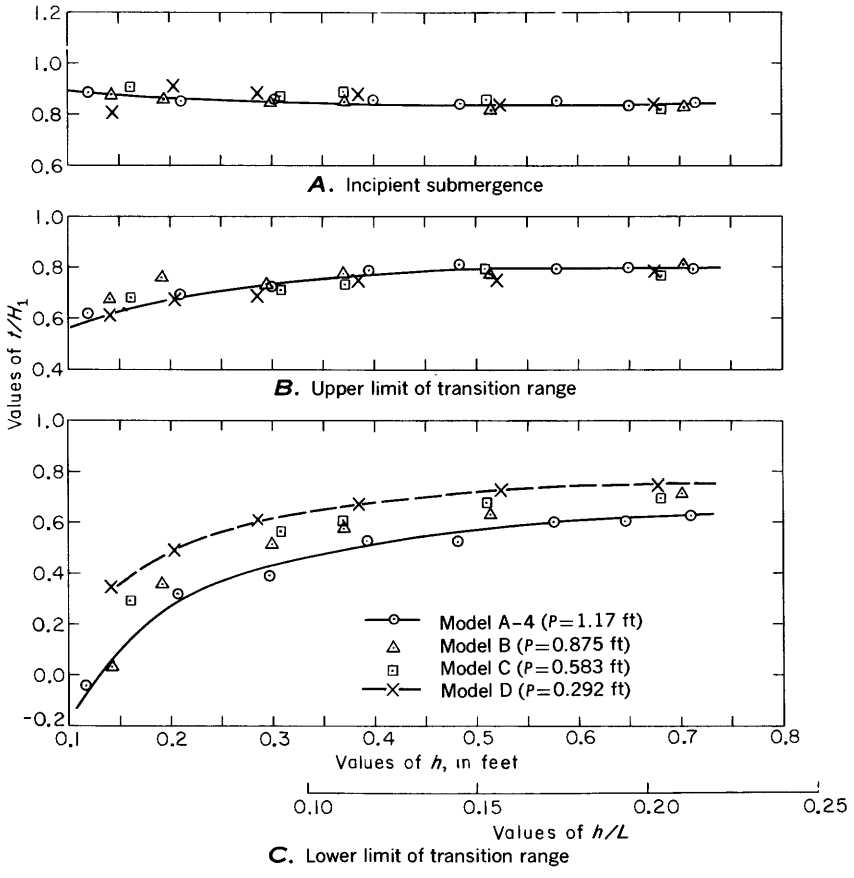

FIGURE 30.—Incipient submergence and free-flow transition range; influence of h/P, with t/H_1 as the submergence ratio

at small values of h is believed to be insignificant, because it is recognized that small values of h correspond to small values of t and relatively large experimental errors in t/H_1.

Figures 35, 36, and 37 show the influence of surface roughness. The results of tests on models AA–2 (fig. 35), AB (fig. 36), and AC (fig. 37) indicate that values of t/H_1 for incipient submergence are smaller for the rough-surfaced models than for the smooth-surfaced models represented by model A. Remarkably, the largest deviation from the model A curve is shown for the screen-roughened model (model AA–2, fig. 35), and the smallest deviation is shown for the model which is completely covered with birdshot (model AC, fig. 37). Furthermore, for model AA–2 the incipient-submergence tailwater ratio varies with h over the full range of test values. For the birdshot-roughened models, as for the smooth-surfaced models, the tailwater ratio at in-

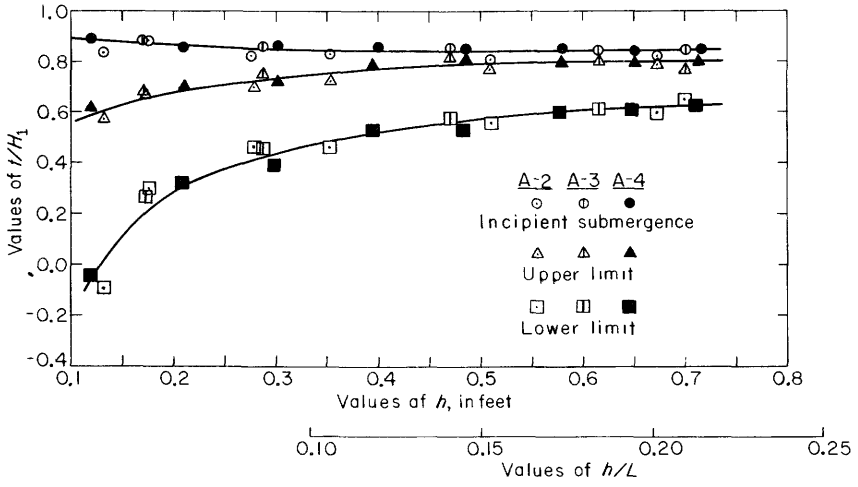

FIGURE 31.—Incipient submergence and free-flow transition range; basic design, model A.

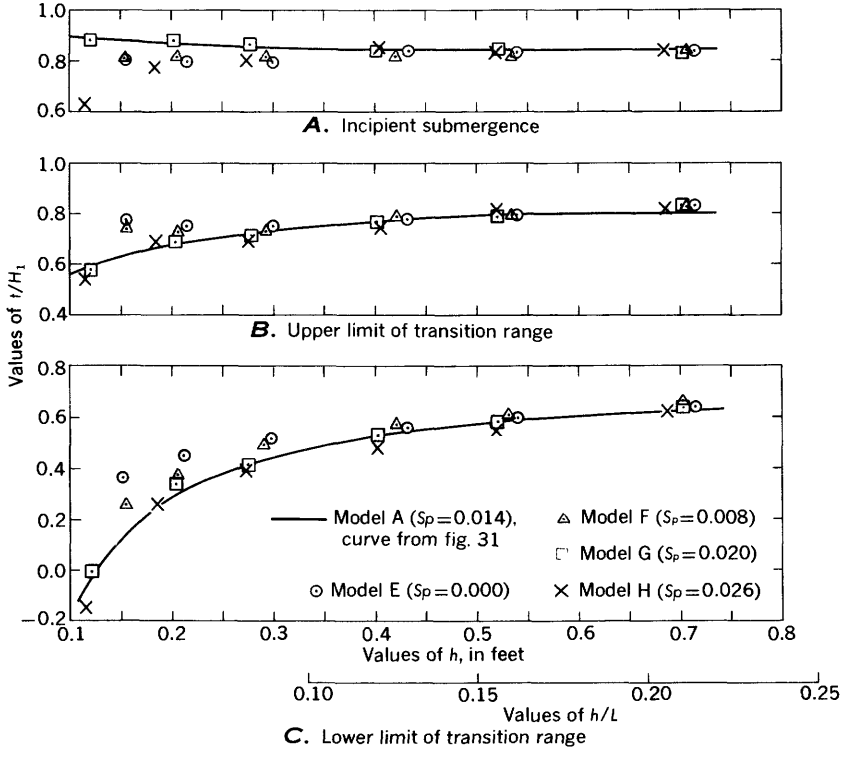

FIGURE 32.—Incipient submergence and free-flow transition range; influence of pavement cross-slope, S_p.

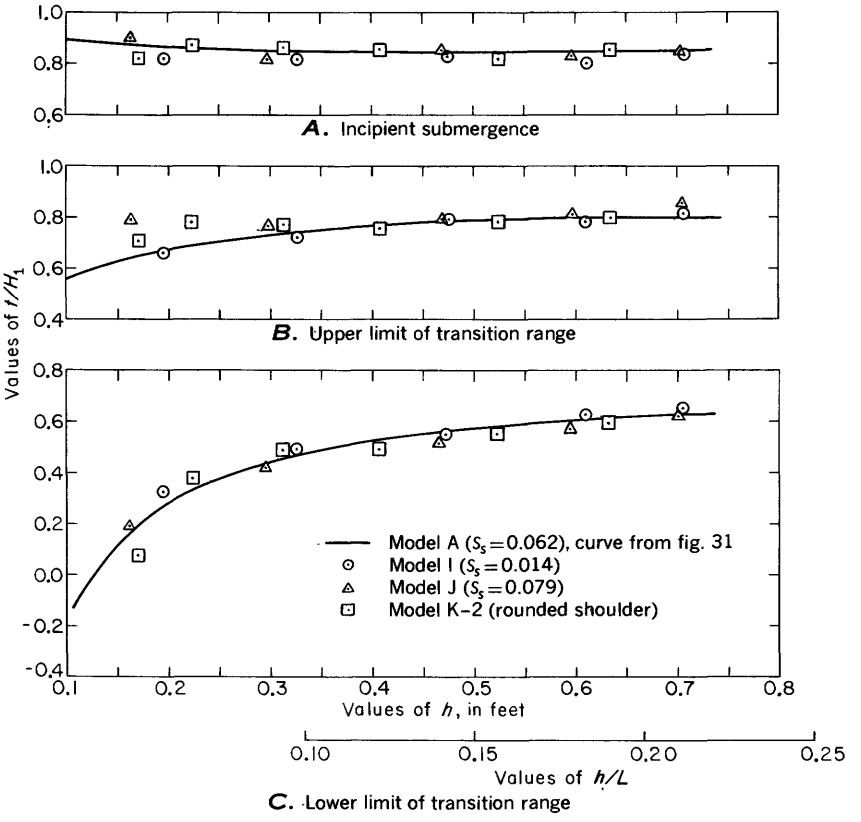

FIGURE 33.—Incipient submergence and free-flow transition range; influence of shoulder slope, S_s.

cipient submergence is constant for heads greater than about 0.4 feet. However, the effect of lower heads is to decrease the ratio for rough-surfaced models and to increase it for the smooth-surfaced models.

FREE-FLOW TRANSITION RANGE

The free-flow transition range is the range of tailwater levels within which a given discharge may produce either a plunging flow or a surface flow on the downstream side of the embankment. The upper and lower limits of the transition range were determined visually by gradually raising and lowering the tailwater and observing the level at which the transitions took place.

The results of tests made to define the free-flow transition range are shown in the middle and lower parts of figures 29 through 37.

690-195 O - 64 - 8

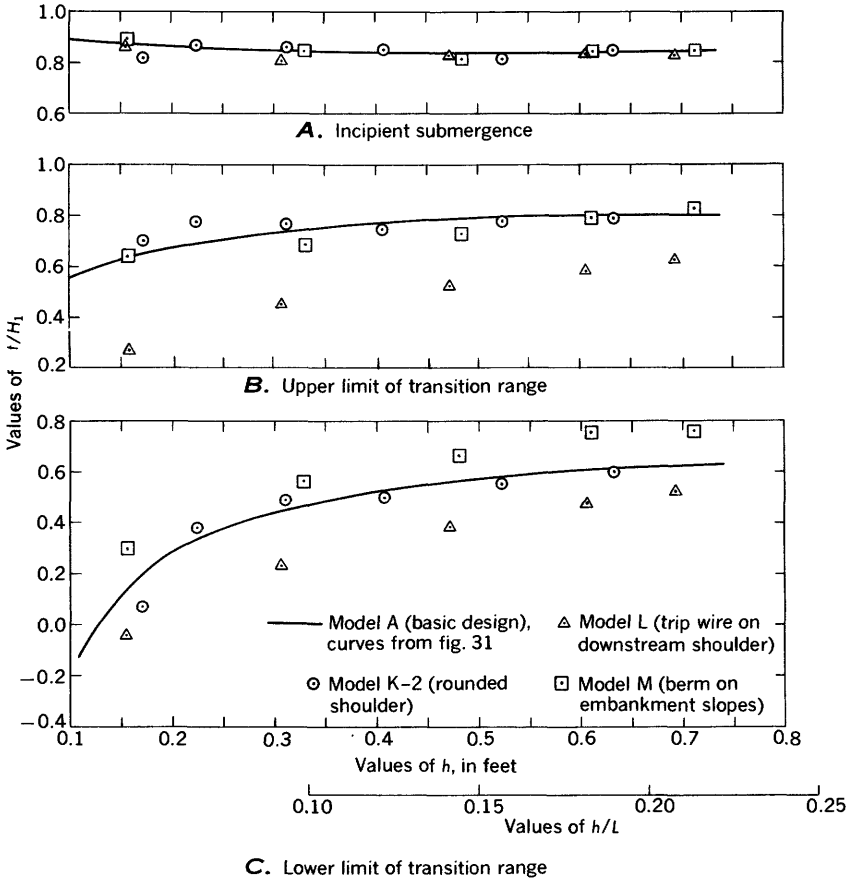

FIGURE 34.—Incipient submergence and free-flow transition range; influence of special design variations.

Figure 30, by comparison with figure 29, shows a slight advantage in using t/H_1 to describe the tailwater levels at which the upper and lower limits occur. In particular, the difference in tailwater levels which reflects the influence of P on the lower limit is smaller when t/H_1 is used. The data show no significant correlation with P for the upper limit.

Figure 31 shows the results of tests on three versions of the basic design. The curves obtained from the figure are shown for comparison on the subsequent figures in this series.

Figures 32 and 33 show the results of tests made with different values of S_p and S_s. In general, these data show good agreement with the curves obtained from model A. A minor correlation with S_p is not believed to be significant in view of the results shown on figure 34.

Figure 34 shows the results of tests made on the smooth-surfaced

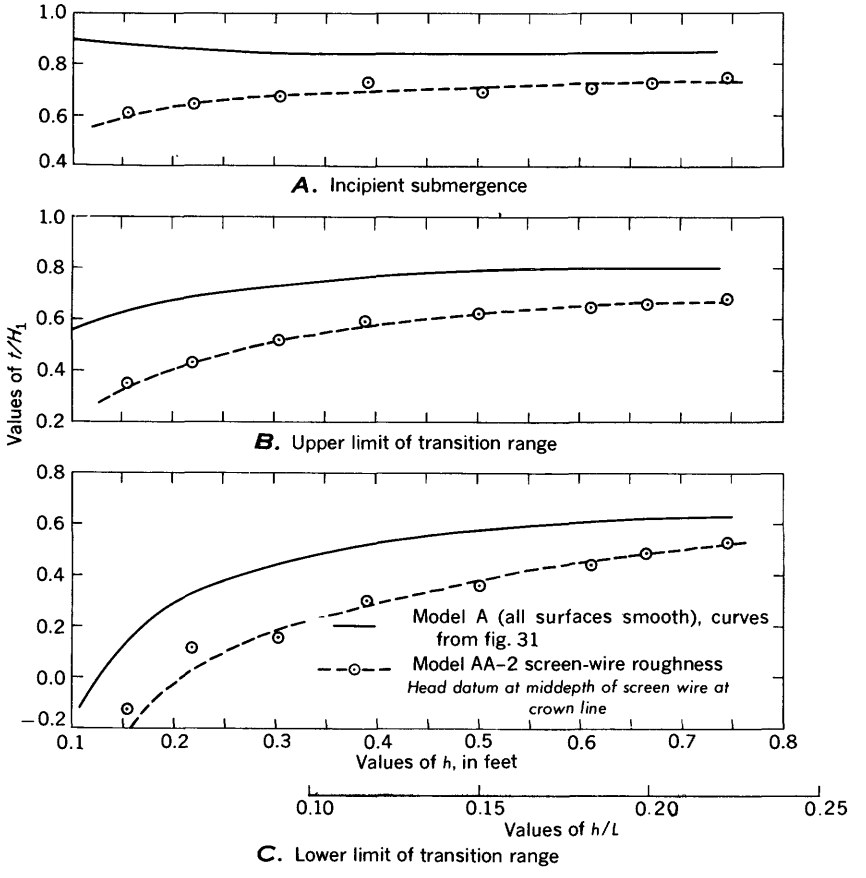

FIGURE 35.—Incipient submergence and free-flow transition range; influence of screen-wire roughness on all surfaces.

models with special design variations. One of these, model L, with a small tripwire located at the downstream edge of the downstream shoulder, was especially designed to demonstrate the sensitivity of the transition-range limits to obstructions on the downstream side of the embankment. From the results of the tests on model L it is obvious that the transition limits cannot be defined with certainty for many natural prototype conditions. This conclusion is substantiated by the results of tests on model M, the model with berms on the embankment slopes. As would be expected, however, tests on model K–2, with the rounded upstream shoulder, agree with the results of tests on the basic design.

Figures 35, 36, and 37 show the influence of roughness on the transition-range limits. The results are remarkably similar for the

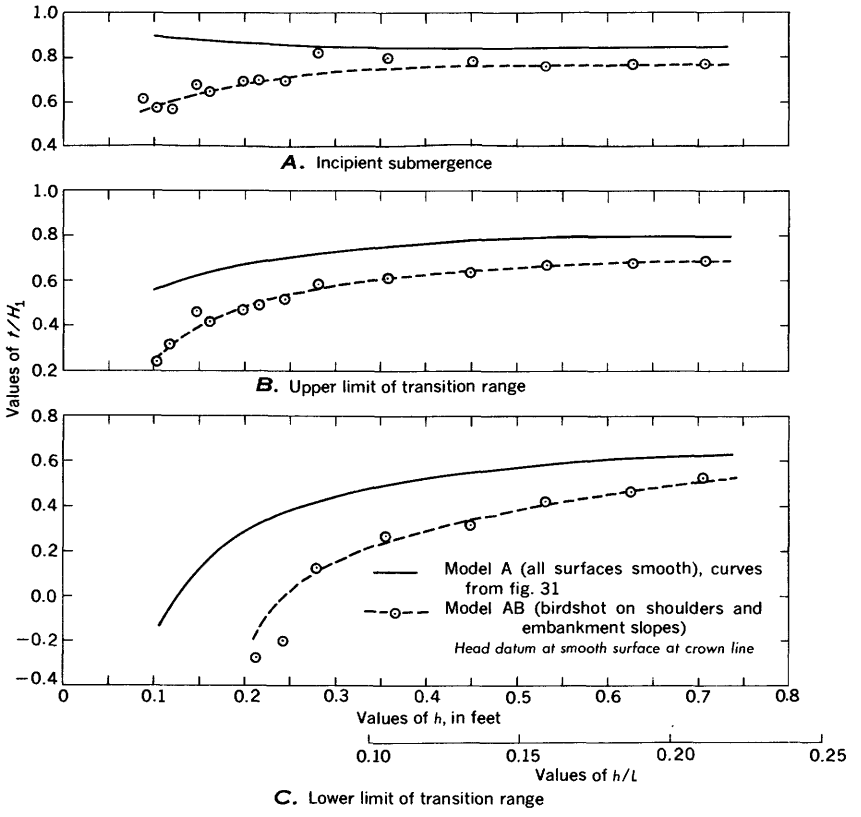

FIGURE 36.—Incipient submergence and free-flow transition range; influence of birdshot roughness on shoulder and embankment slopes.

three conditions of roughness represented by models AA–2, AB, and AC. In general, roughness tends to lower the tailwater levels for both the upper and lower limits. The curves are not well defined for small values of h because of the larger experimental errors which characterize this condition.

DEPTH AT CROWN LINE FOR FREE FLOW

Figures 38, 39, and 40 show the results of tests made to define the depth of flow at the crown line, y_o, in terms of the theoretical critical depth for uniform flow, y_c, where

$$y_c = \sqrt[3]{\frac{q^2}{g}}. \tag{25}$$

Values of y_o used for this purpose were obtained as the average of several point-gage measurements of depth at the crown line. Because

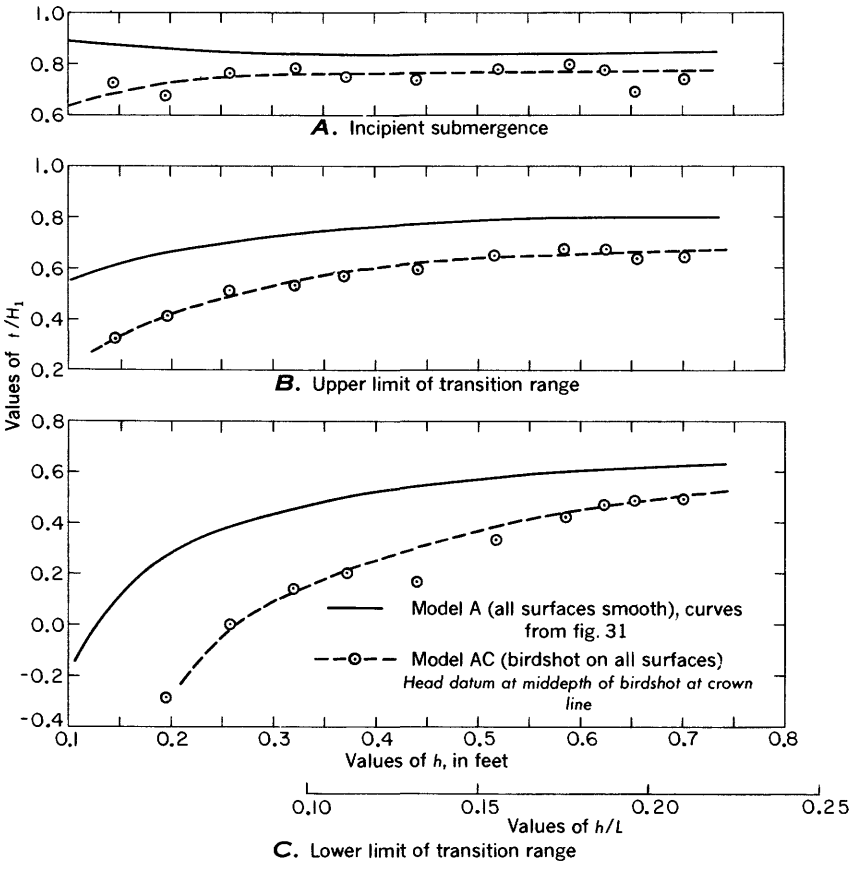

FIGURE 37.—Incipient submergence and free-flow transition range; influence of birdshot roughness on all surfaces.

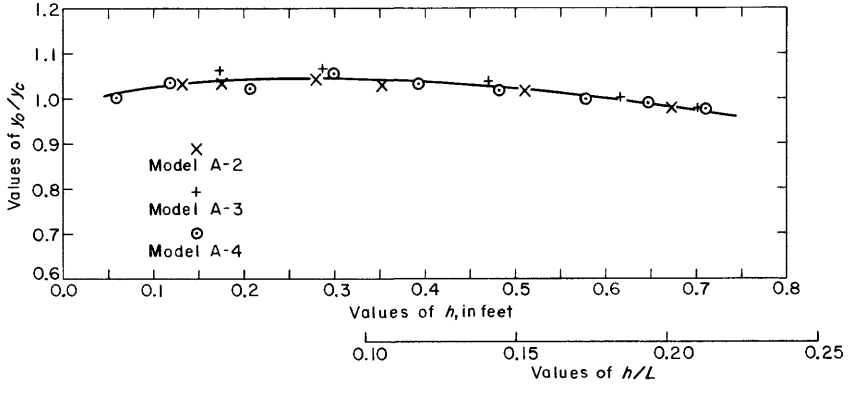

FIGURE 38.—Depth at crown line for free flow; basic design, model A.

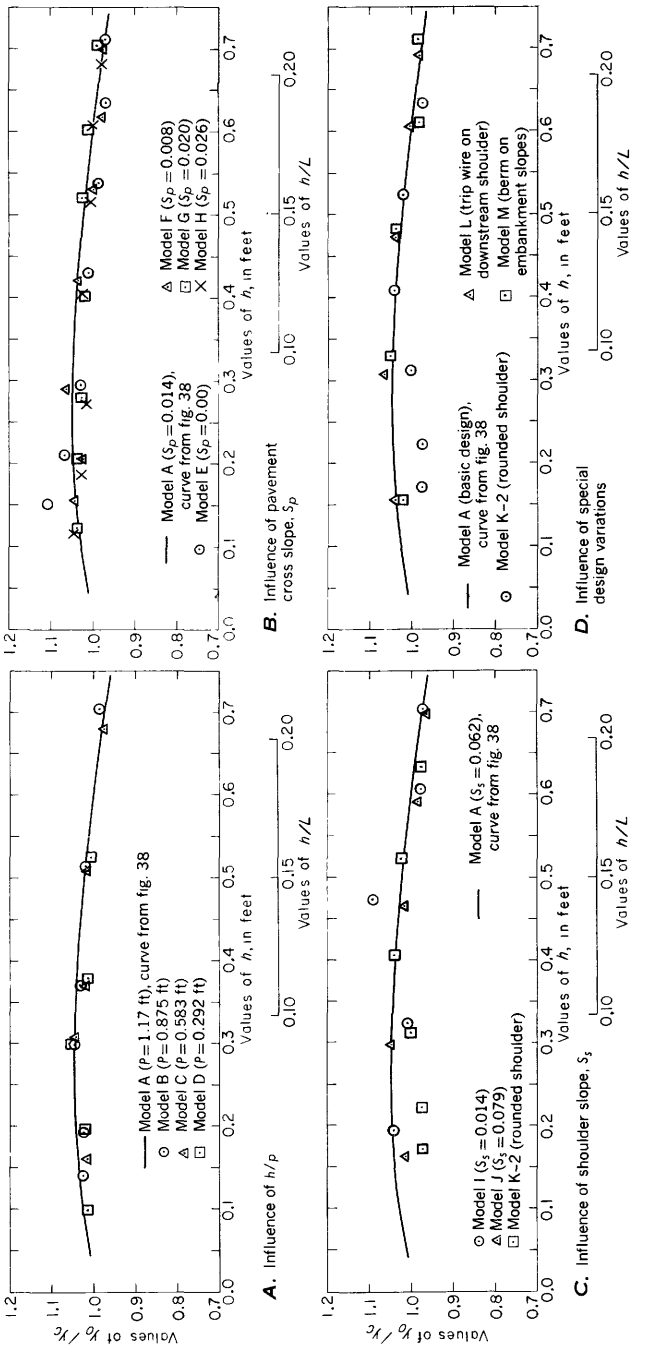

FIGURE 39.—Depth at crown line for free flow; smooth-surfaced models.

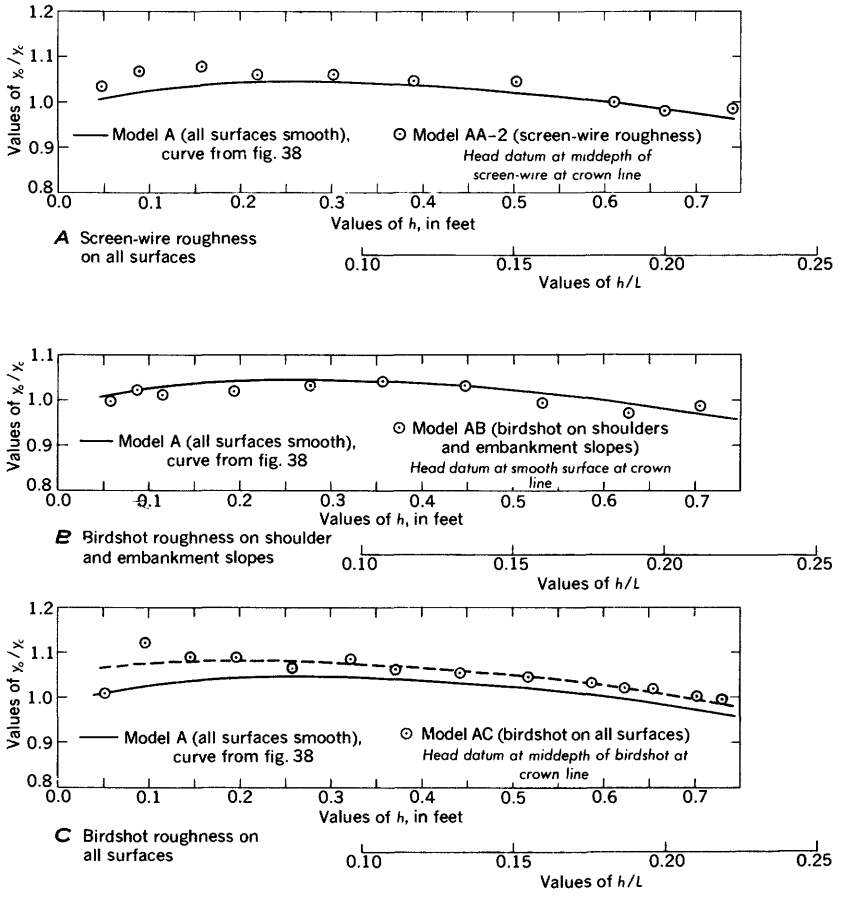

FIGURE 40.—Depth at crown line for free flow; rough-surfaced models.

the roadway level as well as the water-surface level changes rapidly in the vicinity of the crown line, the measurements are not expected to be extremely accurate. Nevertheless, the results shown on the figures are remarkably consistent.

Figure 38 shows the results of tests on the basic design, and the average curve obtained from that figure is shown on figures 39 and 40. The results of all tests on smooth-surfaced models agree well with the model A curve. The maximum deviation from the condition $y_o = y_c$ is about 5 percent. This is believed to be adequate confirmation of the assumption that critical-flow control occurs at the crown line.

Characteristics associated with roughness on the roadway are believed to be related to the thickness of the boundary layer. Thus, a small and not unexpected increase in y_o/y_c characterizes the results of tests on the rough-surfaced models, particularly model AC. Model

AB, with roughness confined to shoulders and embankment slopes, gave results which agree substantially with those obtained from the basic, smooth-surfaced model.

For all designs and flow conditions tested, the test results give reasonably good confirmation of the assumption that critical depth occurs at or very near the crown line.

SUMMARY AND EVALUATION

Tests on 17 different embankment designs indicate that the discharge characteristics are nearly independent of embankment shape. The designs tested were modifications of a basic design which is typical of two-lane paved highways. Two features, embankment slope and roadway width, were identical for all designs. On the basis of the test results, it is believed that embankment slope is insignificant except as it affects the roller on the downstream side. The roller can be expected to have a small influence on the tailwater levels corresponding to incipient submergence and the free-flow transition range. The width of the roadway is believed to be significant only to the extent that it, as well as the discharge and the surface roughness, governs the head loss and the thickness of the boundary layer at the control section. These are effects which will have to be correlated with boundary-layer studies and full-scale prototype tests.

Embankment height, pavement cross-slope, and shoulder slope are insignificant in relation to free-flow discharge characteristics because the embankment comprises a critical-flow control section. Thus, because critical depth occurs very nearly at the crown line for all flows and shapes tested (see figs. 38, 39, and 40), boundary conditions upstream from the crown line have no influence on the free-flow head-discharge relationship. Similarly, because the effect of downstream disturbances cannot be transmitted upstream, through the section of critical flow, boundary conditions downstream from the crown line have no influence on the free-flow coefficient.

Surface roughness has a small but systematic influence on the principal flow characteristics. The effects associated with roughness in the model are difficult to interpret in terms of natural prototype roughness. Nevertheless, the relative influence of a maximum range of prototype roughnesses is believed to be indicated by the results of the model tests. It is emphasized, furthermore, that the smooth-surfaced models are believed to be adequately representative of paved roadways in good condition.

Figure 41 shows a summary of the most important results of the tests made to determine the free-flow coefficient of discharge. A single curve represents all smooth-surfaced models (plus model AB, which was roughened with birdshot on the embankment slopes and shoul-

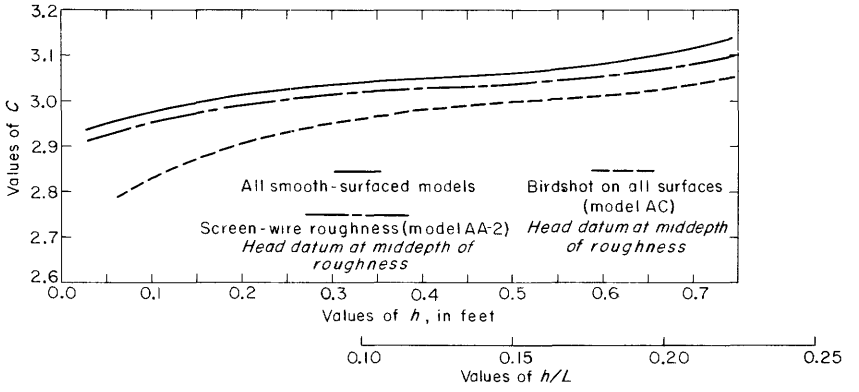

FIGURE 41.—Summary of the coefficient of discharge for free flow.

ders). Different curves show the results of tests on rough-surfaced models AA–2 and AC.

The overlapping abscissa scales shown on figure 41 are independently related to the flow pattern except in the middle range of values. In the lower range of values of h, boundary resistance dominates the flow pattern, and h/L is insignificant (except as L is involved in the loss of energy on the roadway). Conversely, in the upper range of values of h/L, boundary form and flow curvature dominate the flow pattern, and h is insignificant.

It is important to observe that the influence associated with small values of h is a "scale" effect; that is, it is related to the absolute value of h, whether it be a model or a prototype value. This does not imply that model and prototype coefficients will be identical for identical values of h, however, because the characteristics of the boundary layer at the control section are also related to the absolute value of L. Nevertheless, on the basis of the model tests, it is believed that effects associated with values of h less than 0.5 feet seldom would be significant in terms of the prototype. Furthermore, it is observed that the larger values of h/L shown in figure 41 are in excess of the values usually to be expected in the prototype.

Figure 42 shows a summary of the results of the tests made to determine the coefficient of discharge for submerged flow. It is noteworthy that the dependent variable on figure 39 is the simple coefficient of discharge (eq 9) and not, as usual, the ratio of the submerged-flow coefficient to a corresponding free-flow coefficient. This procedure is justified on the basis of the observation that the submerged-flow characteristics are independently related to the parameters which govern free flow. It is also noteworthy that the abscissa scale in figure 42 is the ratio of the downstream (tailwater) piezometric head to the upstream (headwater) total-energy head. This

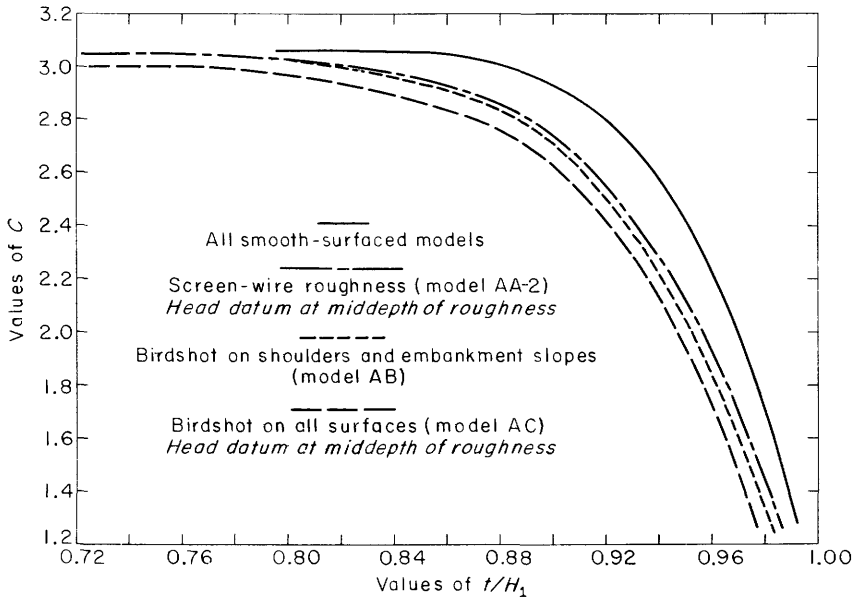

FIGURE 42.—Summary of the coefficient of discharge for submerged flow.

ratio, unlike the commonly used ratio of piezometric heads, results in a relationship with C_{subm} which is virtually free of correlation with embankment height.

A single curve on figure 42 represents the submerged-flow characteristics of all the smooth-surfaced designs. Whereas the results of some of the tests deviated considerably from this smooth curve, the results of other tests showed conclusively that the relationship is extremely sensitive to roughness, irregularities, or obstructions on the downstream side of the embankment. Thus, in view of many uncertainties regarding the occurrence and effect of natural prototype features such as guardrails, windrowed gravel, and vegetation, it is believed to be impractical to seek a very accurate, general solution for submerged flow.

The influence of roughness on C_{subm} is shown by the three dashed curves on figure 42. These curves are believed to indicate the maximum range of the influence of roughness, although it is difficult to relate the model-test results to natural prototype conditions.

Figure 43 shows a summary of the results of tests made to determine the tailwater levels corresponding to incipient submergence and the free-flow transition range. The dependent variable in figure 43, t/H_1, is the same as the independent variable used in figure 42. The overlapping abscissa scales are the same as the corresponding scales in figure 41.

Figure 43 indicates that one curve can be used with sufficient accuracy to describe the incipient-submergence and upper-limit tailwater ratios for all smooth-surfaced designs. A correlation with P shown for the lower-limit tailwater ratio is indicated on figure 43*C*

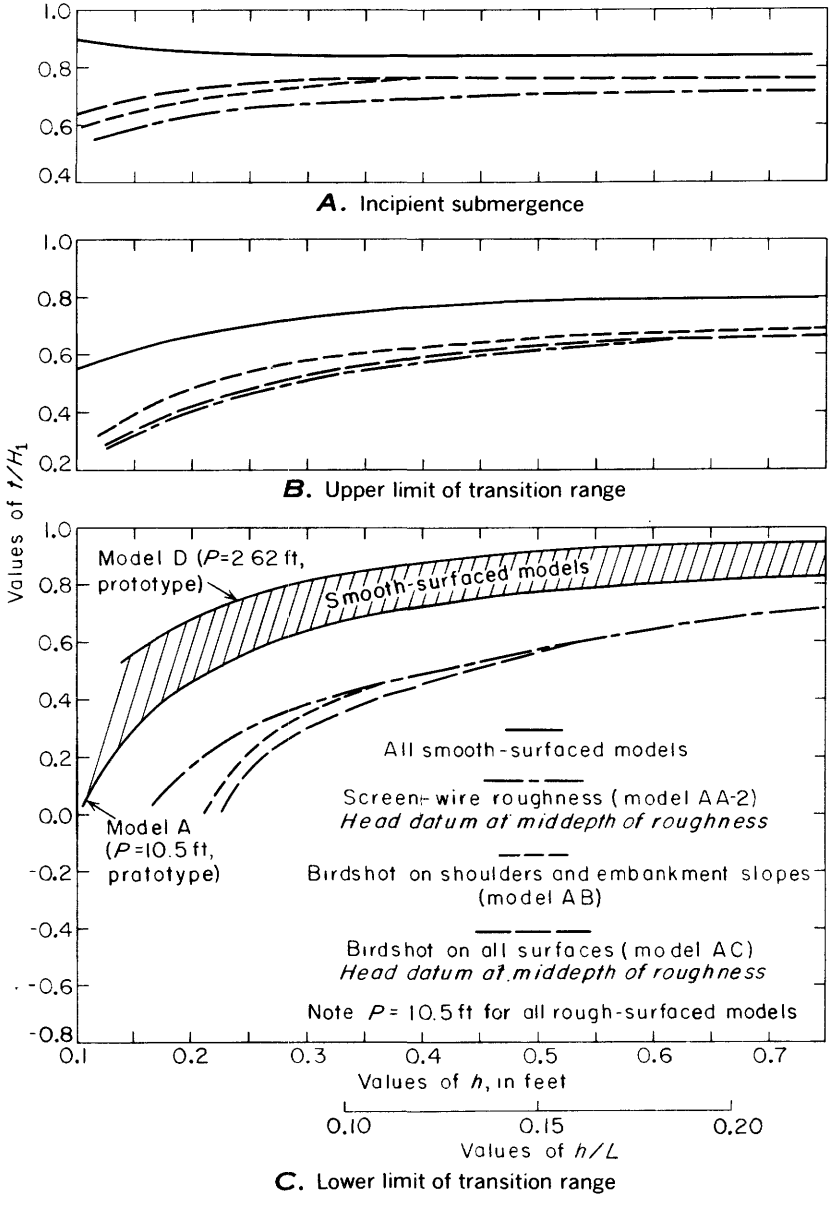

FIGURE 43.—Summary of incipient submergence and free-flow transition range.

by limiting curves for the values of P tested. It is observed that the influence of P was not investigated separately for the rough-surfaced designs. Curves showing the results of tests on the rough-surfaced models are shown on the figure.

It should be emphasized tha the total-energy head, H_1, is involved in the basic discharge equation (eq 8) as well as the tailwater ratio, t/H_1. Also, whereas the solution for discharge requires a trial solution for H_1, the use of h instead of H_1 will ordinarily result in a very small error in the first-trial solution.

It is pertinent in this summary and evaluation of the model test results to observe that, under certain circumstances, the coefficients and ratios used to describe the results are critically influenced by the location of the headwater- and tailwater-level measuring sections. In particular, for high values of h/P, the piezometric level used to determine h is influenced by head losses in the approach channel and flow curvature in the vicinity of the embankment. Thus, in order for the results to be applied accurately to similar model or prototype embankments, the measuring sections should correspond in location to the gage positions shown on figure 7.

INFLUENCE OF THE BOUNDARY LAYER ON FREE-FLOW CHARACTERISTICS

OBJECTIVE

In the preceding pages, dimensional reasoning and a simple discharge equation were used in an empirical analysis of laboratory tests of embankment models. The results provide a practical solution for the discharge characteristics of a variety of embankment forms and surface roughnesses. Like all empirical solutions, this solution is limited in usefulness by the scope of the tests on which it is based.

The second major objective of the investigation was the theoretical and experimental definition of the relationship between free-flow discharge and the boundary layer on the roadway. Here attention is restricted to free flow because the boundary layer is significant in relation to discharge control only when critical flow occurs on the roadway. The results of the studies made to accomplish the second objective are described in the following pages.

The ultimate goal of this part of the investigation could be described as the development of a general, analytical equation of discharge for free flow. More realistically, however, it is to test the validity of the approximate discharge equation (eq 19) in which δ_q and λ are measures of the influence of boundary resistance. The minimum goal is a better understanding of some of the factors which govern the flow pattern. An incidental benefit is a considerable amount of data on boundary layers in accelerated, free-surface flows.

DEFINITION OF δ_q AND λ

The two quantities which represent the influence of boundary resistance in equation 19 are δ_q and λ. The displacement thickness, δ_q, is a measure of the influence of the boundary layer of the continuity equation. From equation 11 (p. 17), for a boundary-layer flow such as that illustrated in figure 6,

$$q=\int_0^y u\,dz=(y-\delta_q)U, \tag{26}$$

from which,

$$\delta_q=\frac{1}{U}\int_0^y (U-u)\,dz=\int_0^y \left(1-\frac{u}{U}\right)dz, \tag{27}$$

or, because $u=U$ when z exceeds the nominal boundary-layer thickness (δ),

$$\delta_q=\int_0^\delta \left(1-\frac{u}{U}\right)dz. \tag{28}$$

From equation 28 it is apparent that δ_q depends on the velocity distribution in the boundary layer.

For intermediate values of the Reynolds number, others (Bauer, 1954; Halbronn, 1954; Delleur, 1957) have concluded that the velocity distribution in partially developed boundary-layer flows in open channels can be described by an equation of the power form,

$$\frac{u}{U}=\left(\frac{z}{\delta}\right)^n, \tag{29}$$

in which n is an exponent which must be evaluated by experiment. If equation 29 is substituted in equation 28, integration yields a simple equation for δ_q,

$$\delta_q=\left(\frac{n}{n+1}\right)\delta, \tag{30}$$

which, of course, is applicable only when the velocity distribution can be described with an equation of the power form.

The velocity-head factor, λ, is a measure of the influence of boundary resistance on the one-dimensional energy equation. It is defined by the relation.

$$\lambda=\frac{U^2}{2g}-\alpha\frac{V^2}{2g}, \tag{31}$$

which is illustrated in figure 6. In this equation $\alpha V^2/(2g)$ is the true average-velocity head, which is given by the equation

$$\alpha\frac{V^2}{2g}=\frac{1}{2gq}\int_0^y u^3\,dz. \tag{32}$$

From equations 31 and 32 and the continuity relationship (eq 26),

$$\lambda=\frac{1}{2gq}\int_0^y (U^2-u^2)\,u\,dz, \tag{33}$$

or, from equations 26 and 33,

$$\lambda=\left(\frac{\frac{U^2}{2g}}{y-\delta_q}\right)\int_0^y \frac{u}{U}\left[1-\left(\frac{u}{U}\right)^2\right]dz. \tag{34}$$

(It is of incidental interest that the integral in equation 34 is equivalent to δ_e, the "energy thickness" of the boundary layer. Thus,

$$\lambda=[(U^2/2g)/(y-\delta_q]\delta_e.)$$

It is now apparent that λ, unlike δ_q depends on q and y as well as the velocity distribution.

In equation 34, the ratio which precedes the integral is proportional to a Froude number. When the flow is critical, the value of the ratio is approximately 1/2. Therefore, at the crown line, where the flow is very nearly critical for all conditions tested (see figures 38, 39, and 40), an adequate approximation is

$$\lambda=\frac{1}{2}\int_0^{y_o} \frac{u}{U}\left[1-\left(\frac{u}{U}\right)^2\right]dz, \tag{35}$$

or, because $u=U$ when z is greater than δ,

$$\lambda=\frac{1}{2}\int_0^{\delta} \frac{u}{U}\left[1-\left(\frac{u}{U}\right)^2\right]dz. \tag{36}$$

It is emphasized that the coefficient 1/2 in equations 35 and 36 restricts their use to the critical-flow section.

For the conditions which warrant the assumption of an n-power velocity distribution (eq 29), equation 36 gives

$$\lambda=\left[\frac{n}{(3n+1)(n+1)}\right]\delta, \tag{37}$$

or, from equation 30,

$$\lambda=\left(\frac{1}{3n+1}\right)\delta_q. \tag{38}$$

BOUNDARY LAYERS IN ACCELERATED MOTION

The most promising solution for the growth of the boundary layer on the roadway is based on von Kármán's semi-analytical equation for boundary layers in accelerated motion (Schlicting, 1955). The equa-

tion is derived from an application of the momentum principle. It presumes a hydrostatic normal-pressure distribution, and it ignores the momentum of the turbulence. It has been substantiated reasonably well for flat plates and circular pipes.

The von Kármán equation can be written in the form

$$\frac{\tau_0}{\rho U^2}=\frac{d\delta_m}{ds}+\left(2+\frac{\delta_q}{\delta_m}\right)\left(\frac{\delta_m}{2U^2}\right)\frac{dU^2}{ds}, \tag{39}$$

in which, in addition to the symbols previously defined, τ_0 is the shear stress at the boundary, s is distance along the boundary in the direction of mean motion, and δ_m is the "momentum thickness" of the boundary layer. Defined by the deficiency of momentum flux which results from the formation of the boundary layer, δ_m is

$$\delta_m=\int_0^{\delta}\frac{u}{U}\left(1-\frac{u}{U}\right)dz. \tag{40}$$

For an n-power velocity distribution (eq 29), equation 40 gives

$$\delta_m=\left[\frac{n}{(2n+1)(n+1)}\right]\delta, \tag{41}$$

which, with equation 30, gives

$$\delta_m=\left(\frac{1}{2n+1}\right)\delta_q. \tag{42}$$

From equation 42 it is apparent that δ_m as well as λ (eq 38) can be defined in terms of δ_q. For convenience, therefore, the von Kármán equation can be converted to the form

$$\frac{\tau_0}{\rho U^2}=\left(\frac{1}{2n+1}\right)\frac{d\delta_q}{ds}+\left(\frac{2n+3}{2n+1}\right)\left(\frac{\delta_q}{2U^2}\right)\frac{dU^2}{ds}, \tag{43}$$

which, of course, is limited by the assumption that the velocity can be described with an equation of the power form.

The left-hand member of equations 39 and 43 is a nondimensional shear coefficient, c_f. In general, c_f is a function of the boundary-layer Reynolds number and the relative roughness,

$$\frac{\tau_0}{\rho U^2}=c_f=f\left(\frac{U\delta}{\nu},\frac{k}{h}\right), \tag{44}$$

in which $\nu=\mu/\rho$ is the kinematic viscosity of the fluid. Approximations for c_f have been derived from analogies with uniform flow in

pipes. One such approximation, for smooth boundaries only, is the equation identified with Blasius,

$$c_f = 0.0225 \left(\frac{U\delta}{\nu}\right)^{-0.25}, \tag{45}$$

which is based on the assumption of a 1/7-power velocity distribution. Equation 45 has been substantiated in application to smooth, flat plates and an intermediate range of Reynolds numbers. Corresponding equations for rough boundaries have been based on the von Kármán logarithmic velocity-distribution equation.

As an implicit equation for the displacement-thickness gradient ($d\delta_q/ds$), equation 43 is limited mainly by the assumption of an n-power velocity distribution. However, its integration, to get δ_q as a function of s, depends on experimental evaluation of n, U, and dU/ds, as well as τ_0. Thus, the most promising means of obtaining a general solution for δ_q is fraught with potential obstacles. The information needed to appraise these obstacles must be obtained from measurements of boundary-layer characteristics under a wide variety of boundary and flow conditions.

BOUNDARY-LAYER MEASUREMENTS

PURPOSE AND SCOPE

The primary purpose of the boundary-layer measurements made as a part of this investigation was to test the validity of the discharge equation (eq 19) which contains δ_q and λ. A simple vertification of equation 19 could have been accomplished with measurements of the velocity distribution at the crown line only. Aside from substantiating certain assumptions regarding the influence of boundary resistance, however, verification by direct determination of the crown-line values of δ_q and λ would lead to nothing more than an empirical solution for q. This solution, like simpler ones involving only the coefficient of discharge (eq 7 or 8), would be limited in usefulness by the range of conditions actually reproduced in the laboratory. On the other hand, if equation 19 is valid, the ideal solution for q would involve the computation of δ_q and λ from a general equation which describes the growth of the boundary layer on the roadway. The ideal solution would be applicable to roadways of all widths, embankments of all shapes within reason, and a full, practical range of discharges. With this ideal as a possible result, the experiments included sufficient vertical velocity traverses and piezometric profile measurements to define the boundary layer between the upstream edge of the upstream shoulder and a point downstream from the control section near the crown line.

Tests were made on four different models, A–1, K–1, AA–1 and KA. The scope of the tests is shown in table 2, and a summary of the velocity measurements is shown in table 4 in the section "Experimental Data." Data used in this part of the report were obtained from tests made by Davidian. To a large extent, the tests duplicate and confirm the results of tests made earlier by Sigurdsson.

TABLE 2.—*Scope of boundary-layer tests made by Davidian*[1]

Model design	Test No.	Head, h, in model (ft)	Discharge, q, in model (cfs per ft)	Number of velocity traverses	Remarks
A–1	1	0.084	0.071	8	Basis design[2], smooth surface.
	2	.183	.234	8	Basic design, smooth surface.
	3	.301	.503	10	Do.
	4	.475	1.01	10	Do.
	5	.632	1.58	10	Do.
K–1	1	.083	.070	5	Rounded shoulder[3], smooth surface.
	2	.183	.238	6	Rounded shoulder, smooth surface.
	3	.301	.511	5	Do.
	4	.475	1.02	6	Do.
	5	.632	1.59	6	Do.
AA–1	1	.183	.225	10	Basic design, screen roughness.
	2	.476	.991	10	Do.
KA	1	.183	.226	6	Rounded shoulder, screen roughness.
	2	.475	.991	6	Do.

[1] Davidian, Jacob, 1959, Influence of the boundary layer on embankment-shaped weirs: Georgia Inst. Technology, Master's degree thesis, 97 p., 38 figs.
[2] See fig. 9 for details of basic design.
[3] Rounded transition between upstream embankment and shoulder surfaces, as shown in fig. 10A. All other shape details as in fig. 9.

Design details of the models are given in table 1 and figures 9 and 10. Model A–1 is the basic design. Model AA–1 is the same embankment section, but with screen roughness added. Details regarding the screen and the method of use are given on page 21. Model K is a design especially created for the boundary-layer tests. As shown in figure 10*A*, it involved a rounded transition between the upstream embankment and shoulder surfaces. The purpose of the rounding was to prevent flow separation at the upstream edge of the shoulder. Tests were also made on this embankment design with screen roughness added (model KA).

SUMMARY OF RESULTS

The basic data for this part of the report are the results of the velocity measurements which are summarized in table 4. Typical data illustrating the growth of the boundary layer on the upstream side of the roadway are shown in figures 44 and 45. Figure 44 shows the results of tests on models A–1 and AA–1, each with a discharge

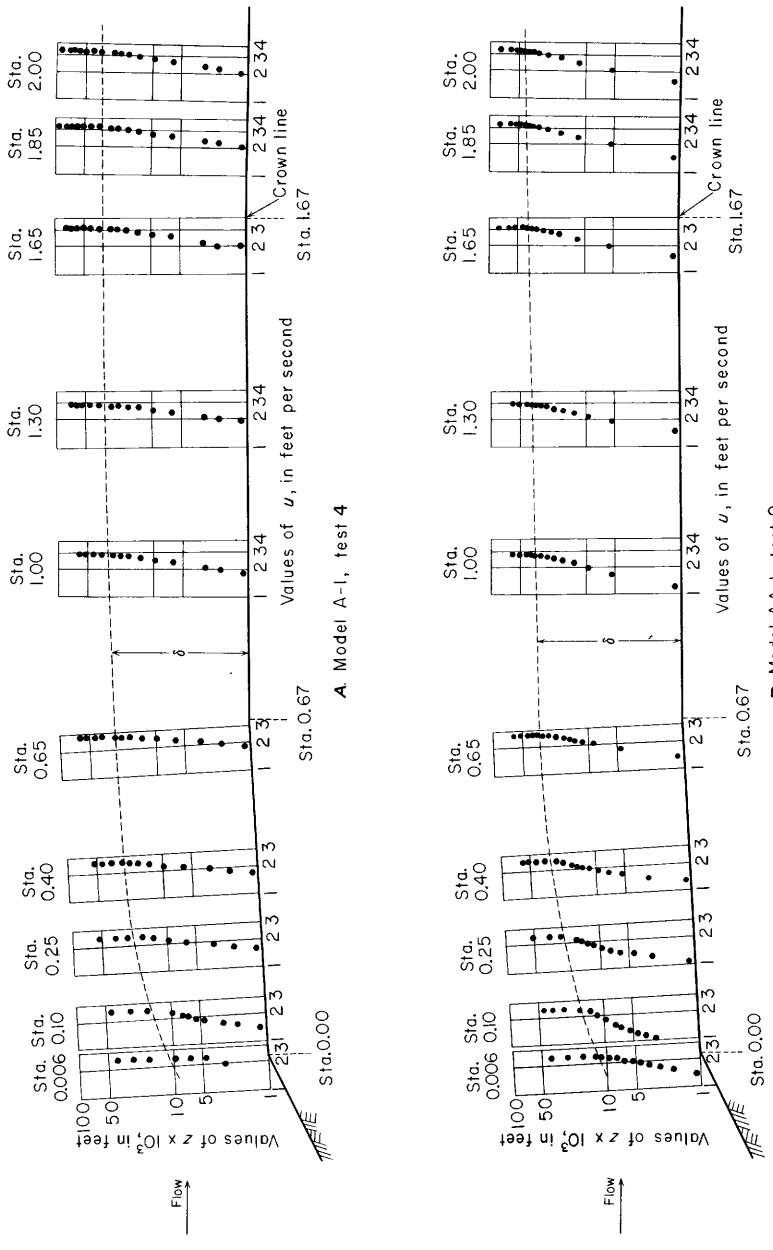

FIGURE 44.—Velocity distribution in boundary layer on upstream side of roadway; basic design, typical discharge.

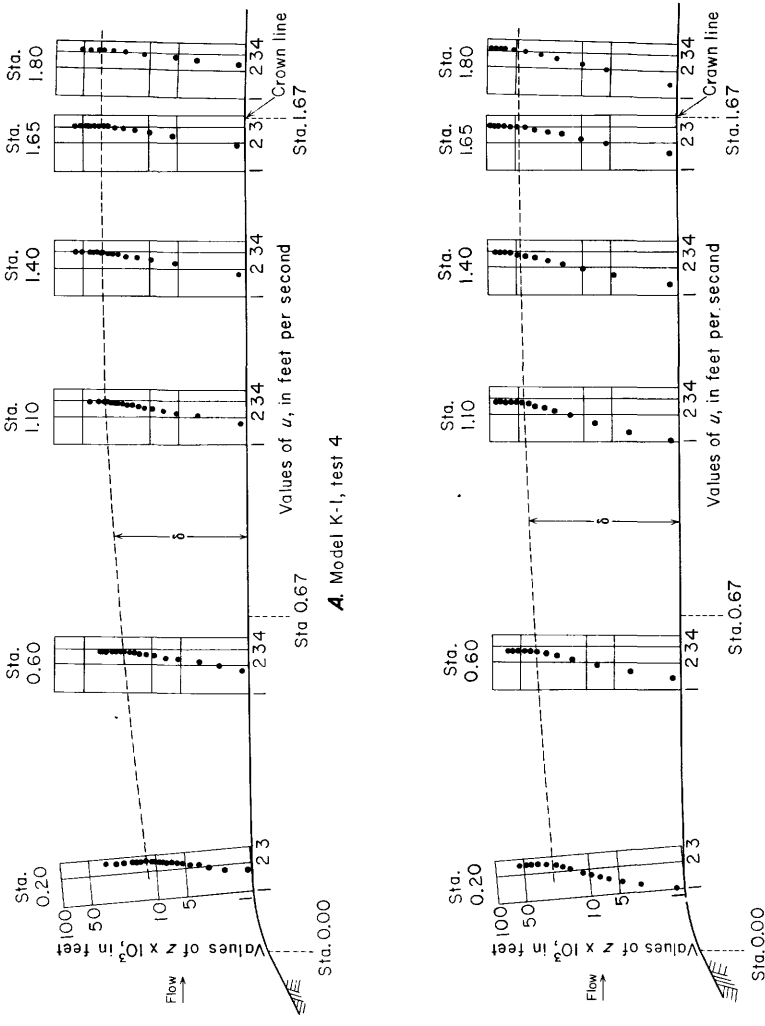

FIGURE 45.—Velocity distribution in boundary layer on upstream side of roadway; rounded shoulder, typical discharge.

(q) of approximately 1 cubic foot per second per foot. Figure 45 shows the results of similar tests on models K–1 and KA.

The boundary layer is indicated in figures 44 and 45 by velocity profiles which are superposed on a silhouette of the embankment cross section. The location of the traverse section for each velocity profile is designated by a station number which is a measure of its distance from the nominal intersection of the upstream embankment slope and shoulder surface. The crown line for all models is at station 1.67. Thus, station 0 for the models with rounded shoulders (models K–1

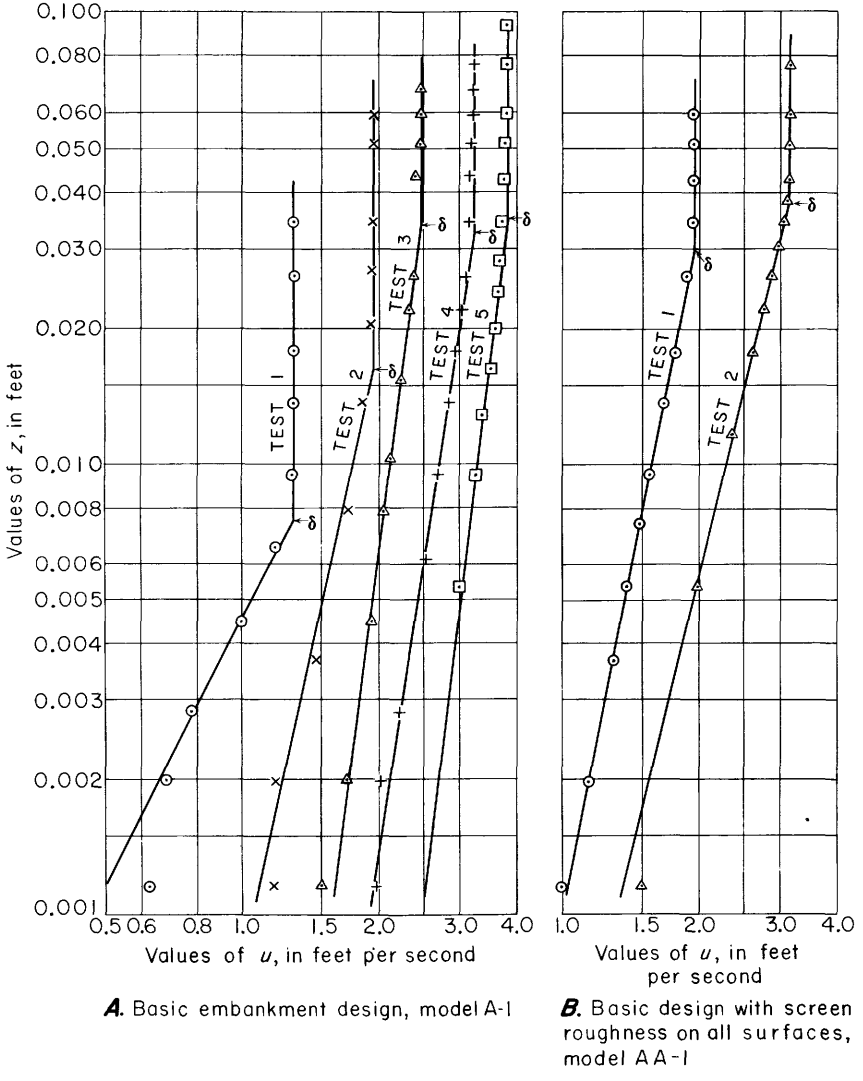

FIGURE 46.—Boundary-layer velocity distribution near crown line (station 1.65), models A–1 and AA–1.

and KA) is on the roundings, at a distance 1.67 feet upstream from the crown line. Measurements were made at station 1.65 instead of station 1.67 in order to avoid the influence of the separation zone which occurs on the downstream side of the crown line.

Figures 46 and 47 show velocity profiles at station 1.65 for all the tests made on models A–1, AA–1, K–1, and KA. The profiles, like those in figures 44 and 45, are plotted on logarithmic coordinates.

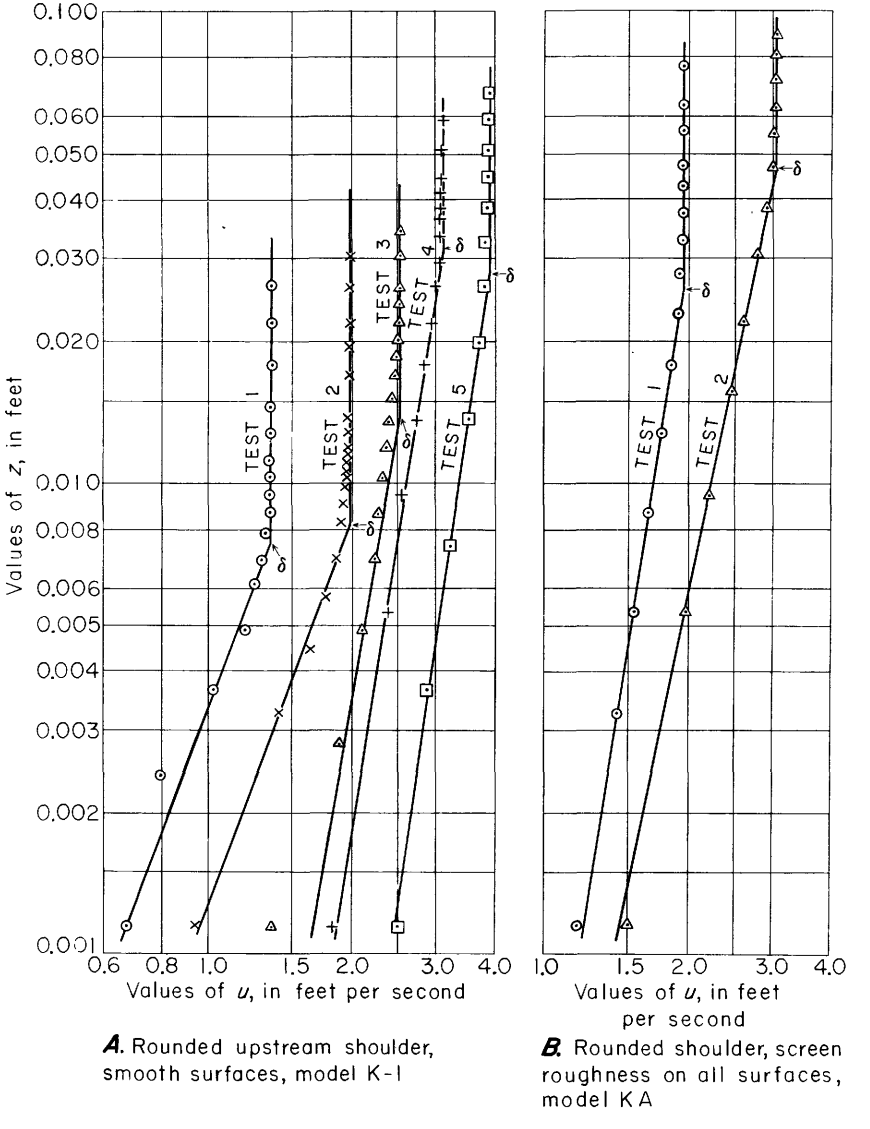

FIGURE 47.—Boundary-layer velocity distribution near crown line (station 1.65), models K–1 and KA.

Straight lines are fitted to the measurements in the boundary layer, and the intersections of the straight lines with the vertical lines signifying the magnitude of U are marked as the outer limit of the nominal boundary layer. The fit of the straight lines with the points in the boundary layer is an indication of the validity of the assumption that the velocity distribution can be described with an equation of the power form, as in equation 29,

$$\frac{u}{U}=\left(\frac{z}{\delta}\right)^n, \tag{29}$$

and the slope of the straight line is a measure of n in that equation.

Values of δ and $1/n$ obtained from figures 46 and 47 are shown plotted as a function of h in figure 48. (Here $1/n$ is used to avoid fractions.)

Values of δ and $1/n$ obtained from figures 44 and 45 by the same procedure are shown plotted in figure 49 as a function of s.

With some exceptions, notably at stations near the upstream edge of the shoulder, the velocity distribution in the boundary layer appears to be reasonably approximated by an equation of the power

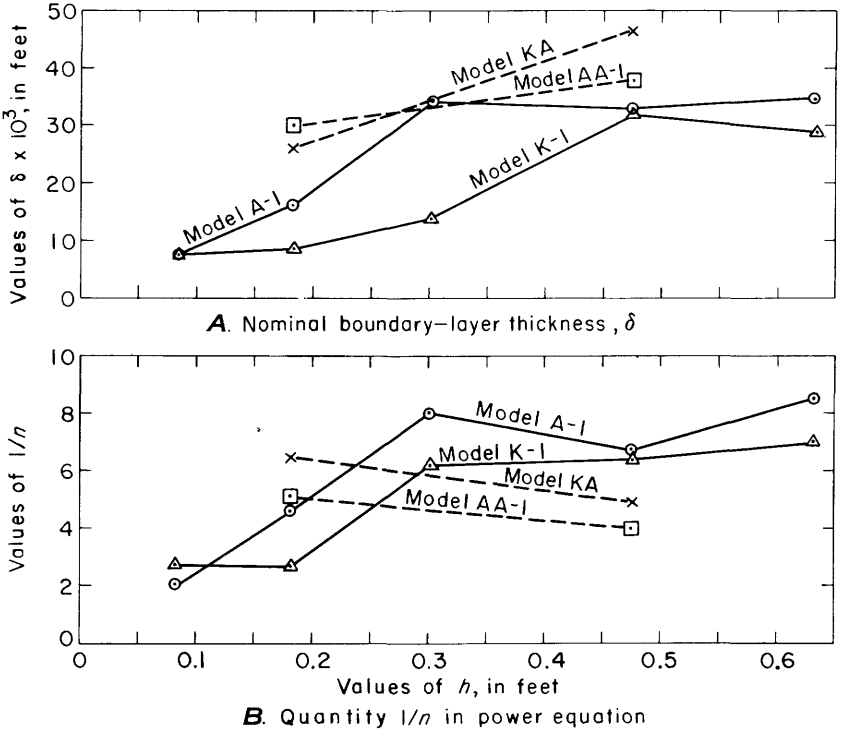

FIGURE 48.—Boundary layer near crown line (station 1.65).

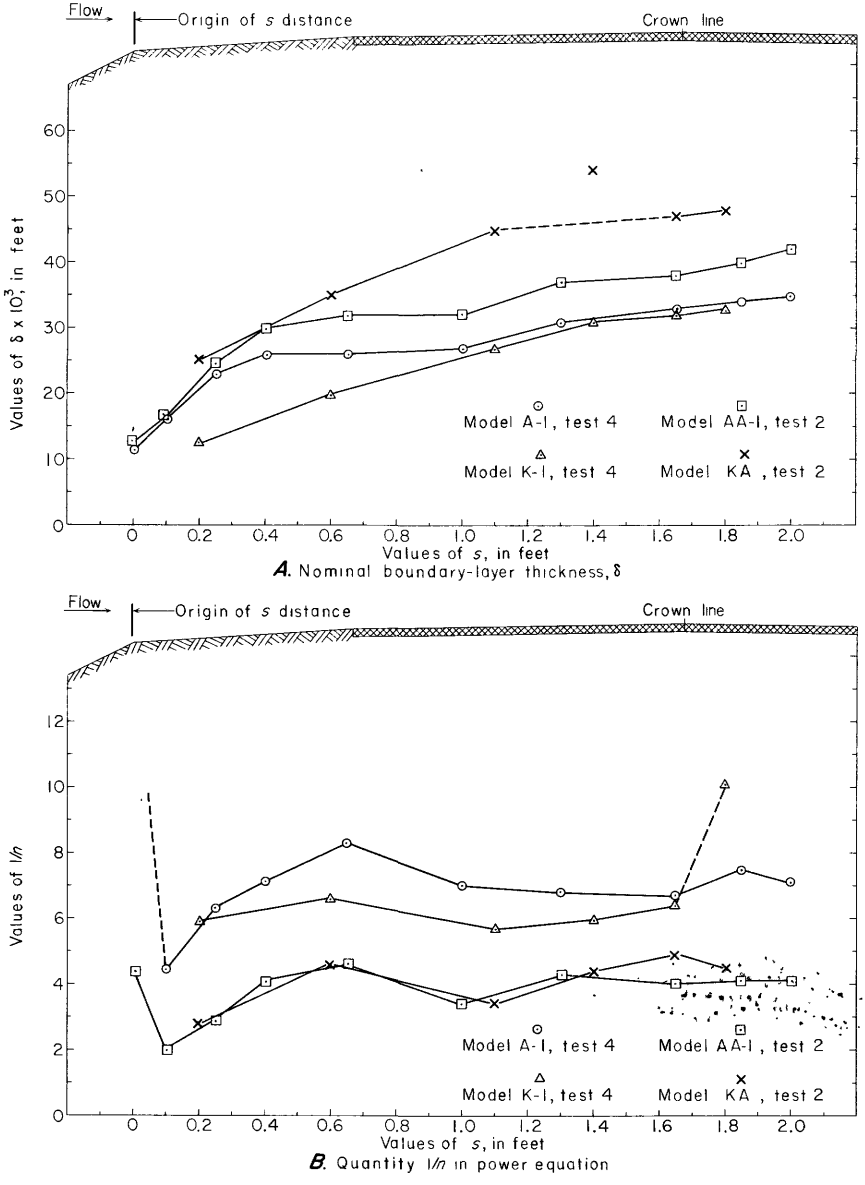

FIGURE 49.—Boundary layer on upstream side of roadway for a typical discharge.

form. However, as shown in figures 48 and 49, δ and $1/n$ are not clearly defined as functions of s and h (or q).

For moderately large discharges, the boundary-layer thickness grows most rapidly in the vicinity of the shoulder. The rate of growth near the crown line is very small. Values $1/n$ are smaller for the rough-surfaced models (AA–1 and KA) than for the smooth-surfaced models (A–1 and K–1), except at small values of h (fig.

48*B*). For larger values of h, the smooth-surfaced models show values of $1/n$ approaching the value 7, which is commonly used for smooth pipes and flat plates.

Values of δ for the smooth-surfaced models indicate an expected decrease in boundary-layer thickness with rounding of the upstream shoulder. This result is attributed to the elimination of the separation zone and the consequent displacement of the boundary layer at the upstream edge of the shoulder. However, the largest values of δ shown on figure 49*A* are those which were measured on the round-shouldered model when it was covered with screen-wire roughness. In general, of course, the effect of roughness is to increase the thickness of the boundary layer. It is suggested that the contradiction which is related to the combined influence of rounding the roughness might be the result of a difference in tautness of the screen wire used on models AA–1 and KA.

In view of the inconsistencies in the data shown in figures 48 and 49, no attempt has been made to draw smooth curves through the plotted points.

COMPUTATION OF *C* BASED ON BOUNDARY-LAYER MEASUREMENTS

Verification of the analysis which led to equation 19 requires that values of δ_q and λ at the crown line be determined from the boundary-layer velocity measurements. Two methods of evaluating δ_q and λ were used. One method, which was evolved from the assumption of an n-power velocity distribution, is suggested by equations 30 and 38, which require prior evaluation of n from the velocity profiles shown in figures 46 and 47. The results based on this method of computation are shown by the solid symbols in figure 50. Here the quantity $(\delta_q-\lambda)$, which appears in equation 19, is plotted as a function of h.

The second and most accurate method of evaluating δ_q and λ requires integration of equations 28 and 36. This was accomplished as a numeral approximation. Values of u/U were plotted on rectilinear graph paper, smooth curves were drawn through the points, mean values of u/U were read from the smooth curves, and the integrals represented by equations 28 and 36 were evaluated as the summation of finite increments. Values of $(\delta_q-\lambda)$ computed by this method are shown in figure 50 with open symbols.

Values of $(\delta_q-\lambda)$ computed by the two different methods agree reasonably well. The paucity of data did not permit accurate definition of the relation between $(\delta_q-\lambda)$ and h for the rough-surfaced models, but a constant value of $(\delta_q-\lambda)=0.001+$ foot was quite well defined for the two smooth-surfaced models. For the purpose of testing the validity of equation 19, a straight-line relationship between h and $(\delta_q-\lambda)$ was assumed for the rough-surfaced models. The

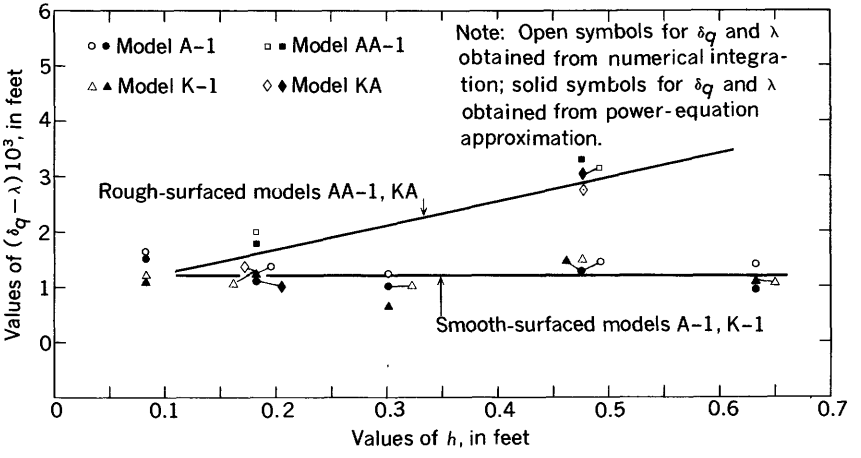

FIGURE 50.—Values of $(\delta_q-\lambda)$ from boundary-layer velocity measurements.

straight line is shown in figure 50. It is observed that the unit divisions on the $(\delta_q-\lambda)$ scale in figure 50 represent differences of only 0.001 foot, and that the approximation represented by the straight line is not critical in determining the validity of equation 19.

Figure 51 shows a comparison of experimentally determined and computed values of the coefficient of discharge for the smooth- and rough-surfaced models. The experimentally determined values were obtained from the summary curves in figure 41. The computed values were determined from equation 20,

$$C=3.09\left[1-\frac{3}{2}\left(\frac{\delta_q-\lambda}{H_1}\right)\right], \tag{20}$$

in which C is the coefficient of discharge defined by equation 19. Values of $(\delta_q-\lambda)$ were determined from figure 50.

The magnitude of the discrepancies between the experimental and computed curves in figure 51 is a measure of the validity of equation 20. The disparity of values of C is reasonably small in the middle range of values of h. For smaller values of h, computed values of C are larger than experimental values. For the largest values of h, computed values of C are smaller. The difference in C values at small values of h can be attributed, perhaps, to a fault in the analytical treatment of boundary resistance. The difference at larger values of h is believed to be associated with boundary-form effects or, specifically, flow curvature at the control section. Thus, this difference is believed to be related to the magnitude of h/L rather than the magnitude of h. The analysis which led to equations 19 and 20 did not involve the

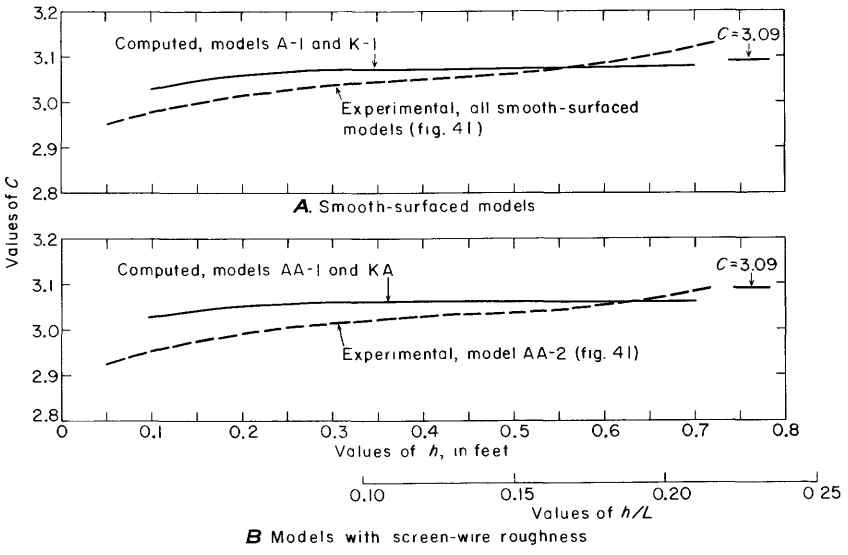

FIGURE 51.—Values of C computed from equation 20 and figure 50.

influence of flow curvature. Consequently, it is not surprising that discrepancies due to this influence are indicated by the comparison shown in figure 51.

The discrepancies between experimental and computed values of C, especially at small values of h, were somewhat greater than was expected. Therefore, a review of the analysis is pertinent.

MODIFIED DISCHARGE EQUATION

In the process of evolving equations 19 and 20 from the one-dimensional energy equation (p. 17), the term H_L, which represents the loss in head between the headwater measuring section and the crown line, was assumed to be negligible. It was particularly convenient to neglect H_L because it is not independently related to the discharge characteristics of the embankment. Furthermore, it is difficult to evaluate, because it depends on the location of the measuring section and the resistance characteristics of the upstream channel.

For the model tests reported herein the headwater was measured at a section which was relatively close to the embankment. Thus, H_L was very small. Nevertheless, it is recognized that neglecting H_L has the effect of making values of C computed from equation 20 larger than they would be if H_L were considered. Moreover, the relative effect of neglecting H_L increases as h decreases. These observations suggest that neglecting H_L is a possible cause of the disparity of computed and experimental values of C at lower values of h in figure 51.

Not only is H_L difficult to compute, but it is also difficult to measure accurately in the laboratory. From the magnitude of the discrepancies shown in figure 51 it is apparent that the effect attributable to H_L is small and, therefore, that H_L in the model tests was a very small quantity. Thus, when it is computed as the difference between total-head quantities determined from pitot-tube and point-gage measurements, the experimental error in H_L is likely to be excessive. This conclusion was confirmed by attempts to determine H_L from the model test data.

As an alternative and admittedly empirical method of handling H_L in equation 14, it is observed that λ is another small term in the equation and that the assumption of equal magnitudes of H_L and λ would result in their mutual elimination from subsequent equations. The resulting counterparts of equations 19 and 20 involve the relative magnitude of δ_q alone:

$$q=3.09\,H_1^{\frac{3}{2}}\left(1-\frac{3}{2}\frac{\delta_q}{H_1}\right), \tag{46}$$

and,

$$C=3.09\left(1-\frac{3}{2}\frac{\delta_q}{H_1}\right). \tag{47}$$

Equation 47, like equation 20, is readily tested by comparison with the experimentally determined values of C.

Values of δ_q corresponding to the values of $(\delta_q-\lambda)$ in figure 50 are shown in figure 52. The relationship between δ_q and h is not well defined, but the straight-line approximations shown on the figure are adequate to test the validity of equation 47.

Figure 53 shows a comparison of experimentally determined values of C from figure 41 with computed values of C from equation 47. At small values of h, for which the influence of boundary resistance is a maximum, the comparable curves are in substantial agreement. Discrepancies at large values of h/L demonstrate, again, the influence which has been attributed to flow curvature at the control section. Thus, for the conditions represented by the models, it is concluded that the influence of boundary resistance is effectively accounted for in equations 46 and 47. It is emphasized that the test conditions include the location of the headwater gage, and that the effect of this condition is reflected in the experimentally determined values of C.

INFLUENCE OF THE SIDEWALL BOUNDARY LAYER

Values of q used to determine C from the model test results were computed from equation 24,

$$q=\frac{Q}{B}, \tag{24}$$

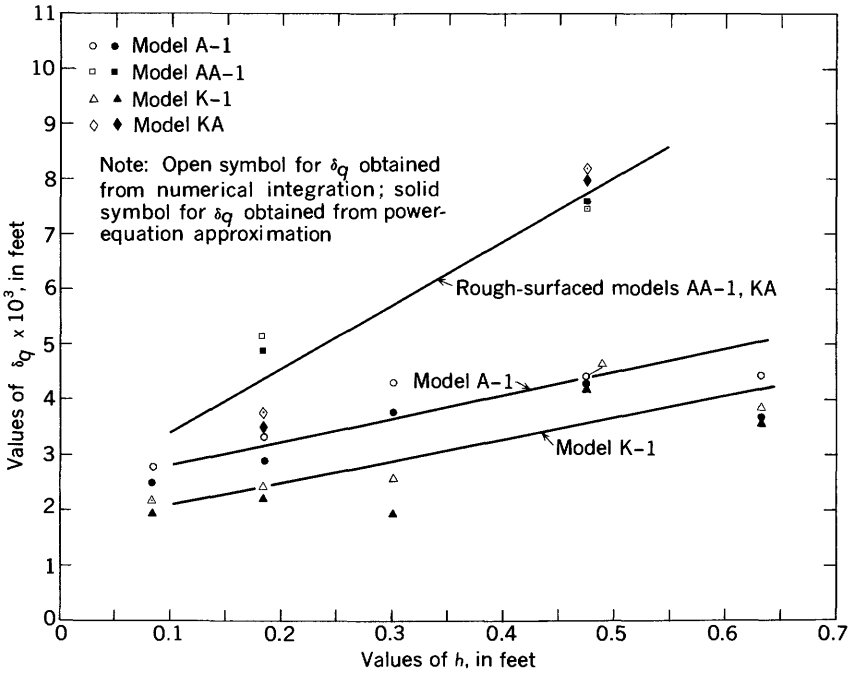

FIGURE 52.—Values of δ_q from boundary-layer velocity measurements.

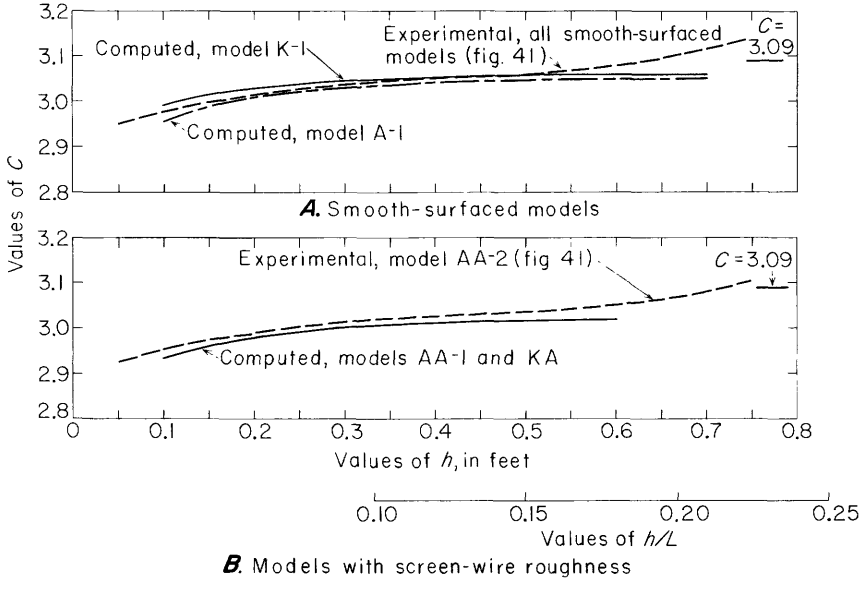

FIGURE 53.—Values of C computed from equation 47 and figure 52.

in which B is the average width of the test flume in the vicinity of the control section. It is recognized that this procedure ignores the effect of the boundary layer which occurs on both sides of the flume. Thus, if δ'_q is defined as the displacement thickness on the side walls, at the control section, a better definition of q is

$$q=\frac{Q}{B-2\delta'_q}. \tag{48}$$

The experiments made for this investigation did not include measurements of δ'_q. It might be assumed, however, that values of δ'_q are commensurate with values of δ_q measured for the round-shouldered, smooth-surfaced model. (The walls of the flume are plate glass.) Thus, a reasonable approximation of an average value of δ'_q, corresponding to the average value of δ_q for model K–1 on figure 52, is 0.003 foot. The corresponding error in the computation of q (and C) is indicated by the ratio

$$\frac{\frac{Q}{B}}{\frac{Q}{(B-2\delta'_q)}}=\frac{3.010-2(0.003)}{3.010}=0.998. \tag{49}$$

Therefore, in the experimentally determined values of C used in the report, the average relative error due to neglecting the sidewall boundary layer is estimated to be approximately 0.2 percent. This is less than the experimental error to be expected.

GENERAL SOLUTION FOR δ_q

Equation 47 has been substantiated as an effective means of accounting for the influence of the boundary layer on free discharge. However, the verification shown in figure 53 is based on measured crown-line values of δ_q. Practical use of equation 47 requires a convenient, general solution for δ_q. Anything less than this would result in an empirical discharge solution of limited usefulness and considerably less convenience than that which involves the simple, experimentally determined coefficient of discharge.

Equation 43 was proposed as a basis for a general solution for δ_q. Potential obstacles to its use are associated with the evaluation of τ_0 (or c_f), n, U, and dU/ds. It is now possible to appraise these obstacles on the basis of the boundary-layer measurements. The following observations are concerned with the practicality of integrating equation 43 to obtain δ_q as a function of s:

1. Equation 43 involves the assumption that the velocity distribution in the boundary layer can be described with an equation of the

power form. In general, the measurements confirm the use of this assumption for rough-surfaced as well as smooth-surfaced models. Values of n are not clearly defined as functions of s and h (or q). Nevertheless, for all but the smallest values of h, and for virtually the full distance upstream from the crown line, figures 48B and 49B support the use of a different, approximate, constant value of n for each of the models tested. Whereas the assumption of constant values of n facilitates the integration of equation 43 for specific models, the substantial variation of n with shape and roughness is an obstacle to a general solution.

2. Figures 44, 45, and 49A show that a secondary layer of considerable thickness exists at station 0 (at the nominal intersection of the upstream shoulder and embankment surfaces). The data show that the thickness of the layer at station 0 varies with model design and discharge, and that it is sensitive to the occurrence of a separation zone immediately downstream from station 0. These observations confirm the assumption that the effective origin of the boundary layer is upstream from station 0. Although the data are inadequate to provide a general method of accurately determining the location of the origin, it is observed that the thickness of the layer changes very rapidly in the vicinity of station 0 and very slowly in the vicinity of the crown line. Consequently, the use of an approximate origin probably would result in a relatively small error in crown-line values of δ_q computed from equation 43.
3. The experimental data show that the boundary layer is displaced by the separation zone which occurs at station 0, especially in models A–1 and AA–1. The thickness of the layer downstream from the point of reattachment is increased as a result of this displacement, but the increase, as indicated by a comparison of boundary layers on models A–1 and K–1, diminishes with distance from station 0. The influence on crown-line values of δ_q is not believed to be substantial.
4. The boundary-layer measurements do not provide a direct means of evaluating the effects of curvilinear flow in relation to the assumptions made in deriving equation 43. This influence remains an unknown but probably minor source of error in the application of the equation to the computation of δ_q.
5. Integration of equation 43 requires evaluation of the relationship between U and s. Figures 54 and 55 show the experimentally determined values from the boundary-layer tests. For each test

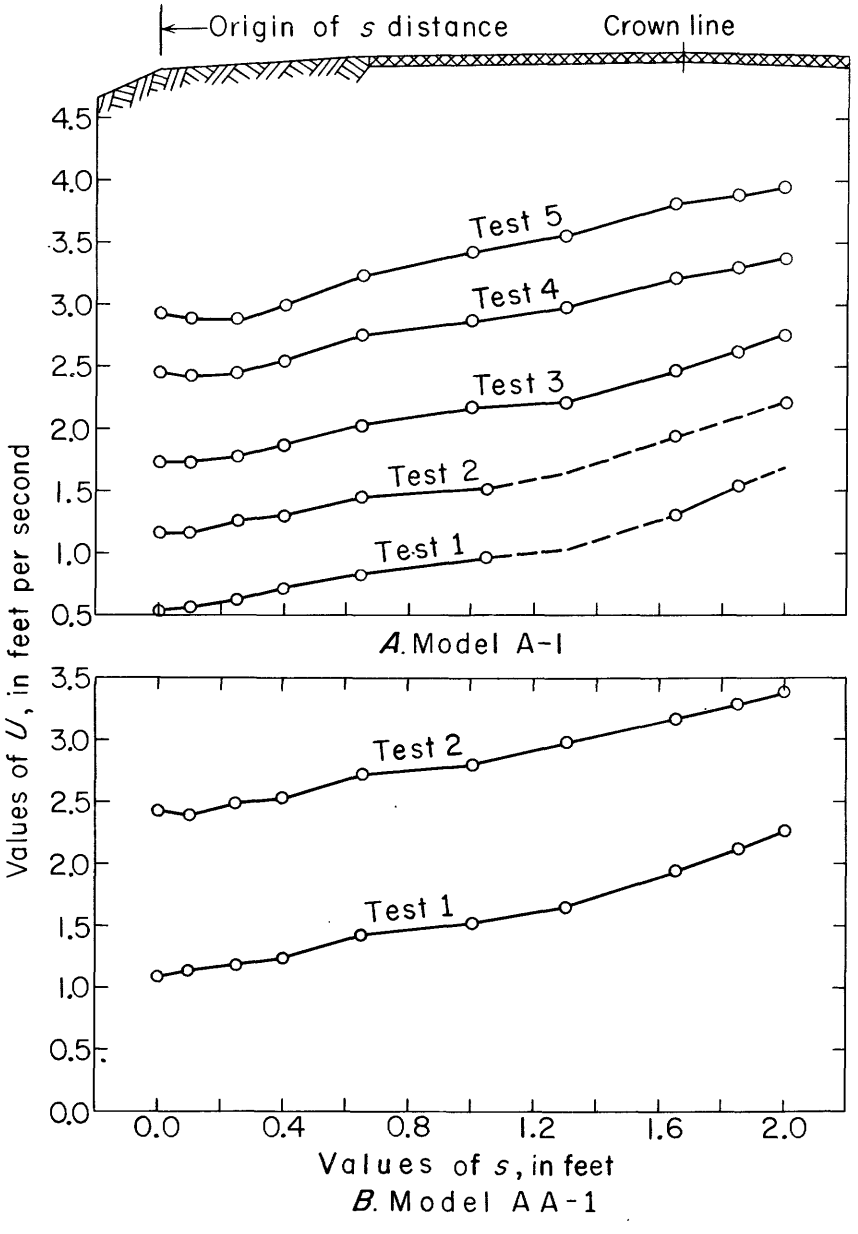

FIGURE 54.—Velocity outside the boundary layer, model of basic design.

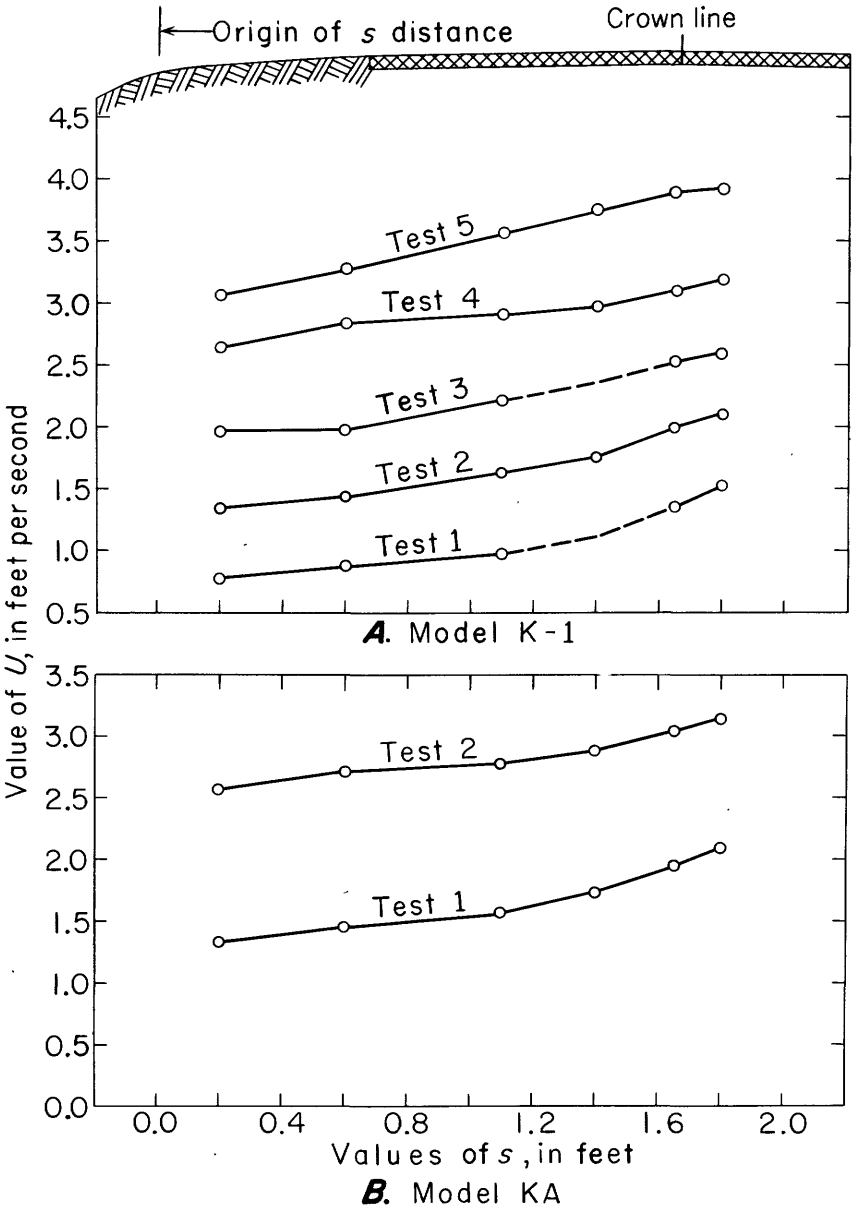

FIGURE 55.—Velocity outside the boundary layer, model with rounded upstream shoulder.

the relationship is described approximately by an equation in the straight-line form,

$$U=U_0+ms, \tag{50}$$

in which U_0 is the velocity outside the boundary layer at station 0, and m is the slope of a straight line fitted to the plotted points, Comparison of the data shown in figures 54 and 55 indicates that m varies with the shape of the upstream shoulder, whereas it is virtually independent of discharge and embankment roughness. (Thus, m is approximately 0.5 for most tests on models A–1 and AA–1 and 0.3 for tests on models K–1 and KA.) The quantity U_0, of course, varies with the discharge. It also varies with the shape of the upstream shoulders; but it, too, is virtually independent of embankment roughness. The form of equation 50 does not preclude integration of equation 43. However, because U_0 varies with discharge, the computation of q by means of equations 43 and 46 would require a tedious successive-approximations procedure.

6. The principal effects of embankment roughness are related to its influence on c_f in equation 44 and and the exponent n in the velocity-distribution equation. Equation 43 does not account specifically for the influence of roughness, and the experimental data do not provide a general means of evaluating that influence in terms of a nondimensional relative-roughness parameter. Consequently, it is impossible to use the model test data to determine the effect of roughness in the prototype.

The foregoing observations lead to the conclusion that a discharge equation which depends on equation 43 for the crown-line value of δ_q is neither general nor practical. In summary, the decisive obstacles revealed by the experimental data are: (a) n varies substantially with both boundary form and roughness and, less critically, with s and q; (b) U_0 varies with boundary form and discharge; and (c) m varies with boundary form. Furthermore, the data are inadequate to provide a general solution for τ_0 in terms of discharge and relative roughness. Whereas the combination of these obstacles precludes a satisfactory general solution for q, it neither disproves nor proves the validity of equation 43 as applied to embankment-shaped weirs. For academic interest, at least, the validity test is a logical, terminal objective of the boundary-layer measurements.

On the assumption that the Blasius equation for c_f (page 66) is applicable to the smooth-surfaced models, equations 30 and 45 can be substituted in equation 43 to give

$$0.0225\left(\frac{U\delta_q}{\nu}\right)^{-0.25}\left(\frac{n}{n+1}\right)^{0.25}=\left(\frac{1}{2n+1}\right)\frac{d\delta_q}{ds}+\left(\frac{2n+3}{2n+1}\right)\left(\frac{\delta_q}{2U^2}\right)\frac{dU^2}{ds}, \tag{51}$$

which is an implicit equation for the displacement-thickness gradient ($d\delta_q/ds$), in terms of the local values of n, U, δ_q, and dU/ds at distance s from the origin of the boundary layer. If equation 50 is substituted for U, equation 51 can be integrated, whence

$$\delta_q=\left\{\frac{K_1(U_0+ms)^{0.75}}{mK_2}\left[1-\left(\frac{U_0}{U_0+ms}\right)^{K_2}\right]\right\}^{0.8}, \tag{52}$$

in which,

$$K_1=0.028(2n+1)\left(\frac{m}{n+1}\right)^{0.25}, \tag{53}$$

and,

$$K_2=2.5n+4.5. \tag{54}$$

The tests selected for verification of equation 52 are test 4, model A–1, and test 4, model K–1, tests which previously were used to represent the smooth-surfaced models in figure 49. The experimental data required for the evaluation of equation 52 were obtained from figures 48, 49, 54, and 55. For comparison with computed values of δ_q from equation 52, measured values of δ from figure 49 were converted to values of δ_q by means of equation 30, using average values of n. Values of U_0, m, and $1/n$ used in equation 52, and values of n used in the conversion of δ are shown on figure 56.

Figure 56 shows a comparison of the computed and experimentally determined values of δ_q. The s-origin for the values computed from equation 52 was assumed to correspond with station 0 for the boundary-layer measurements. For this condition, experimental values of δ_q compare favorably with the computed values at the crown-line station. Experimental values are larger than computed values at upstream stations, and values for model A–1 show the effect of the separation zone at station 0. A small s-distance displacement of the computed curve would cause it to show good agreement with the K–1 curve over a large part of the roadway. This displacement could be defined as the distance from station 0 to the effective origin of the boundary layer for that test. However, it is observed that only the crown-line value of δ_q is involved in the discharge equation (eq. 46), and the crown-line value is best defined by the computed curve when its origin is at station 0, as in figure 56.

The comparison shown on figure 56 is limited evidence of the validity of the analysis which led to equations 43 and 52. Nothing more is expected from this phase of the investigation, which previously was acknowledged to be of academic interest only.

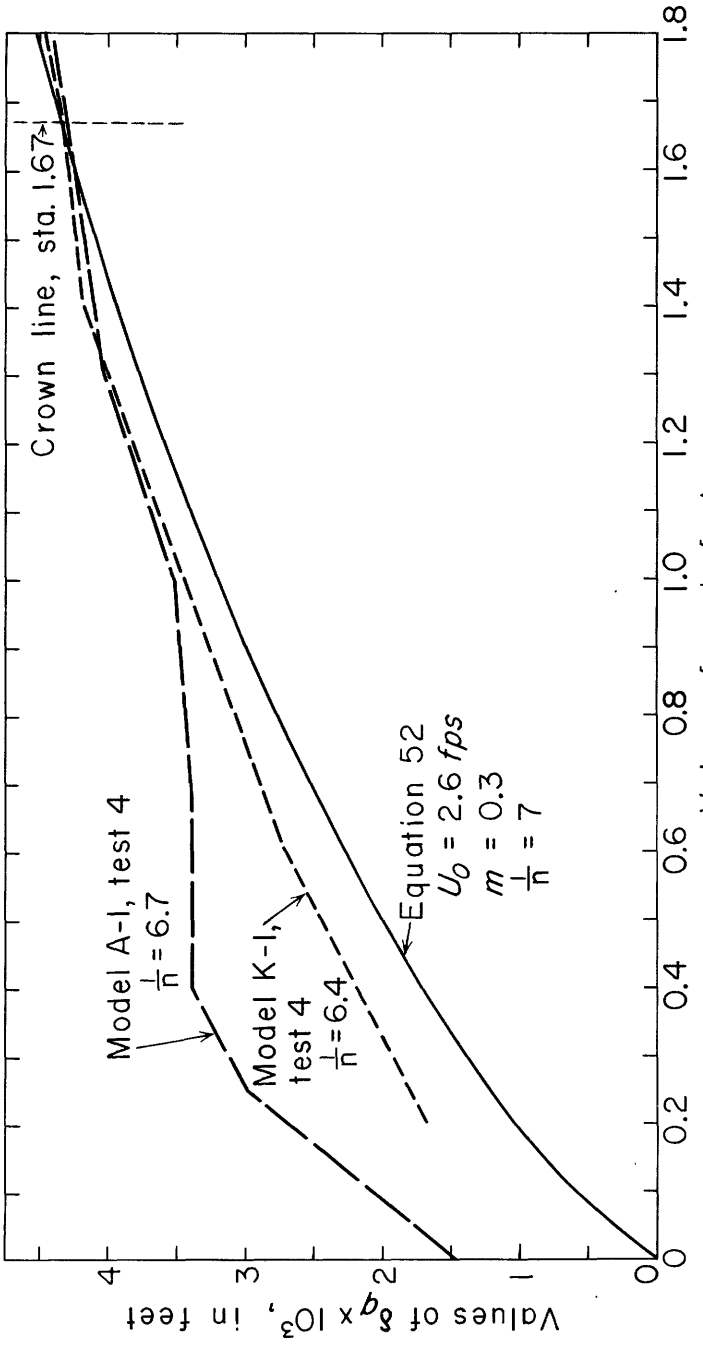

FIGURE 56.—Values of δ_q computed from equation 52 compared with experimental values from figure 49.

COMPUTATION OF C FOR THE PROTOTYPE

The search for a general solution for boundary-layer growth was previously (p. 79) related to the need for a means of computing the crown-line value of δ_q for prototype embankments of various forms, widths, and roughnesses. Equation 52 already has been described as impractical as a general solution for the boundary layer. Furthermore, the approximate confirmation of model values shown on figure 56 is limited to a small range of model conditions. Nevertheless, this limited evidence of the validity of equation 52 is encouragement for an attempt to compute C for prototype embankments similar to the basic, smooth-surfaced model.

Prototype values of δ_q were computed from equation 52 with $m=0.3$, $1/n=7$, and values of U_0 equal to the square root of the prototype-model length ratio (9:1) times the corresponding model values of U_0 from figure 55*A*. Using these values of δ_q, values of C were computed from equation 47. The results are shown by the solid line in figure 57.

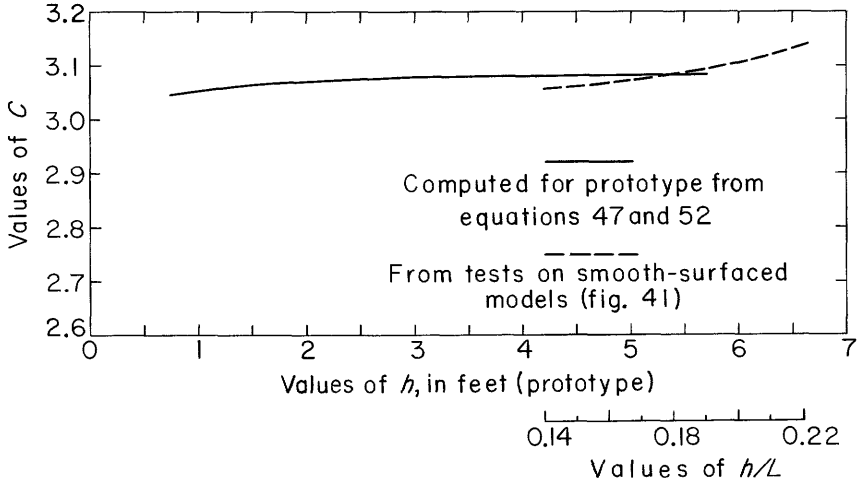

FIGURE 57.—Computed prototype values and measured model values of C, smooth-surfaced embankments.

Considering the limitations of the data on model boundary layers and the lack of data on model-prototype conformity, the solid-line curve shown in figure 57 is of doubtful accuracy. Nevertheless, it is reasonable to describe the curve as an estimate of the relative influence of the boundary layer on a 9:1-scale prototype which corresponds in design to the smooth-surfaced models.

Shown for comparison in figure 57 is the curve from figure 41 which is the average for all smooth-surfaced models. Actually, the model curve is shown in two parts. On the left, the dashed-line curve covers the range of values of head in which the influence of boundary resistance is dominant in the model. (The corresponding range of heads for a 9:1-scale prototype is represented by the solid-line curve in the middle.) On the right, the dashed-line curve covers the range of h/L values in which the influence of flow curvature was dominant in the model. The prototype counterpart of this curve can be expected to be similar to the model curve. However, it cannot be predicted accurately without experimental data from tests on models of different size (scale) or from tests on prototype embankments.

CONCLUSIONS

From the results of the model tests summarized on page 58, it is concluded that the coefficient of discharge for free flow is primarily a function of head, roadway roughness, and the head-width ratio (h/L). The coefficient of discharge for submerged flow is primarily a function of the submergence ratio (t/H_1) and the roughness of the roadway surface. These conclusions are substantiated by the summary curves in figures 41 and 42. In general, values of t/H_1 corresponding to incipient submergence and the free-flow transition-range limits vary with head, roadway roughness, and h/L. This conclusion is substantiated by the curves shown in figure 43.

For intermediate values of head, the coefficient of discharge for free flow is nearly equal to the ideal value (3.09) which corresponds to the assumption of critical-depth control at the crown. For smaller values of head, the influence of boundary resistance causes the coefficient to be smaller than the ideal value. For larger values of head (or, actually, larger values of h/L), the influence of flow curvature at the control section causes the coefficient to be larger than the ideal value.

The influence of boundary resistance on the free-flow coefficient of discharge is related to the relative thickness of the boundary layer at the crown line of the embankment. The growth of the boundary layer and, therefore, the thickness of the boundary layer at the crown line can be computed approximately with empirical equations which are based on well-known general equations for turbulent boundary layers in accelerated motion. Consequently, the coefficient of discharge for free-flow, in the range of low and intermediate values of head, can be computed with equations which involve boundary-layer parameters. However, the equations are not sufficiently general and convenient to be practical. Therefore, the most practical solution for free-flow discharge is that which is based on the simple equation of

discharge and experimentally determined coefficients which are related directly to the basic geometric and flow variables. This is the solution which makes use of the curves in figure 41.

The ultimate goal of this research is a satisfactory solution for the discharge characteristics of a full, practical variety of prototype embankments. The model tests show that the most significant characteristics of both free and submerged flow are virtually independent of embankment shape and relative height (h/P). However, the influence of boundary resistance is appreciable, and it depends on roadway width as well as roughness. The model test data are not adequate to define accurately the boundary-resistance effects for prototype-size embankments. For a more accurate evaluation of these effects, the results of the model studies should be correlated with a limited number of prototype tests.

REFERENCES CITED

Bauer, W. J., 1954, Turbulent boundary layer on steep slopes: Am. Soc. Civil Engineers Trans., v. 119, p. 1212.

Delleur, J. W., 1957, The boundary layer development in open channels: Am. Soc. Civil Engineers Proc., Journal of the Engineering Mechanics Div., EMI, January, Paper 1138.

Halbronn, G., 1954, Turbulent boundary layer on steep slopes [discussion of paper by Bauer (1954)]: Am. Soc. Civil Engineers Trans., v. 119, p. 1234.

Kindsvater, C. E., 1957, Flood-erosion protection for highway fills [discussion of paper by Chesley J. Posey]: Am. Soc. Civil Engineers Trans., v. 122, p. 548.

Schlichting, Hermann, 1955, Boundary layer theory: New York, Pergamon Press, 535 p.

Tracy, H. J., 1957, Discharge characteristics of broad-crested weirs: U.S. Geol. Survey Circ. 397, 15 p., 11 figs.

Yarnell, D. L., and Nagler, F. A., 1930, Flow of flood water over railway and highway embankments: Public Roads, v. 11, no. 2 (April), p. 30.

EXPERIMENTAL DATA

TABLE 3.—*Summary of data for discharge characteristics* [1]

[F, free flow, tailwater below lower limit of transition range; LL, free flow, tailwater at lower limit of transition range; UL, free flow, tailwater at upper limit of transition range; IS, incipient submergence; S, submerged flow]

Run No.	q (cfs per ft)	t (feet)	h (feet)	H_o (feet)	C	Remarks	Run No.	q (cfs per ft)	t (feet)	h (feet)	H_o (feet)	C	Remarks
MODEL A-2													
Test 1													
[y_o=0.120 ft; y_o/y_c=1.04]													
1	0.222		0.175	0.175	3.03	F	5	.222	.204	.212	.212	2.27	S
2	.222	0.118	.174	.174	3.05	UL	6	.222	.233	.239	.239	1.90	S
3	.222	.155	.175	.175	3.03	IS	7	.222	.258	.262	.262	1.65	S
4	.222	.179	.191	.191	2.65	S	8	.222	.052	.175	.175	3.03	LL
Test 2													
[y_o=0.194 ft, y_o/y_c=1.04]													
1	0.451		0.278	0.280	3.05	F	6	.451	.350	.363	.364	2.05	S
2	.451	0.196	.278	.280	3.05	UL	7	.451	.381	.390	.391	1.84	S
3	.451	.231	278	.280	3.05	IS	8	.451	.409	.418	.419	1.66	S
4	.451	.271	.295	.296	2.79	S	9	.451	.443	.450	.451	1.49	S
5	.451	.315	.332	.333	2.34	S	10	.451	.129	.278	.280	3.05	LL
Test 3													
[y_o=0.244 ft, y_o/y_c=1.03]													
1	0.650		0.353	0.356	3.06	F	6	.650	.418	.438	.440	2.23	S
2	.650	0.258	.353	.356	3.06	UL	7	.650	.461	.476	.478	1.96	S
3	.650	.295	.353	.356	3.06	IS	8	.650	.498	.511	.513	1.77	S
4	.650	.324	.361	.364	2.96	S	9	.650	.543	.553	.555	1.57	S
5	.650	.388	.411	.414	2.44	S	10	.650	.164	.353	.356	3.06	LL
Test 4													
[y_o=0.089 ft, y_o/y_c=1.03]													
1	0.143		0.132	0.132	2.98	F	5	.143	.119	.134	.134	2.91	S
2	.143	0.076	.132	.132	2.98	UL	6	.143	.178	.181	.181	1.86	S
3	.143	.111	.132	.132	2.98	IS	7	.143	.012	.132	.132	2.98	LL
4	.143	.149	.156	.156	2.32	S							
Test 5													
[y_o=0.451 ft, y_o/y_c=0.977]													
1	1.78		0.647	0.688	3.12	F	3	1.78	.561	.674	.688	3.12	IS
2	1.78	0.543	.674	.688	3.12	UL	4	1.78	.414	.672	.687	3.12	LL

See footnote at end of table, p. A106.

TABLE 3.—*Summary of data for discharge characteristics*—Continued

Run No.	q (cfs per ft)	t (feet)	h (feet)	H_o (feet)	C	Remarks	Run No.	q (cfs per ft)	t (feet)	h (feet)	H_o (feet)	C	Remarks
MODEL A-2—Continued													
Test 6													
[y_o=0.349 ft, y_o/y_c=1.02]													
1	1.14		0.510	0.517	3.06	F	6	1.14	.534	.570	.576	2.60	S
2	1.14	0.399	.510	.517	3.06	UL	7	1.14	.584	.612	.618	2.34	S
3	1.14	.417	.510	.517	3.06	IS	8	1.14	.637	.660	.667	2.09	S
4	1.14	.459	.516	.523	3.01	S	9	1.14	.689	.706	.712	1.90	S
5	1.14	.499	.542	.550	2.80	S	10	1.14	.289	.510	.517	3.06	LL
MODEL A-3													
Test 1													
[y_o=0.122 ft, y_o/y_c=1.06]													
1	0.221		0.174	0.174	3.04	F	5	.221	.233	.239	.239	1.89	S
2	.221	0.117	.174	.174	3.04	UL	6	.221	.260	.264	.264	1.63	S
3	.221	.153	.174	.174	3.04	IS	7	.221	.305	.307	.307	1.30	S
4	.221	.191	.202	.202	2.43	S	8	.221	.047	.174	.174	3.04	LL
Test 2													
[y_o=0.204 ft, y_o/y_c=1.06]													
1	0.476		0.289	0.291	3.04	F	6	.476	.359	.372	.374	2.09	S
2	.476	0.216	.289	.291	3.04	UL	7	.476	.410	.418	.420	1.75	S
3	.476	.249	.289	.291	3.04	IS	8	.476	.463	.469	.470	1.48	S
4	.476	.278	.304	.306	2.82	S	9	.476	.132	.289	.291	3.04	LL
5	.476	.312	.331	.333	2.48	S							
Test 3													
[y_o=0.328 ft, y_o/y_c=1.03]													
1	1.01		0.472	0.478	3.06	F	5	1.01	.520	.547	.553	2.46	S
2	1.01	0.387	.473	.479	3.06	UL	6	1.01	.610	.628	.633	2.01	S
3	1.01	.404	.473	.479	3.06	IS	7	1.01	.274	.472	.478	3.06	LL
4	1.01	.468	.505	.511	2.77	S							
Test 4													
[y_o=0.417 ft, y_o/y_c=0.998]													
1	1.53		0.617	0.629	3.08	F	4	1.53	.611	.655	.666	2.82	S
2	1.53	0.501	.618	.630	3.07	UL	5	1.53	.682	.709	.720	2.51	S
3	1.53	.531	.618	.630	3.07	IS	6	1.53	.388	.617	.629	3.08	LL
Test 5													
[y_o=0.471 ft, y_o/y_c=0.977]													
1	1.89		0.701	0.718	3.12	F	3	1.89	.608	.702	.719	3.11	IS
3	1.89	0.549	.702	.719	3.11	UL	4	1.89	.463	.701	.718	3.12	LL
MODEL A-4													
Test 1													
[y_o=0.037 ft, y_o/y_c=1.00]													
1	0.0402		0.058	0.058	2.91	F	3	0402	.018	.061	.061	2.70	IS
2	.0402	0.001	.060	.060	2.77	UL	4	.0402	−.089	.058	.058	2.91	LL
Test 2													
[y_o=0.078 ft, y_o/y_c=1.04]													
1	0.117		0.117	0.117	2.93	F	3	.117	.106	.120	.120	2.82	IS
2	.117	0.073	.119	.119	2.86	UL	4	.117	−.005	.117	.117	2.93	LL

TABLE 3.—*Summary of data for discharge characteristics*—Continued

Run No.	q (cfs per ft)	t (feet)	h (feet)	H_o (feet)	C	Remarks	Run No.	q (cfs per ft)	t (feet)	h (feet)	H_o (feet)	C	Remarks
MODEL A–4—Continued													
Test 3													
[y_o=0.140 ft, y_o/y_c=1.03]													
1	0.284	0.146	0.208	0.208	2.99	F	3	.284	.180	.211	.211	2.93	IS
2	.284		.210	.210	2.95	UL	4	.284	.067	.208	.208	2.99	LL
Test 4													
[y_o=0.209 ft, y_o/y_c=1.06]													
1	0.498	0.218	0.299	0.300	3.03	F	3	.498	.260	.303	.304	2.97	IS
2	.498		.301	.302	3.00	UL	4	.498	.117	.299	.300	3.03	LL
Test 5													
[y_o=0.271 ft, y_o/y_c=1.03]													
1	0.765	0.315	0.394	0.397	3.06	F	3	.765	.345	.399	.402	3.00	IS
2	.765		.397	.400	3.02	UL	4	.765	.209	.394	.397	3.06	LL
Test 6													
[y_o=0.330 ft, y_o/y_c=1.02]													
1	1.05	0.397	0.483	0.489	3.06	F	3	1.05	.417	.487	.493	3.03	IS
2	1.05		.486	.492	3.04	UL	4	1.05	.259	.483	.489	3.06	LL
Test 7													
[y_o=0.390 ft, y_o/y_c=0.999]													
1	1.39	0.466	0.577	0.586	3.09	F	3	1.39	.504	.581	.590	3.06	IS
2	1.39		.580	.589	3.07	UL	4	1.39	.354	.576	.586	3.09	LL
Test 8													
[y_o=0.435 ft, y_o/y_c=0.986]													
1	1.66	0.530	0.648	0.661	3.09	F	3	1.66	.558	.652	.665	3.06	IS
2	1.66		.651	.664	3.07	UL	4	1.66	.402	.648	.661	3.09	LL
Test 9													
[y_o=0.474 ft, y_o/y_c=0.976]													
1	1.92	0.586	0.711	0.727	3.10	F	3	1.92	.623	.716	.732	3.07	IS
2	1.92		.714	.730	3.08	UL	4	1.92	.457	.711	.727	3.10	LL
Test 10													
1	0.0592		0.07	0.074	2.97	F	4	.386		.252	.253	3.04	F
2	.172		.14	.148	3.03	F	5	1.59		.628	.640	3.10	F
3	.277		.202	.203	3.02	F	6	1.88		.702	.718	3.06	F
Test 11													
1	0.0343		0.050	0.050	3.02	F	7	.888		.435	.449	3.04	F
2	.0900		.097	.097	2.97	F	8	1.12		.505	.512	3.06	F
3	.187		.156	.153	3.02	F	9	1.40		.581	.594	3.08	F
4	.323		.224	.225	3.02	F	10	1.71		.656	.670	3.11	F
5	.451		.278	.280	3.04	F	11	1.93		.710	.726	3.11	F
6	.674		.362	.366	3.05	F							

TABLE 3.—*Summary of data for discharge characteristics*—Continued

Run No.	q (cfs per ft)	t (feet)	h (feet)	H_o (feet)	C	Remarks	Run No.	q (cfs per ft)	t (feet)	h (feet)	H_o (feet)	C	Remarks
MODEL A-4—Continued													
Test 12													
1	0.0335		0.050	0.050	2.95	F	6	.967		.460	.465	3.05	F
2	.109		.110	.110	2.99	F	7	1.28		.550	.559	3.07	F
3	.228		.179	.179	3.00	F	8	1.61		.636	.648	3.08	F
4	.375		.248	.250	3.01	F	9	1.91		.708	.725	3.09	F
5	.640		.352	.354	3.04	F							
MODEL B													
Test 1													
[y_o=0.096 ft, y_o/y_c=1.02]													
1	0.163	0.097	0.142	0.142	3.02	F, UL	5	.163	.182	.186	.186	2.02	S
2	.163	.126	.142	.142	3.02	IS	6	.163	.218	.221	.221	1.56	S
3	.163	.133	.145	.145	2.93	S	7	.163	.005	.142	.142	3.02	LL
4	.163	.150	.158	.158	2.58	S							
Test 2													
[y_o=0.131 ft, y_o/y_c=1.02]													
1	0.259	0.148	0.194	0.195	3.01	F, UL	4	.259	.197	.210	.211	2.67	S
2	.259	.167	.194	.195	3.01	IS	5	.259	.217	.227	.228	2.38	S
3	.259	.182	.198	.199	2.92	S	6	.259	.070	.194	.195	3.01	LL
Test 3													
[y_o=0.209 ft, y_o/y_c=1.04]													
1	0.506	0.233	0.300	0.303	3.03	F, UL	7	.506	.389	.399	.402	1.99	S
2	.506	.260	.300	.303	3.03	IS	8	.506	.408	.417	.419	1.86	S
3	.506	.294	.316	.319	2.81	S	9	.506	.438	.445	.447	1.69	S
4	.506	.314	.332	.335	2.61	S	10	.506	.464	.470	.472	1.56	S
5	.506	.336	.352	.355	2.40	S	11	.506	.155	.300	.303	3.03	LL
6	.506	.365	.377	.380	2.16	S							
Test 4													
[y_o=0.256 ft, y_o/y_c=1.03]													
1	0.706	0.291	0.371	0.376	3.06	F, UL	6	.706	.521	.529	.533	1.81	S
2	.706	.321	.371	.376	3.06	IS	7	.706	.579	.585	.589	1.56	S
3	.706	.379	.400	.405	2.74	S	8	.706	.631	.636	.639	1.38	S
4	.706	.437	.451	.455	2.30	S	9	.706	.216	.371	.376	3.06	LL
5	.706	.475	.486	.490	2.06	S							
Test 5													
[y_o=0.353 ft, y_o/y_c=1.02]													
1	1.16	0.405	0.515	0.526	3.03	F, UL	6	1.16	.608	.628	.637	2.27	S
2	1.16	.432	.515	.526	3.03	IS	7	1.16	.677	.692	.701	1.97	S
3	1.16	.485	.529	.540	2.92	S	8	1.16	.747	.756	.764	1.73	S
4	1.16	.527	.559	.569	2.69	S	9	1.16	.327	.515	.526	3.03	LL
5	1.16	.558	.584	.594	2.53	S							
Test 6													
[y_o=0.477 ft, y_o/y_c=0.981]													
1	1.92	0.582	0.703	0.726	3.11	F, UL	3	1.92	.513	.702	.725	3.12	LL
2	1.92	.603	.703	.726	3.11	IS							
Test 7													
1	1.48		0.601	0.617	3.06	F	3	1.30		.551	.564	3.06	F
2	.618		.342	.346	3.04	F	4	1.84		.683	.705	3.11	F

TABLE 3.—*Summary of data for discharge characteristics*—Continued

Run No.	q (cfs per ft)	t (feet)	h (feet)	H_o (feet)	C	Remarks	Run No.	q (cfs per ft)	t (feet)	h (feet)	H_o (feet)	C	Remarks
MODEL C													
Test 1													
[y_o=0.108 ft, y_o/y_c=1.02]													
1	0.197	0.112	0.161	0.162	3.01	F, UL	4	.197	.214	.218	.219	1.92	S
2	.197	.147	.161	.162	3.01	IS	5	.197	.243	.246	.247	1.60	S
3	.197	.182	.189	.190	2.37	S	6	.197	.048	.161	.162	3.01	LL
Test 2													
[y_o=0.216 ft, y_o/y_c=1.04]													
1	0.534	0.226	0.307	0.313	3.06	F, UL	5	.534	.370	.378	.383	2.26	S
2	.534	.270	.307	.313	3.06	IS	6	.534	.419	.425	.429	1.90	S
3	.534	.296	.315	.320	2.94	S	7	.534	.458	.461	.465	1.68	S
4	.534	.325	.339	.344	2.64	S	8	.534	.175	.307	.313	3.06	LL
Test 3													
[y_o=0.257 ft, y_o/y_c=1.02]													
1	0.715	0.283	0.371	0.380	3.06	F, UL	5	.715	.440	.452	.459	2.30	S
2	.715	.337	.371	.380	3.06	IS	6	.715	.500	.507	.514	1.94	S
3	.715	.367	.388	.396	2.86	S	7	.715	.579	.583	.589	1.58	S
4	.715	.401	418	.426	2.57	S	8	.715	.228	.370	.379	3.06	LL
Test 4													
[y_o=0.358 ft, y_o/y_c=1.02]													
1	1.18	0.417	0.510	0.528	3.08	F, UL	5	1.18	.592	.606	.621	2.41	S
2	1.18	.452	.510	.528	3.08	IS	6	1.18	.663	.671	.685	2.09	S
3	1.18	.487	.519	.537	3.01	S	7	1.18	.359	.510	.528	3.08	LL
4	1.18	.541	.561	.578	2.70	S							
Test 5													
[y_o=0.468 ft, y_o/y_c=0.977]													
1	1.88	0.549	0.682	0.716	3.10	F, UL	3	1.88	.501	.682	7.16	3.10	LL
2	1.88	.593	.682	.716	3.10	IS							
Test 6													
1	1.47		0.586	0.610	3.08	F	2	0.873		.426	.438	3.02	F
MODEL D													
Test 1													
[y_o=0.067 ft, y_o/y_c=1.01]													
1	0.0959		0.101	0.102	2.94	F	4	.0959	.150	.153	.154	1.59	S
2	.0959	0.087	.101	.102	2.94	IS	5	.0959	.105	.111	.112	2.56	S
3	.0959	.109	.113	.114	2.49	S							
Test 2													
[y_o=0.094 ft, y_o/y_c=1.02]													
1	0 159		0.141	0.143	2.93	F	5	.159	.160	.165	.167	2.33	S
2	.159	0.116	.141	.143	2.93	IS	6	.159	.171	.175	.177	2.13	S
3	.159	.134	.145	.147	2.81	S	7	.159	.183	.187	.189	1.94	S
4	.159	.147	.154	.156	2.57	S							

TABLE 3.—*Summary of data for discharge characteristics*—Continued

Run No.	q (cfs per ft)	t (feet)	h (feet)	H_o (feet)	C	Remarks	Run No.	q (cfs per ft)	t (feet)	h (feet)	H_o (feet)	C	Remarks
MODEL D—Continued													
Test 3													
[y_o=0.135 ft, y_o/y_c=1.02]													
1	0.272		0.196	0.201	3.02	F	5	.272	.207	.215	.220	2.65	S
2	.272	0.166	.196	.201	3.02	IS	6	.272	.220	.226	.230	2.46	S
3	.272	.181	.197	.202	3.00	S	7	.272	.240	.243	.247	2.22	S
4	.272	.191	.202	.207	2.89	S							
Test 4													
[y_c=0.216 ft, y_o/y_c=1.05]													
1	0.525		0.300	0.312	3.01	F	5	.525	.328	.338	.349	2.55	S
2	.525	0.270	.300	.312	3.01	IS	6	.525	.355	.362	.372	2.31	S
3	.525	.282	.303	.315	2.97	S	7	.525	.375	.381	.391	2.15	S
4	.525	.310	.323	.334	2.72	S	8	.525	.396	.400	.408	2.02	S
Test 5													
[y_o=0.265 ft, y_o/y_c=1.01]													
1	0.763		0.378	0.398	3.04	F	5	.763	.374	.394	.413	2.87	S
2	.763	0.335	.378	.398	3.04	IS	6	.763	.400	.415	.433	2.68	S
3	.763	.342	.379	.399	3.02	S	7	.763	.446	.454	.470	2.36	S
4	.763	.351	.380	.400	3.01	S	8	.763	.488	.493	.508	2.11	S
Test 6													
[y_o=0.367 ft, y_o/y_c=1.01]													
1	1.25		0.527	0.563	2.95	F	4	1.25	.520	.551	.585	2.78	S
2	1.25	0.475	.527	.563	2.95	IS	5	1.25	.547	.571	.604	2.66	S
3	1.25	.498	.536	.571	2.88	S	6	1.25	.591	.605	.635	2.46	S
Test 7													
1	0.288	0.138	0.203	0.208	3.03	F, UL	12	1.29	.409	.523	.562	3.07	LL
2	.288	.189	.203	.208	3.03	IS	13	1.97	.581	.676	.741	3.09	F, UL
3	.288	.101	.203	.208	3.03	LL	14	1.97	.625	.676	.741	3.09	IS
4	.490	.206	.285	.296	3.04	F, UL	15	1.97	.549	.676	.741	3.09	LL
5	.490	.261	.285	.296	3.04	IS	16	.159	.087	.141	.143	2.94	IS
6	.490	.181	.285	.296	3.04	LL	17	.159	.116	.141	.143	2.94	IS
7	.793	.301	.385	.406	3.06	F, UL	18	.159	.050	.141	.143	2.94	LL
8	.793	.357	.385	.406	3.06	IS	19	.970		.437	.464	3.07	F
9	.793	.275	.385	.406	3.06	LL	20	1.58		.590	.640	3.08	F
10	1.29	.423	.523	.562	3.07	F, UL	21	.777		.380	.401	3.06	F
11	1.29	.469	.523	.562	3.07	IS							
MODEL E													
Test 1													
[y_o=0.109 ft, y_o/y_c=1.11]													
1	0.175		0.151	0.151	2.97	F	5	.175	.187	.192	.192	2.08	S
2	.175	0.121	.155	.155	2.86	UL	6	.175	.208	2.11	.211	1.80	S
3	.175	.125	.155	.155	2.86	IS	7	.175	.054	.152	.152	2.95	LL
4	.175	.163	.172	.172	2.45	S							
Test 2													
[y_o=0.147 ft, y_o/y_c=1.06]													
1	0.292		0.211	0.212	2.99	F	5	.292	.225	.238	.239	2.50	S
2	.292	0.159	.213	.214	2.95	UL	6	.292	.252	.260	.261	2.19	S
3	.292	.171	.213	.214	2.95	IS	7	.292	.285	.290	.291	1.86	S
4	.292	.195	.216	.217	2.89	S	8	.292	.095	.212	.213	2.97	LL

TABLE 3.—*Summary of data for discharge characteristics*—Continued

Run No.	q (cfs per ft)	t (feet)	h (feet)	H_o (feet)	C	Remarks	Run No.	q (cfs per ft)	t (feet)	h (feet)	H_o (feet)	C	Remarks
MODEL E—Continued													
Test 3 [y_o=0.203 ft, y_o/y_c=1.03]													
1	0.496		0.296	0.298	3.05	F	6	.496	.361	.373	.375	2.16	S
2	.496	0.226	.299	.301	3.00	UL	7	.496	.415	.421	.423	1.80	S
3	.496	.240	.299	.301	3.00	IS	8	.496	.467	.471	.473	1.53	S
4	.496	.261	.301	.303	2.98	S	9	.496	.152	.297	.299	3.04	LL
5	.496	.306	.325	.327	2.66	S							
Test 4 [y_o=0.289 ft, y_o/y_c=1.01]													
1	0.871		0.430	0.435	3.04	F	6	.871	.539	.553	.557	2.09	S
2	.871	0.341	.432	.437	3.01	UL	7	.871	.578	.588	.592	1.91	S
3	.871	.367	.432	.437	3.01	IS	8	.871	.673	.680	.684	1.54	S
4	.871	.399	.442	.447	2.92	S	9	.871	.245	.431	.436	3.02	LL
5	.871	.459	.487	.492	2.53	S							
Test 5 [y_o=0.351 ft, y_o/y_c=0.982]													
1	1.22		0.538	0.546	3.01	F	6	1.22	.541	.583	.588	2.70	S
2	1.22	0.434	.539	.547	3.00	UL	7	1.22	.616	.641	.648	2.33	S
3	1.22	.459	.539	.547	3.00	IS	8	1.22	.672	.690	.697	2.09	S
4	1.22	.474	.543	.551	2.97	S	9	1.22	.326	.539	.547	3.00	LL
5	1.22	.507	.557	.565	2.86	S							
Test 6 [y_o=0.470 ft, y_o/y_c=0.968]													
1	1.92		0.711	0.728	3.09	F	3	1.92	.607	.714	.731	3.07	IS
2	1.92	0.603	.714	.731	3.07	UL	4	1.92	.475	.714	.731	3.07	LL
Test 7 [y_o=0.415 ft, y_o/y_c=0.965]													
1	1.60		0.635	0.648	3.06	F							
MODEL F													
Test 1 [y_o=0.106 ft, y_o/y_c=1.04]													
1	0.183		0.155	0.155	3.00	F	5	.183	.184	.190	.190	2.21	S
2	.183	0.116	.156	.156	2.97	UL	6	.183	.234	.237	.237	1.59	S
3	.183	.127	.156	.156	2.97	IS	7	.183	.040	.156	.156	2.97	LL
4	.183	.152	.165	.165	2.73	S							
Test 2 [y_o=0.138 ft, y_o/y_c=1.02]													
1	0.281		0.205	0.206	3.01	F	6	.281	.265	.271	.272	1.98	S
2	.281	0.150	.206	.207	2.99	UL	7	.281	.299	.304	.305	1.67	S
3	.281	.169	.206	.207	2.99	IS	8	.281	.328	.331	.332	1.47	S
4	.281	.199	.215	.216	2.80	S	9	.281	.076	.206	.207	2.99	LL
5	.281	.229	.240	.241	2.38	S							
Test 3 [y_o=0.206 ft, y_o/y_c=1.06]													
1	0.484		0.291	0.293	3.06	F	7	.484	.325	.342	.344	2.40	S
2	.484	0.217	.293	.295	3.02	UL	8	.484	.338	.352	.354	2.30	S
3	.484	.240	.293	.295	3.02	IS	9	.484	.381	.390	.392	1.98	S
4	.484	.246	.294	.296	3.01	S	10	.484	.428	.435	.436	1.68	S
5	.484	.264	.297	.299	2.96	S	11	.484	.491	.495	.496	1.38	S
6	.484	.285	.309	.311	2.80	S	12	.484	.142	.292	.294	3.04	LL

TABLE 3.—*Summary of data for discharge characteristics*—Continued

Run No.	q (cfs per ft)	t (feet)	h (feet)	H_o (feet)	C	Remarks	Run No.	q (cfs per ft)	t (feet)	h (feet)	H_o (feet)	C	Remarks
MODEL F—Continued													
Test 4													
[y_o=0.289 ft, y_o/y_c=1.03]													
1	0.841		0.420	0.425	3.04	F	7	.841	.446	.472	.476	2.56	S
2	.841	0.335	.421	.426	3.03	UL	8	.841	.492	.512	.516	2.27	S
3	.841	.346	.421	.426	3.03	IS	9	.841	.539	.554	.558	2.02	S
4	.841	.373	.423	.428	3.01	S	10	.841	.592	.602	.606	1.78	S
5	.841	.393	.433	.438	2.99	S	11	.841	.646	.655	660	1.57	S
6	.841	.427	.458	.462	2.67	S	12	.841	.245	.421	426	3.03	LL
Test 5													
[y_o=0.356 ft, y_o/y_c=0.994]													
1	1.21		0.532	0.540	3.05	F	5	1.21	.542	.579	.587	2.69	S
2	1.21	0.432	.534	.542	3.03	UL	6	1.21	.614	.608	.645	2.34	S
3	1.21	.444	.534	.542	3.03	IS	7	1.21	.676	.691	.697	2.08	S
4	1.21	.464	.535	.543	3.02	S	8	1.21	.329	.532	.540	3.05	LL
Test 6													
[y_o=0.465 ft, y_o/y_c=0.974]													
1	1.88		0.701	0.717	3.09	F	3	1.88	.601	.703	719	3.08	IS
2	1.88	0.594	.703	.719	3.08	UL	4	1.88	.477	.701	.717	3.09	LL
Test 7													
[y_o=0.409 ft, y_o/y_c=0.979]													
1	1.53		0.617	0.629	3.07	F							
MODEL G													
Test 1													
[y_o=0.084 ft, y_o/y_c=1.04]													
1	0.130		0.122	0.122	3.05	F	4	.130	.127	132	132	2.71	S
2	.130	0.071	.122	.122	3.05	UL	5	.130	.157	.160	.160	2.03	S
3	.130	.107	.122	.122	3.05	IS	6	.130	—.001	.122	.122	3.05	LL
Test 2													
[y_o=0.140 ft, y_o/y_c=1.04]													
1	0.282		0.203	0.204	3.06	F	6	.282	.244	.251	.252	2.23	S
2	.282	0.140	.203	.204	3.06	UL	7	.282	.273	.278	.279	1.91	S
3	.282	.178	.203	.204	3.06	IS	8	.282	.300	.304	.305	1.68	S
4	.282	.197	.212	.213	2.87	S	9	.282	.069	.203	.204	3.06	LL
5	.282	.217	.229	.230	2.56	S							
Test 3													
[y_o=0.189 ft, y_o/y_c=1.03]													
1	0.447		0.277	0.278	3.04	F	6	.447	.326	338	.339	2.26	S
2	.447	0.199	.277	.278	3.04	UL	7	.447	.368	.376	.377	1.93	S
3	.447	.243	.277	278	3.04	IS	8	.447	.409	.415	.416	1.66	S
4	.447	.257	.282	.284	2.96	S	9	.447	.456	.459	.460	1.43	S
5	.447	.288	.303	.304	2.66	S	10	.447	.114	.277	.278	3.04	LL
Test 4													
[y_o=0.274 ft, y_o/y_c=1.02]													
1	0.789		0.402	0.406	3.05	F	6	.789	.427	.451	.455	2.57	S
2	.789	0.311	.402	.406	3.05	UL	7	.789	.459	.477	.481	2.37	S
3	.789	.341	.402	.406	3.05	IS	8	.789	.538	.549	.552	1.92	S
4	.789	.363	.406	.410	3.01	S	9	.789	.616	.623	.626	1.59	S
5	.789	.393	.424	.428	2.82	S	10	.789	.213	.402	.406	3.05	LL

TABLE 3.—*Summary of data for discharge characteristics*—Continued

Run No.	q (cfs per ft)	t (feet)	h (feet)	H_o (feet)	C	Remarks	Run No.	q (cfs per ft)	t (feet)	h (feet)	H_o (feet)	C	Remarks
MODEL G—Continued													
Test 5													
[y_o=0.359 ft, y_o/y_c=1.02]													
1	1.17		0.520	0.528	3.06	F	6	1.17	.553	.583	.590	2.58	S
2	1.17	0.418	.520	.528	3.06	UL	7	1.17	.607	.628	.635	2.32	S
3	1.17	.447	.520	.528	3.06	IS	8	1.17	.660	.676	.682	2.08	S
4	1.17	.457	.523	.531	3.03	S	9	1.17	.309	.520	.528	3.06	LL
5	1.17	.483	.530	.538	2.97	S							
Test 6													
[y_o=0.474 ft, y_o/y_c=0.980]													
1	1.91		0.701	0.718	3.14	F	3	1.91	.598	.702	.719	3.13	IS
2	1.91	0.592	.702	.719	3.13	UL	4	1.91	.462	.702	.719	3.13	LL
Test 7													
[y_o=0.411 ft, y_o/y_c=1.01]													
1	1.48		0.602	0.613	3.08	F							
MODEL H													
Test 1													
[y_o=0.081 ft, y_o/y_c=1.04]													
1	0.123		0.118	0.118	3.02	F	5	.123	.109	.120	.120	2.94	S
2	.123	0.065	.118	.118	3.02	UL	6	.123	.128	.131	.131	2.58	S
3	.123	.074	.118	.118	3.02	IS	7	.123	.142	.144	.144	2.24	S
4	.123	.084	.119	.119	2.98	S	8	.123	−.017	.118	.118	3.02	LL
Test 2													
[y_o=0.127 ft, y_o/y_c=1.02]													
1	0.247		0.186	0.187	3.07	F	6	.247	.199	.208	.209	2.60	S
2	.247	0.129	.187	.188	3.05	UL	7	.247	.219	.226	.227	2.30	S
3	.247	.145	.187	.188	3.05	IS	8	.247	.255	.259	.260	1.87	S
4	.247	.161	.188	.198	3.02	S	9	.247	.048	.186	.187	3.07	LL
5	.247	.181	.193	.194	2.91	S							
Test 3													
[y_o=0.187 ft, y_o/y_c=1.02]													
1	0.446		0.274	0.276	3.08	F	7	.446	.312	.325	.326	2.39	S
2	.446	0.196	.275	.277	3.06	UL	8	.446	.345	.355	.356	2.10	S
3	.446	.223	.275	.277	3.06	IS	9	.446	.380	.387	.388	1.84	S
4	.446	.232	.276	.278	3.05	S	10	.446	.427	.431	.432	1.57	S
5	.446	.250	.278	.280	3.02	S	11	.446	.108	.274	.276	3.08	LL
6	.446	.269	.290	.292	2.83	S							
Test 4													
[y_o=0.277 ft, y_o/y_c=1.02]													
1	0.799		0.404	0.408	3.06	F	6	.799	.431	.454	.458	2.58	S
2	.799	0.309	.405	.409	3.05	UL	7	.799	.488	.504	.508	2.21	S
3	.799	.347	.405	.409	3.05	IS	8	.799	.539	.550	.553	1.94	S
4	.799	.353	.406	.410	3.04	S	9	.799	.591	.598	.601	1.71	S
5	.799	.378	.415	.419	2.95	S	10	.799	.198	.404	.408	3.06	LL
Test 5													
[y_o=0.353 ft, y_o/y_c=1.01]													
1	1.17		0.517	0.525	3.09	F	5	1.17	.534	.568	.575	2.69	S
2	1.17	0.426	.520	.528	3.07	UL	6	1.17	.599	.622	.629	2.36	S
3	1.17	.442	.520	.528	3.07	IS	7	1.17	.647	.665	.672	2.14	S
4	1.17	.465	.523	.531	3.04	S	8	1.17	.291	.518	.526	3.08	LL

TABLE 3.—*Summary of data for discharge characteristics*—Continued

Run No.	q (cfs per ft)	t (feet)	h (feet)	H_o (feet)	C	Remarks	Run No.	q (cfs per ft)	t (feet)	h (feet)	H_o (feet)	C	Remarks
MODEL H—Continued													
Test 6													
[y_o=0.463 ft, y_o/y_c=0.977]													
1	1.84		0.682	0.698	3.16	F	3	1.84	.583	.687	.702	3.12	IS
2	1.84	0.580	.687	.702	3.12	UL	4	1.84	.446	.685	.700	3.14	LL
Test 7													
[y_o=0.416 ft, y_o/y_c=0.998]													
1	1.52		0.606	0.618	3.14	F							
MODEL I													
Test 1													
[y_o=0.135 ft, y_o/y_c=1.04]													
1	0.266		0.196	0.197	3.05	F	5	.266	.219	.235	.236	2.33	S
2	.266	0.130	.197	.198	3.03	UL	6	.266	.270	.279	.280	1.80	S
3	.266	.161	.197	.198	3.03	IS	7	.266	.355	.259	.360	1.23	S
4	.266	.185	.208	.209	2.79	S	8	.266	.065	.197	.198	3.03	LL
Test 2													
[y_o=0.219 ft, y_o/y_c=1.01]													
1	0.573		0.325	0.327	3.06	F	5	.573	.348	.373	.375	2.49	S
2	.573	0.236	.326	.328	3.04	UL	6	.573	.400	.418	.420	2.10	S
3	.573	.265	.326	.328	3.04	IS	7	.573	.551	.558	.560	1.37	S
4	.573	.303	.342	.344	2.83	S	8	.573	.164	.326	.328	3.04	LL
Test 3													
[y_o=0.345 ft, y_o/y_c=1.09]													
1	1.01		0.473	0.479	3.05	F	6	1.01	.552	.584	.589	2.24	S
2	1.01	0.380	.475	.481	3.03	UL	7	1.01	.615	.635	.640	1.98	S
3	1.01	.395	.475	.481	3.03	IS	8	1.01	.689	.704	.709	1.70	S
4	1.01	.434	.491	.497	2.89	S	9	1.01	.265	.473	.479	3.05	LL
5	1.01	.479	.521	.527	2.64	S							
Test 4													
[y_o=0.404 ft, y_o/y_c=0.978]													
1	1.50		0.608	0.620	3.08	F	5	1.50	.593	.650	.661	2.80	S
2	1.50	0.489	.610	.622	3.07	UL	6	1.50	.673	.711	.721	2.45	S
3	1.50	.496	.610	.622	3.07	IS	7	1.50	.389	.609	.620	3.08	LL
4	1.50	.538	.617	.628	3.02	S							
Test 5													
[y_o=0.467 ft, y_o/y_c=0.967]													
1	1.90		0.704	0.721	3.11	F	3	1.90	.600	.705	.722	3.10	IS
2	1.90	0.585	.705	.722	3.10	UL	4	1.90	.473	.704	.721	3.11	LL
MODEL J													
Test 1													
[y_o=0.111 ft, y_o/y_c=1.01]													
1	0.205		0.164	0.164	3.08	F	5	.205	.202	.209	.209	2.14	S
2	.205	0.128	.164	.164	3.08	UL	6	.205	.239	.242	.242	1.72	S
3	.205	.148	.164	.164	3.08	IS	7	.205	.032	.164	.164	3.08	LL
4	.205	.171	.182	.182	2.62	S							

TABLE 3.—*Summary of data for discharge characteristics*—Continued

Run No.	q (cfs per ft)	t (feet)	h (feet)	H_o (feet)	C	Remarks	Run No.	q (cfs per ft)	t (feet)	h (feet)	H_o (feet)	C	Remarks
MODEL J—Continued													
Test 2													
[y_o=0.210 ft, y_o/y_c=1.05]													
1	0.508		0.298	0.300	3.10	F	6	.508	.328	.346	.348	2.48	S
2	.508	0.228	.298	.300	3.10	UL	7	.508	.407	.415	.417	1.89	S
3	.508	.245	.298	.300	3.10	IS	8	.508	.483	.489	.491	1.48	S
4	.508	.259	.299	.301	3.08	S	9	.508	.127	.298	.300	3.10	LL
5	.508	.286	.312	.314	2.89	S							
Test 3													
[y_o=0.321 ft, y_o/y_c=1.02]													
1	1.01		0.467	0.473	3.10	F	5	1.01	.533	.558	.563	2.38	S
2	1.01	0.374	.468	.474	3.09	UL	6	1.01	.619	.636	.641	1.96	S
3	1.01	.402	.468	.474	3.09	IS	7	1.01	.246	.467	.473	3.10	LL
4	1.01	.452	.491	.497	2.88	S							
Test 4													
[y_o=0.399 ft, y_o/y_c=0.982]													
1	1.47		0.594	0.605	3.12	F	5	1.47	.591	.634	.645	2.84	S
2	1.47	0.493	.597	.608	3.10	UL	6	1.47	.673	.700	.710	2.46	S
3	1.47	.503	.597	.608	3.10	IS	7	1.47	.346	.595	.606	3.11	LL
4	1.47	.547	.606	.617	3.03	S							
Test 5													
[y_o=0.471 ft, y_o/y_c=0.967]													
1	1.93		0.699	0.716	3.18	F	3	1.93	.609	.704	.721	3.15	IS
2	1.93	0.588	.704	.721	3.15	UL	4	1.93	.451	.701	.718	3.17	LL
MODEL K-2													
Test 1													
[y_o=0.111 ft, y_o/y_c=0.974]													
1	0.219		0.172	0.172	3.06	F	7	.219	.238	.243	.243	1.83	S
2	.219	0.121	.172	.172	3.06	UL	8	.219	.251	.255	.255	1.70	S
3	.219	.141	.172	.172	3.06	IS	9	.219	.284	.287	.287	1.42	S
4	.219	.148	.173	.173	3.04	S	10	.219	.202	.208	.208	2.30	S
5	.219	.166	.178	.178	2.91	S	11	.219	.184	.190	.190	2.64	S
6	.219	.207	.214	.214	2.21	S	12	.219	.015	.172	.172	3.06	LL
Test 2													
[y_o=0.144 ft, y_o/y_c=0.972]													
1	0.324		0.223	0.224	3.06	F	6	.324	.238	.252	.253	2.55	S
2	.324	0.174	.233	.224	3.06	UL	7	.324	.279	.286	.287	2.11	S
3	.324	.194	.223	.224	3.06	IS	8	.324	.314	.320	.320	1.79	S
4	.324	.196	.224	.225	3.04	S	9	.324	.086	.223	.224	3.06	LL
5	.324	.201	.225	.226	3.02	S							
Test 3													
[y_o=0.208 ft, y_o/y_c=1.00]													
1	0.538		0.312	0.314	3.06	F	7	.538	.395	.408	.409	2.06	S
2	.538	0.241	.312	.314	3.06	UL	8	.538	.445	.454	.455	1.75	S
3	.538	.269	.312	.314	3.06	IS	9	.538	.482	.490	491	1.56	S
4	.538	.274	.314	.316	3.03	S	10	.538	.541	.548	.548	1.32	S
5	.538	.302	.328	.330	2.83	S	11	.538	.155	.312	.314	3.06	LL
6	.538	.344	.363	.364	2.45	S							

TABLE 3.—*Summary of data for discharge characteristics*—Continued

Run No.	q (cfs per ft)	t (feet)	h (feet)	H_o (feet)	C	Remarks	Run No.	q (cfs per ft)	t (feet)	h (feet)	H_o (feet)	C	Remarks
MODEL K-2—Continued													
Test 4													
[y_o=0.283 ft, y_o/y_c=1.04]													
1	0.805		0.407	0.411	3.05	F	7	.805	.493	.511	.515	2.18	S
2	.805	0.307	.407	.411	3.05	UL	8	.805	.525	.542	.546	1.99	S
3	.805	.349	.407	.411	3.05	IS	9	.805	.556	.570	.573	1.86	S
4	.805	.386	.424	.428	2.87	S	10	.805	.593	.606	.609	1.69	S
5	.805	.437	.462	.466	2.53	S	11	.805	.621	.631	.634	1.59	S
6	.805	.463	.485	.489	2.36	S	12	.805	.206	.407	.411	3.05	LL
Test 5													
[y_o=0.363 ft, y_o/y_c=1.02]													
1	1.20		0.524	0.532	3.09	F	6	1.20	.581	.612	.619	2.46	S
2	1.20	0.413	.524	.532	3.09	UL	7	1.20	.642	.664	.670	2.19	S
3	1.20	.433	.524	.532	3.09	IS	8	1.20	.702	.719	.725	1.94	S
4	1.20	.480	.534	.542	3.00	S	9	1.20	.297	.523	.531	3.10	LL
5	1.20	.528	.570	.577	2.74	S							
Test 6													
[y_o=0.420 ft, y_o/y_c=0.975]													
1	1.60		0.633	0.645	3.09	F	3	1.60	.549	.633	.645	3.09	IS
2	1.60	0.510	.633	.645	3.09	UL	4	1.60	.388	.632	.644	3.10	LL
MODEL L													
Test 1													
[y_o=0.106 ft, y_o/y_c=1.04]													
1	0.183		0.155	0.155	3.00	F	4	.183	.169	.179	.179	2.42	S
2	.183	0.043	.155	.155	3.00	UL	5	.183	.209	.212	.212	1.88	S
3	.183	.133	.155	.155	3.00	IS	6	.183	−.006	.155	.155	3.00	LL
Test 2													
[y_o=0.218 ft, y_o/y_c=1.07]													
1	0.524		0.307	0.309	3.05	F	5	.524	.323	.349	.351	2.52	S
2	.524	0.142	.307	.309	3.05	UL	6	.524	.440	.451	.453	1.72	S
3	.524	.250	.307	.309	3.05	IS	7	.524	.505	.513	.515	1.42	S
4	.524	.280	.317	.319	2.91	S	8	.524	.072	.307	.309	3.05	LL
Test 3													
[y_o=0.328 ft, y_o/y_c=1.04]													
1	1.01		0.472	0.478	3.06	F	6	1.01	.512	.549	.555	2.45	S
2	1.01	0.252	.472	.478	3.06	UL	7	1.01	.573	.600	.605	2.15	S
3	1.01	.396	.472	.478	3.06	IS	8	1.01	.650	.667	.672	1.84	S
4	1.01	.434	.492	.498	2.88	S	9	1.01	.740	.752	.756	1.54	S
5	1.01	.455	.504	.510	2.78	S	10	1.01	.187	.472	.478	3.06	LL
Test 4													
[y_o=0.411 ft, y_o/y_c=1.00]													
1	1.49		0.605	0.616	3.07	F	5	1.49	.633	.680	.682	2.64	S
2	1.49	0.364	.605	.616	3.07	UL	6	1.49	.680	.717	.727	2.40	S
3	1.49	.513	.606	.617	3.06	IS	7	1.49	.299	.605	.616	3.07	LL
4	1.49	.579	.640	.651	2.84	S							
Test 5													
[y_o=0.467 ft, y_o/y_c=0.983]													
1	1.86		0.693	0.709	3 11	F	3	1.86	.590	.694	.710	3.10	IS
2	1.86	0.448	.693	.709	3.11	UL	4	1.86	.375	.693	.709	3.11	LL

TABLE 3.—*Summary of data for discharge characteristics*—Continued

Run No.	q (cfs per ft)	t (feet)	h (feet)	H_o (feet)	C	Remarks	Run No.	q (cfs per ft)	t (feet)	h (feet)	H_o (feet)	C	Remarks
MODEL M													
Test 1													
[y_o=0.106 ft, y_o/y_c=1.02]													
1	0.190		0.155	0.155	3.10	F	5	.190	.182	.189	.189	2.30	S
2	.190	0.101	.157	.157	3.04	UL	6	.190	.217	.221	.221	1.82	S
3	.190	.140	.157	.157	3.04	IS	7	.190	.247	.250	.250	1.52	S
4	.190	.160	.171	.171	2.68	S	8	.190	.049	.157	.157	3.04	LL
Test 2													
[y_o=0.230 ft, y_o/y_c=1.05]													
1	0.581		0.327	0.330	3.07	F	6	.581	.362	.379	.381	2.47	S
2	.581	0.227	.328	.331	3.06	UL	7	.581	.399	.412	.414	2.18	S
3	.581	.278	.328	.331	3.06	IS	8	.581	.443	.452	.454	1.90	S
4	.581	.296	.331	.334	3.02	S	9	.581	.499	.506	.508	1.61	S
5	.581	.323	.348	.350	2.80	S	10	.581	.189	.328	.331	3.06	LL
Test 3													
[y_o=0.334 ft, y_o/y_c=1.03]													
1	1.04		0.482	0.488	3.05	F	6	1.04	.510	.537	.543	2.60	S
2	1.04	0.356	.483	.490	3.04	UL	7	1.04	.554	.574	.580	2.36	S
3	1.04	.400	.483	.490	3.04	IS	8	1.04	.615	.629	.634	2.06	S
4	1.04	.430	.485	.492	3.02	S	9	1.04	.330	.482	.488	3.05	LL
5	1.04	.471	.506	.512	2.84	S							
Test 4													
[y_o=0.407 ft, y_o/y_c=0.981]													
1	1.51		0.610	0.622	3.08	F	5	1.51	.620	.650	.661	2.81	S
2	1.51	0.496	.611	.623	3.08	UL	6	1.51	.669	.689	.700	2.58	S
3	1.51	.526	.611	.623	3.08	IS	7	1.51	.475	.611	.623	3.08	LL
4	1.51	.565	616	.628	3.04	S							
Test 5													
[y_o=0.481 ft, y_o/y_c=0.985]													
1	1.94		0.710	0.727	3.13	F	3	1.94	.621	.712	.729	3.12	IS
2	1.94	0.603	.712	.729	3.12	UL	4	1.94	.555	712	729	3.12	LL
MODEL AA-2 [2]													
Test 1													
[y_o=0.032 ft, y_o/y_c=1.03]													
1	0.0306		0.048	0.048	2.96	F	4	.0306	.068	.072	.072	1.60	S
2	.0306	−0.011	.049	.049	2.88	UL	5	.0306	.123	.126	.126	0.689	S
3	.0306	.016	.050	.050	2.78	IS	6	.0306	−.062	.048	.048	2.96	LL
Test 2													
[y_o=0.063 ft, y_o/y_c=1.07]													
1	0.0814		0.091	0.091	2.98	F	5	.0184	.130	.135	.135	1.73	S
2	.0814	0.008	.091	.091	2.98	UL	6	.0814	.184	.187	.187	1.06	S
3	.0814	.039	.092	.092	2.94	IS	7	.0814	.232	234	.234	0.756	S
4	.0814	.082	.095	.095	2.80	S	8	.0814	−.059	.091	.091	2.98	LL
Test 3													
[y_o=0.110 ft, y_o/y_c=1.08]													
1	0.185		0.157	0.157	2.98	F	5	.185	.235	.241	.241	1.56	S
2	.185	0.055	.157	.157	2.98	UL	6	.185	.296	.300	.300	1.12	S
3	.185	.096	.158	.158	2.95	IS	7	.185	.336	.339	.339	0.937	S
4	.185	.181	.192	.192	2.20	S	8	.185	−.019	.157	.157	2.98	LL

See footnote at end of table, p. A106.

TABLE 3.—*Summary of data for discharge characteristics*—Continued

Run No.	q (cfs per ft)	t (feet)	h (feet)	H_o (feet)	C	Remarks	Run No.	q (cfs per ft)	t (feet)	h (feet)	H_o (feet)	C	Remarks
MODEL AA-2—Continued													
Test 4 [y_o=0.142 ft, y_o/y_c=1.06]													
1	0.304		0.218	0.218	2.98	F	5	.304	.221	.250	.250	2.43	S
2	.304	0.096	.220	.220	2.94	UL	6	.304	.305	.323	.323	1.65	S
3	.304	.142	.221	.221	2.92	IS	7	.304	.412	.425	.425	1.10	S
4	.304	.185	.223	.223	2.88	S	8	.304	.026	.219	.219	2.96	LL
Test 5 [y_o=0.199 ft, y_o/y_c=1.06]													
1	0.504		0.304	0.305	2.99	F	5	.504	.343	.366	.367	2.27	S
2	.504	0.158	.305	.306	2.98	UL	6	.504	.418	432	.433	1.77	S
3	.504	.206	.306	.307	2.96	IS	7	.504	.479	.490	.491	1.46	S
4	.504	.250	.307	.308	2.95	S	8	.504	.046	.304	.305	2.99	LL
Test 6 [y_o=0.260 ft, y_o/y_c=1.05]													
1	0.750		0.392	0.395	3.02	F	6	.750	.452	.479	.482	2.24	S
2	.750	0.233	.393	.396	3.01	UL	7	.750	.487	.507	.510	2.06	S
3	.750	.291	.394	.397	3.00	IS	8	.750	.530	.546	.549	1.84	S
4	.750	.347	.403	.406	2.90	S	9	.750	.116	.392	.395	3.02	LL
5	.750	.407	.441	.444	2.53	S							
Test 7 [y_o=0.350 ft, y_o/y_c=1.04]													
1	1.11		0.503	0.510	3.04	F	6	1.11	.521	.563	.569	2.57	S
2	1.11	0.318	.504	.511	3.03	UL	7	1.11	.567	.600	.606	2.34	S
3	1.11	.357	.505	.512	3.02	IS	8	1.11	.620	.645	.651	2.10	S
4	1.11	.395	.506	.513	3.01	S	9	1.11	.186	.503	.510	3.04	LL
5	1.11	.467	.526	.532	2.84	S							
Test 8 [y_o=0.412 ft, y_o/y_c=1.00]													
1	1.50		0.611	0.622	3.06	F	6	1.50	.624	.673	.684	2.65	S
2	1.50	0.402	.612	.623	3.05	UL	7	1.50	.679	.715	.726	2.42	S
3	1.50	.443	.613	.624	3.04	IS	8	1.50	.706	.739	.750	2.31	S
4	1.50	.498	.616	.627	3.02	S	9	1.50	.274	.611	.622	3.06	LL
5	1.50	.560	.630	.641	2.92	S							
Test 9 [y_o=0.451 ft, y_o/y_c=0.978]													
1	1.72		0.668	0.682	3.06	F	3	1.72	.503	.671	.685	3.04	IS
2	1.72	0.449	.670	.684	3.05	UL	4	1.72	.333	.668	.682	3.06	LL
Test 10 [y_o=0.499 ft, y_o/y_c=0.982]													
1	2.06		0.744	0.762	3.09	F	3	2.06	.577	.747	.765	3.07	IS
2	2.06	0.515	.746	.764	3.08	UL	4	2.06	.405	.744	.762	3.09	LL
MODEL AB[3]													
Test 1 [y_o=0.038 ft, y_o/y_c=1.00]													
1	0.0421		0.058	0.058	3.05	F	5	.0421	.096	.099	.099	1.36	S
2	.0421	0.000	.058	.058	3.05	UL	6	.0421	.124	.126	.126	0.948	S
3	.0421	.036	.059	.059	2.98	IS	7	.0421	.159	.162	.162	.649	S
4	.0421	.070	.073	.073	2.16	S	8	.0421	−.105	.058	.058	3.05	LL

See footnote at end of table, p. A106.

TABLE 3.—*Summary of data for discharge characteristics*—Continued

Run No.	q (cfs per ft)	t (feet)	h (feet)	H_o (feet)	C	Remarks	Run No.	q (cfs per ft)	t (feet)	h (feet)	H_o (feet)	C	Remarks
MODEL AB—Continued													
Test 2													
[y_o=0.076 ft, y_o/y_c=1.01]													
1	0.117		0.115	0.115	3.02	F	6	.117	.147	.154	.154	1.95	S
2	.117	0.036	.117	.117	2.95	UL	7	.117	.166	.172	.172	1.65	S
3	.117	.067	.118	.118	2.91	IS	8	.117	.199	.203	.203	1.29	S
4	.117	.101	.119	.119	2.87	S	9	.117	−.092	.115	.115	3.02	LL
5	.117	.125	.135	.135	2.37	S							
Test 3													
[y_o=0.132 ft, y_o/y_c=1.02]													
1	0.262		0.195	0.195	3.04	F	6	.262	.234	.249	.249	2.11	S
2	.262	0.092	.197	.197	3.00	UL	7	.262	.273	.283	.283	1.74	S
3	.262	.136	.198	.198	2.97	IS	8	.262	.305	.313	.313	1.50	S
4	.262	.169	.201	.201	2.91	S	9	.262	−.093	.195	.195	3.04	LL
5	.262	.201	.221	.221	2.52	S							
Test 4													
[y_o=0.189 ft, y_o/y_c=1.03]													
1	0.446		0.279	0.280	3.01	F	6	.446	.339	.357	.358	2.08	S
2	.446	0.162	.281	.282	2.98	UL	7	.446	.365	.380	.381	1.90	S
3	.446	.232	.282	.283	2.96	IS	8	.446	.415	.427	.428	1.60	S
4	.446	.269	.300	.301	2.70	S	9	.446	.035	.279	.280	3.01	LL
5	.446	.297	.322	.323	2.43	S							
Test 5													
[y_o=0.245 ft, y_o/y_c=1.04]													
1	0.649		0.356	0.358	3.03	F	6	.649	.370	.402	.404	2.53	S
2	.649	0.218	.358	.360	3.00	UL	7	.649	.408	.433	.435	2.26	S
3	.649	.286	.359	.361	2.99	IS	8	.649	.450	.470	.472	2.00	S
4	.649	.314	.363	.365	2.94	S	9	.649	.095	.356	.358	3.03	LL
5	.649	.341	.382	.384	2.73	S							
Test 6													
[y_o=0.308 ft, y_o/y_c=1.03]													
1	0.930		0.449	0.454	3.04	F	6	.930	.444	.488	.493	2.69	S
2	.930	0.285	.450	.455	3.03	UL	7	.930	.489	.524	.528	2.42	S
3	.930	.356	.451	.456	3.02	IS	8	.930	.535	.561	.565	2.19	S
4	.930	.382	.453	.458	3.00	S	9	.930	.141	.449	.454	3.04	LL
5	.930	.412	.467	.472	2.87	S							
Test 7													
[y_o=0.354 ft, y_o/y_c=0.995]													
1	1.21		0.532	0.540	3.06	F	6	1.21	.512	.567	.571	2.78	S
2	1.21	0.356	.533	.541	3.05	UL	7	1.21	.564	.604	.611	2.54	S
3	1.21	.409	.534	.542	3.04	IS	8	1.21	.604	.637	.644	2.35	S
4	1.21	.452	.537	.544	3.02	S	9	1 21	.221	.532	.540	3.06	LL
5	1.21	.480	.546	.553	2.94	S							
Test 8													
[y_o=0.409 ft, y_o/y_c=0.970]													
1	1.56		0.627	0.638	3.06	F	6	1.56	.619	.675	.686	2.75	S
2	1.56	0.430	.628	.639	3.05	UL	7	1.56	.664	.710	.720	2.55	S
3	1.56	.491	.629	.640	3.04	IS	8	1.56	.711	.758	.768	2.32	S
4	1.56	.520	.631	.642	3.03	S	9	1.56	.295	.627	.638	3.06	LL
5	1.56	.561	.639	.650	2.97	S							

TABLE 3.—*Summary of data for discharge characteristics*—Continued

Run No.	q (cfs per ft)	t (feet)	h (feet)	H_o (feet)	C	Remarks	Run No.	q (cfs per ft)	t (feet)	h (feet)	H_o (feet)	C	Remarks
MODEL AB—Continued													
Test 9													
[y_o=0.459 ft, y_o/y_c=0.987]													
1	1.87		0.705	0.720	3.06	F	4	1.87	.615	.712	.727	3.01	S
2	1.87	0.492	.706	.721	3.05	UL	5	1.87	.376	.705	.720	3.06	LL
3	1.87	.555	.708	.723	3.04	IS							
Test 10													
[y_o=0.057 ft, y_o/y_c=1.02]													
1	0.0748		0.087	0.087	2.93	F	3	.0748	.054	.089	.089	2.84	IS
2	.0748	0.017	.088	.088	2.88	UL	4	.0748	—.141	.087	.087	2.93	LL
Test 11													
[y_o=0.098 ft, y_o/y_c=1.03]													
1	0.167		0.146	0.146	3.00	F	3	.167	.100	.149	.149	2.91	IS
2	.167	0.068	.148	.148	2.94	UL	4	.167	—.156	.146	.146	3.00	LL
Test 12													
1	1.31		0.556	0.565	3.08	F	15	.193	—.134	.160	.160	3.02	LL
2	1.55		.624	.635	3.06	F	16	.297		.213	.213	3.02	F
3	1.83		.692	.707	3.08	F	17	.297	.104	.214	.214	3.00	UL
4	.0400		.056	.056	3.07	F	18	.297	.150	.215	.215	2.98	IS
5	.0400	—.010	.057	.057	2.99	UL	19	.297	—.059	.213	.213	3.02	LL
6	.0400	.027	.058	.058	2.90	IS	20	.362		.243	.244	3.01	F
7	.0400	—.116	.056	.056	3.07	LL	21	.362	.127	.244	.245	3.00	UL
8	.0969		.101	.101	3.04	F	22	.362	.170	.245	.246	2.98	IS
9	.0969	.024	.102	.102	2.99	UL	23	.362	—.005	.243	.244	3.01	LL
10	.0969	.059	.103	.103	2.95	IS	24	1.49		.611	.622	3.04	F
11	.0969	—.115	.101	.101	3.04	LL	25	1.61		.642	.654	3.05	F
12	.193		.160	.160	3.02	F	26	1.77		.682	.696	3.05	F
13	.193	.062	.161	.161	2.99	UL	27	2.02		.741	.758	3.06	F
14	.193	.104	.162	.162	2.96	IS							
MODEL AC [4]													
Test 1													
[y_o=0.038 ft, y_o/y_c=1.01]													
1	0.0346		0.052	0.052	2.90	F	5	.0346	.074	.076	.076	1.64	S
2	.0346	—0.021	.053	.053	2.82	UL	6	.0346	.098	.098	.098	1.12	S
3	.0346	.003	.054	.054	2.75	IS	7	.0346	.129	.129	.129	0.746	S
4	.0346	.045	.057	.057	2.53	S	8	.0346	—.074	.052	.052	2.90	LL
Test 2													
[y_o=0.068 ft, y_o/y_c=1.12]													
1	0.0844		0.096	0.096	2.83	F	5	.0844	.107	.116	.116	2.13	S
2	.0844	0.011	.097	.097	2.78	UL	6	.0844	.140	.145	.145	1.52	S
3	.0844	.043	.098	.098	2.74	IS	7	.0844	.185	.187	.187	1.04	S
4	.0844	.074	.099	.099	2.70	S	8	.0844	—.129	.096	.096	2.83	LL
Test 3													
[y_o=0.100 ft, y_o/y_c=1.08]													
1	0.159		0.145	0.145	2.86	F	6	.159	.204	.212	.212	1.62	S
2	.159	0.048	.147	.147	2.80	UL	7	.159	.231	.237	.237	1.37	S
3	.159	.107	.148	.148	2.78	IS	8	.159	.264	.268	.268	1.14	S
4	.159	.135	.155	.155	2.59	S	9	.159	—.098	.145	.145	2.86	LL
5	.159	.168	.179	.179	2.09	S							

See footnote at end of table, p. A106.

TABLE 3.—*Summary of data for discharge characteristics*—Continued

Run No.	q (cfs per ft)	t (feet)	h (feet)	H_o (feet)	C	Remarks	Run No.	q (cfs per ft)	t (feet)	h (feet)	H_o (feet)	C	Remarks
MODEL AC—Continued													
Test 4													
[y_o=0.137 ft, y_o/y_c=1.09]													
1	0.253		0.196	0.197	2.90	F	6	.253	.241	.254	.255	1.97	S
2	.253	0.081	.198	.199	2.85	UL	7	.253	.278	.287	.288	1.64	S
3	.253	.135	.199	.200	2.83	IS	8	.253	.319	.327	.328	1.35	S
4	.253	.171	.203	.204	2.75	S	9	.253	−.048	.197	.198	2.88	LL
5	.253	.212	.229	.230	2.30	S							
Test 5													
[y_o=0.175 ft, y_o/y_c=1.06]													
1	0.379		0.256	0.257	2.90	F	6	.379	.319	.335	.336	1.94	S
2	.379	0.131	.258	.259	2.87	UL	7	.379	.379	.390	.391	1.55	S
3	.379	.199	.259	.260	2.85	IS	8	.379	.427	.436	.437	1.31	S
4	.379	.227	.266	.267	2.74	S	9	.379	−.001	.257	.258	2.89	LL
5	.379	.264	.289	.290	2.42	S							
Test 6													
[y_o=0.226 ft, y_o/y_c=1.08]													
1	0.541		0.320	0.322	2.96	F	6	.541	.379	.398	.400	2.14	S
2	.541	0.174	.321	.323	2.94	UL	7	.541	.431	.445	.447	1.81	S
3	.541	.254	.322	.324	2.93	IS	8	.541	.477	.489	.491	1.57	S
4	.541	.304	.340	.342	2.70	S	9	.541	.044	.319	.321	2.97	LL
5	.541	.343	.368	.370	2.40	S							
Test 7													
[y_o=0.257 ft, y_o/y_c=1.06]													
1	0.678		0.370	0.373	2.97	F	6	.678	.406	.434	.437	2.35	S
2	.678	0.212	.371	.374	2.96	UL	7	.678	.452	.473	.476	2.07	S
3	.678	.280	.372	.375	2.95	IS	8	.678	.489	.506	.509	1.87	S
4	.678	.329	.381	.384	2.85	S	9	.678	.075	.370	.373	2.97	LL
5	.678	.368	.405	.408	2.60	S							
Test 8													
[y_o=0.306 ft, y_o/y_c=1.05]													
1	0.890		0.440	0.445	3.00	F	5	.890	.416	.466	.471	2.75	S
2	.890	0.264	.442	.447	2.98	UL	6	.890	.452	.491	.496	2.55	S
3	.890	.329	.443	.448	2.97	IS	7	890	.492	.523	.528	2.32	S
4	.890	.370	.446	.451	2.94	S	8	.890	.528	.553	.557	2.14	S
							9	.890	.076	.441	.446	2.99	LL
Test 9													
[y_o=0.360 ft, y_o/y_c=1.05]													
1	1.14		0.517	0.524	3.00	F	5	1.14	.549	.590	.597	2.47	S
2	1.14	0.338	.519	.526	2.99	UL	6	1.14	.598	.630	.637	2.25	S
3	1.14	.405	.520	.527	2.98	IS	7	1.14	.657	.684	.690	1.99	S
4	1.14	.468	.535	.542	2.86	S	8	1.14	.702	.724	.730	1.83	S
							9	1.14	.176	518	.525	3.00	LL
Test 10													
[y_o=0.402 ft, y_o/y_c=1.03]													
1	1.39		0.586	0.596	3.01	F	6	1.39	.666	.701	.710	2.32	S
2	1.39	0.401	.588	.598	3.00	UL	7	1.39	.721	.750	.759	2.10	S
3	1.39	.479	.590	.600	2.98	IS	8	1.39	.775	.798	.806	1.92	S
4	1.39	.551	.613	.620	2.84	S	9	1.39	.251	.586	.596	3.01	LL
5	1.39	.611	.657	.666	2.55	S							

TABLE 3.—*Summary of data for discharge characteristics*—Continued

Run No.	q (cfs per ft)	t (feet)	h (feet)	H_o (feet)	C	Remarks	Run No.	q (cfs per ft)	t (feet)	h (feet)	H_o (feet)	C	Remarks
MODEL AC—Continued													
Test 11													
[y_o=0.426 ft, y_o/y_c=1.02]													
1	1.53	0.421	0.623	0.635	3.03	F	3	1.53	.492	.626	.638	3.01	IS
2	1.53		.625	.637	3.02	UL	4	1.53	.303	.623	.635	3.03	LL
Test 12													
[y_o=0.445 ft, y_o/y_c=1.01]													
1	1.65	0.427	0.654	0.667	3.03	F	3	1.65	.461	.657	.670	3.01	IS
2	1.65		.656	.669	3.02	UL	4	1.65	.323	.654	.667	3.03	LL
Test 13													
[y_o=0.471 ft, y_o/y_c=0.999]													
1	1.84	0.464	0.700	0.715	3.04	F	3	1.84	.532	.704	.719	3.01	IS
2	1.84		.703	.718	3.02	UL	4	1.84	.352	.701	.716	3.03	LL
Test 14													
[y_o=0.488 ft, y_o/y_c=0.993]													
1	1.95		0.729	0.746	3.03	F							

[1] Model dimensions and other details are given in table 1.
[2] Head datum taken at mid-depth of screen on crown line.
[3] Head datum taken at smooth surface on crown line.
[4] Head datum taken at mid-depth of shot on crown line.

TABLE 4.—*Summary of data for boundary-layer velocity distribution* [1]

Station [2] (feet)	z [3] (feet $\times 10^3$)	u (fps)	U (fps)	Station [2] (feet)	z [3] (feet $\times 10^3$)	u (fps)	U (fps)	Station [2] (feet)	z [3] (feet $\times 10^3$)	u (fps)	U (fps)
MODEL A-1											
Test 1											
0.006	1.15	−0.264	0.532	.25	17.8	.629	.629	1.05	26.2	.961	.961
.006	1.57	.073	.532	.40	1.15	−.057	.720	1.05	34.5	.961	.961
.006	1.98	.264	.532	.40	1.98	.359	.720	1.65	1.15	.625	1.309
.006	2.40	.394	.532	.40	2.82	.474	.720	1.65	1.98	.687	1.309
.006	2.82	.532	.532	.40	4.48	.576	.720	1.65	2.82	.779	1.309
.006	4.48	.532	.532	.40	6.57	.717	.720	1.65	4.48	1.003	1.309
.006	9.48	.532	.532	.40	9.48	.717	.720	1.65	6.57	1.186	1.309
.006	12.8	.532	.532	.40	17.8	.717	.720	1.65	9.48	1.276	1.309
.006	14.9	.518	.532	.40	26.2	.724	.720	1.65	13.7	1.298	1.309
.006	17.8	.512	.532	.65	1.15	−.433	.830	1.65	17.8	1.309	1.309
.006	26.2	.532	.532	.65	1.98	.264	.830	1.65	26.2	1.309	1.309
.10	1.15	.401	.567	.65	2.82	.420	.830	1.65	34.5	1.309	1.309
.10	1.98	.469	.567	.65	4.48	.532	.830	1.85	1.15	.955	1.543
.10	2.82	.543	.567	.65	6.57	.743	.830	1.85	1.98	1.008	1.543
.10	4.48	.543	.567	.65	9.48	.825	.830	1.85	3.23	1.128	1.543
.10	6.57	.558	.567	.65	17.8	.832	.830	1.85	5.32	1.393	1.543
.10	9.48	.567	.567	.65	26.2	.828	.830	1.85	7.82	1.505	1.543
.10	18.0	.567	.567	1.05	1.15	−.057	.961	1.85	10.3	1.522	1.543
.25	1.15	−.073	.629	1.05	1.98	.414	.961	1.85	13.7	1.543	1.543
.25	1.98	.351	.629	1.95	2.82	.558	.961	1.85	17.8	1.543	1.543
.25	2.82	.469	.629	1.05	4.48	.751	.961	1.85	26.2	1.543	1.543
.25	4.48	.603	.629	1.05	6.57	.918	.961	1.85	34.5	1.543	1.543
.25	6.57	.625	.629	1.05	9.48	.964	.961				
.25	9.48	.621	.629	1.05	17.8	.961	.961				

See footnotes at end of table, p. A114.

TABLE 4.—*Summary of data for boundary-layer velocity distribution*—Continued

Station [2] (feet)	z^3 (feet $\times 10^3$)	u (fps)	U (fps)	Station [2] (feet)	z^3 (feet $\times 10^3$)	u (fps)	U (fps)	Station [2] (feet)	z^3 (feet $\times 10^3$)	u (fps)	U (fps)
MODEL A-1—Continued											
Test 2											
.006	1.15	.451	1.151	.40	1.15	.469	1.302	1.05	27.0	1.508	1.520
.006	1.98	.533	1.151	.40	1.98	.691	1.302	1.05	34.5	1.513	1.520
.006	2.82	.918	1.151	.40	2.82	.930	1.302	1.05	51.2	1.520	1.520
.006	4.48	1.098	1.151	.40	4.48	1.089	1.302	1.65	1.15	1.172	1.954
.006	6.57	1.151	1.151	.40	6.57	1.123	1.302	1.65	1.98	1.194	1.954
.006	9.48	1.151	1.151	.40	9.48	1.239	1.302	1.65	3.65	1.458	1.954
.006	17.8	1.151	1.151	.40	17.8	1.282	1.302	1.65	7.82	1.707	1.954
.006	26.2	1.151	1.151	.40	26.2	1.302	1.302	1.65	13.7	1.834	1.954
.10	1.15	.613	1.158	.40	34.5	1.302	1.302	1.65	20.3	1.907	1.954
.10	1.98	.733	1.158	.65	1.15	.765	1.455	1.65	27.0	1.933	1.954
.10	2.82	.819	1.158	.65	1.98	.988	1.455	1.65	34.5	1.945	1.954
.10	4.48	1.006	1.158	.65	3.23	1.148	1.455	1.65	51.2	1.950	1.954
.10	6.57	1.111	1.158	.65	5.73	1.269	1.455	1.65	59.5	1.954	1.954
.10	9.48	1.158	1.158	.65	9.48	1.346	1.455	2.00	1.15	1.593	2.212
.10	17.8	1.158	1.158	.65	15.7	1.420	1.455	2.00	1.98	1.637	2.212
.10	26.2	1.158	1.158	.65	22.0	1.437	1.455	2.00	3.65	1.849	2.212
.10	34.5	1.149	1.158	.65	28.2	1.441	1.455	2.00	7.82	2.030	2.212
.25	1.15	.809	1.258	.65	34.5	1.448	1.455	2.00	13.7	2.089	2.212
.25	1.98	.938	1.258	.65	51.2	1.451	1.455	2.00	20.3	2.125	2.212
.25	2.82	.994	1.258	.65	59.5	1.455	1.455	2.00	27.0	2.172	2.212
.25	4.48	1.069	1.258	1.05	1.15	.702	1.520	2.00	34.5	2.188	2.122
.25	6.57	1.153	1.258	1.05	1.98	.776	1.520	2.00	42.8	2.212	2.212
.25	9.48	1.204	1.258	1.05	3.65	1.014	1.520	2.00	51.2	2.212	2.212
.25	17.8	1.260	1.258	1.05	7.82	1.284	1.520	2.00	59.5	2.212	2.212
.25	26.2	1.258	1.258	1.05	13.7	1.413	1.520				
.25	34.5	1.258	1.258	1.05	20.3	1 455	1.520				
Test 3											
.006	1.15	.753	1.733	.40	51.2	1.867	1.867	1.65	4.48	1.943	2.475
.006	1.98	1.365	1.733	.65	1.15	1.275	2.032	1.65	7.40	2.050	2.475
.006	2.82	1.563	1.733	.65	1.98	1.407	2.032	1.65	10.3	2.125	2.475
.006	4.48	1.682	1.733	.65	4.48	1.658	2.032	1.65	15.3	2.240	2.475
.006	6.57	1.712	1.733	.65	7.82	1.784	2.032	1.65	22.0	2.327	2.475
.006	9.48	1.733	1.733	.65	12.0	1.866	2.032	1.65	26.2	2.384	2.475
.006	17.8	1.733	1.733	.65	17.8	1.945	2.032	1.65	42.8	2.410	2.475
.006	26.2	1.733	1.733	.65	26.2	2.003	2.032	1.65	51.2	2.470	2.475
.10	1.15	1.156	1.736	.65	34.5	2.030	2.032	1.65	59.5	2.475	2.475
.10	1.98	1.203	1.736	.65	42.8	2.030	2.032	1.65	67.8	2.475	2.475
.10	2.82	1.308	1.736	.65	51.2	2.032	2.032	1.85	1.15	1.598	2.624
.10	4.48	1.404	1.736	1.00	1.15	1.314	2.172	1.85	1.98	1.806	2.624
.10	6.57	1.530	1.736	1.00	1.98	1.494	2.172	1.85	4.48	2.060	2.624
.10	9.48	1.688	1.736	1.00	5.32	1.786	2.172	1.85	7.40	2.196	2.624
.10	17.8	1.736	1.736	1.00	9.48	1.915	2.172	1.85	10.3	2.295	2.624
.10	26.2	1.736	1.736	1.00	13.7	2.015	2.172	1.85	15.3	2.420	2.624
.10	34.5	1.732	1.736	1.00	17.8	2.090	2.172	1.85	22.0	2.500	2.624
.25	1.15	1.106	1.772	1.00	26.2	2.150	2.172	1.85	26.2	2.560	2.624
.25	1.98	1.186	1.772	1.00	34.5	2.172	2.172	1.85	34.5	2.580	2.624
.25	4.48	1.453	1.772	1.00	42.8	2.172	2.172	1.85	42.8	2.620	2.624
.25	7.82	1.559	1.772	1.00	51.2	2.172	2.172	1.85	51.2	2.624	2.624
.25	12 0	1.657	1.772	1.30	1.15	1.254	2.226	1.85	59.5	2.624	2.624
.25	17.8	1.746	1.772	1.30	1.98	1.474	2.226	2.00	1.15	1.722	2.759
.25	26.2	1.772	1.772	1.30	5.32	1.797	2.226	2.00	1.98	1.803	2.759
.25	34.5	1.772	1.772	1.30	9.48	1.904	2.226	2 00	4.48	2.176	2.759
.25	47.0	1.772	1.772	1.30	13.7	2.024	2.226	2.00	7.40	2.302	2.759
.40	1.15	1.195	1.867	1.30	17.8	2.097	2.226	2.00	10.3	2.394	2.759
.40	1.98	1.260	1.867	1.30	26.2	2.180	2.226	2.00	15.3	2.532	2.759
.40	4.48	1.552	1.867	1.30	34.5	2.220	2.226	2.00	22.0	2.620	2.759
.40	7.82	1.628	1.867	1.30	42.8	2.222	2.226	2.00	26.2	2.684	2.759
.40	12.0	1.716	1.867	1.30	51.2	2.226	2.226	2.00	34.5	2.702	2.759
.40	17.8	1.808	1.867	1.30	59.5	2.226	2.226	2.00	42.8	2.755	2.759
.40	26.2	1.860	1.867	1.65	1.15	1.504	2.475	2.00	51.2	2.755	2.759
.40	34.5	1.864	1.867	1.65	1.98	1.710	2.475	2.00	59.5	2.759	2.759
.40	42.8	1.867	1.867								

See footnotes at end of table, p. A114.

TABLE 4.—*Summary of data for boundary-layer velocity distribution*—Continued

Station [2] (feet)	z^3 (feet $\times 10^3$)	u^* (fps)	U (fps)	Station [2] (feet)	z^3 (feet $\times 10^3$)	u (fps)	U (fps)	Station [2] (feet)	z^3 (feet $\times 10^3$)	u (fps)	U (fps)
MODEL A-1—Continued											
Test 4											
.006	1.15	−1.718	2.452	.65	3.23	2.163	2.752	1.65	9.48	2.682	3.210
.006	1.98	−1.222	2.452	.65	6.15	2.331	2.752	1.65	13.7	2.851	3.210
.006	2.82	1.920	2.452	.65	9.48	2.436	2.752	1.65	17.8	2.947	3.210
.006	4.48	2.292	2.452	.65	13.7	2.538	2.752	1.65	22.0	3.040	3.210
.006	6.57	2.376	2.452	.65	17.8	2.627	2.752	1.65	26.2	3.104	3.210
.006	9.48	2.424	2.452	.65	22.0	2.676	2.752	1.65	34.5	3.160	3.210
.006	17.8	2.447	2.452	.65	26.2	2.706	2.752	1.65	42.8	3.192	3.210
.006	26.2	2.450	2.452	.65	34.5	2.740	2.752	1.65	51.2	3.198	3.210
.006	38.7	2.452	2.452	.65	42.8	2.750	2.752	1.65	59.5	3.210	3.210
.10	1.15	1.379	2.426	.65	51.2	2.752	2.752	1.65	67.8	3.210	3.210
.10	1.98	1.547	2.426	.65	59.5	2.752	2.752	1.65	76.2	3.210	3.210
.10	2.82	1.637	2.426	1.00	1.15	1.757	2.862	1.85	1.15	2.047	3.297
.10	4.48	1.776	2.426	1.00	1.98	1.946	2.862	1.85	1.98	2.252	3.297
.10	5.32	1.892	2.426	1.00	2.82	2.075	2.862	1.85	2.82	2.382	3.297
.10	6.57	2.016	2.426	1.00	6.15	2.312	2.862	1.85	6.15	2.623	3.297
.10	7.40	2.067	2.426	1.00	9.48	2.464	2.862	1.85	9.48	2.728	3.297
.10	9.48	2.255	2.426	1.00	13.7	2.610	2.862	1.85	13.7	2.947	3.297
.10	17.8	2.413	2.426	1.00	17.8	2.707	2.862	1.85	17.2	3.058	3.297
.10	26.2	2.426	2.426	1.00	22.0	2.765	2.862	1.85	22.0	3.142	3.297
.10	42.8	2.426	2.426	1.00	26.2	2.811	2.862	1.85	26.2	3.203	3.297
.25	1.15	1.562	2.458	1.00	34.5	2.843	2.862	1.85	34.5	3.260	3.297
.25	1.98	1.706	2.458	1.00	42.8	2.862	2.862	1.85	42.8	3.290	3.397
.25	3.23	1.836	2.458	1.00	51.2	2.862	2.862	1.85	51.2	3.292	3.297
.25	6.15	2.007	2.458	1.00	59.5	2.862	2.862	1.85	59.5	3.297	3.297
.25	9.48	2.139	2.458	1.30	1.15	1.828	2.976	1.85	67.8	3.297	3.297
.25	13.7	2.277	2.458	1.30	1.98	1.963	2.976	1.85	76.2	3.297	3.297
.25	17.8	2.377	2.458	1.30	2.82	2.092	2.976	1.85	92.8	3.297	3.297
.25	26.2	2.458	2.458	1.30	6.15	2.354	2.976	2.00	1.15	2.045	3.385
.25	34.5	2.458	2.458	1.30	9.48	2.503	2.976	2.00	1.98	2.270	3.385
.25	51.2	2.458	2.458	1.30	13.7	2.652	2.976	2.00	2.82	2.394	3.385
.40	1.15	1.631	2.545	1.30	17.8	2.736	2.976	2.00	6.15	2.643	3.385
.40	1.98	1.777	2.545	1.30	19.9	2.794	2.976	2.00	9.48	2.810	3.385
.40	3.23	1.948	2.545	1.30	22.0	2.812	2.976	2.00	13.7	2.976	3.385
.40	6.15	2.106	2.545	1.30	26.2	2.854	2.976	2.00	17.8	3.106	3.385
.40	9.48	2.204	2.545	1.30	34.5	2.917	2.976	2.00	22.0	3.194	3.385
.40	13.7	2.347	2.545	1.30	42.8	2.968	2.976	2.00	26.2	3.250	3.385
.40	17.8	2.424	2.545	1.30	51.2	2.976	2.976	2.00	34.5	3.333	3.385
.40	22.0	2.475	2.545	1.30	59.5	2.976	2.976	2.00	42.8	3.361	3.385
.40	26.2	2.516	2.545	1.30	67.8	2.976	2.976	2.00	51.2	3.372	3.385
.40	34.5	2.545	2.545	1.65	1.15	1.982	3.210	2.00	59.5	3.382	3.385
.40	42.8	2.545	2.545	1.65	1.98	2.006	3.210	2.00	67.8	3.385	3.385
.40	51.2	2.545	2.545	1.65	2.82	2.220	3.210	2.00	76.2	3.385	3.385
.65	1.15	1.779	2.752	1.65	6.15	2.536	2.210	2.00	92.8	3.385	3.385
.65	1.98	2.020	2.752								

See footnotes at end of table, p. A114.

TABLE 4.—*Summary of data for boundary-layer velocity distribution*—Continued

Station [2] (feet)	z^3 (feet $\times 10^3$)	u (fps)	U (fps)	Station [2] (feet)	z^3 (feet $\times 10^3$)	u (fps)	U (fps)	Station [2] (feet)	z^3 (feet $\times 10^3$)	u (fps)	U (fps)
MODEL A-1—Continued											
Test 5											
.006	1.15	−2.124	2.937	.40	22.0	2.908	2.997	1.65	5.32	3.008	3.815
.006	2.82	2.108	2.937	.40	26.2	2.933	2.997	1.65	9.48	3.261	3.815
.006	4.48	2.710	2.937	.40	34.5	2.982	2.997	1.65	12.8	3.377	3.815
.006	6.98	2.824	2.937	.40	42.8	2.997	2.997	1.65	16.2	3.498	3.815
.006	7.82	2.854	2.937	.40	59.5	2.997	2.997	1.65	19.9	3.600	3.815
.006	9.48	2.862	2.937	.40	76.2	2.997	2.997	1.65	24.1	3.642	3.815
.006	13.7	2.904	2.937	.65	5.32	2.618	3.232	1.65	28.2	3.676	3.815
.006	17.8	2.934	2.937	.65	9.48	2.840	3.232	1.65	34.5	3.732	3.815
.006	26.2	2.936	2.937	.65	12.8	2.922	3.232	1.65	42.8	3.752	3.815
.006	34.5	2.936	2.937	.65	16.2	2.992	3.232	1.65	51.2	3.782	3.815
.006	47.0	2.937	2.937	.65	19.9	3.080	3.232	1.65	59.5	3.815	3.815
.10	1.15	1.678	2.883	.65	24.1	3.124	3.232	1.65	76.2	3.815	3.815
.10	3.23	2.028	2.883	.65	28.2	3.162	3.232	1.65	92.8	3.815	3.815
.10	5.32	2.256	2.883	.65	34.5	3.204	3.232	1.85	5.32	2.973	3.880
.10	9.48	2.653	2.883	.65	42.8	3.230	3.232	1.85	9.48	3.255	3.880
.10	11.6	2.747	2.883	.65	59.5	3.232	3.232	1.85	12.8	3.364	3.880
.10	13.7	2.816	2.883	.65	76.2	3.232	3.232	1.85	16.2	3.558	3.880
.10	15.7	2.840	2.883	1.00	5.32	2.740	3.428	1.85	19.9	3.657	3.880
.10	17.8	2.850	2.883	1.00	9.48	2.974	3.428	1.85	24.1	3.708	3.880
.10	26.2	2.881	2.883	1.00	12.8	3.074	3.428	1.85	28.2	3.754	3.880
.10	38.7	2.883	2.883	1.00	16.2	3.190	3.428	1.85	34.5	3.805	3.880
.10	51.2	2.883	2.883	1.00	19.9	3.273	3.428	1.85	42.8	3.848	3.880
.25	1.15	1.640	2.872	1.00	24.1	3.320	3.428	1.85	51.2	3.858	3.880
.25	3.23	2.072	2.872	1.00	28.2	3.353	3.428	1.85	59.5	3.876	3.880
.25	5.32	2.236	2.872	1.00	34.5	3.384	3.428	1.85	76.2	3.876	3.880
.25	9.48	2.466	2.872	1.00	42.8	3.402	3.428	1.85	92.8	3.880	3.880
.25	11.6	2.576	2.872	1.00	59.5	3.428	3.428	2.00	5.32	3.026	3.955
.25	13.7	2.704	2.872	1.00	76.2	3.428	3.428	2.00	9.48	3.300	3.955
.25	15.7	2.728	2.872	1.30	5.32	2.794	3.562	2.00	12.8	3.455	3.955
.25	17.8	2.787	2.872	1.30	9.48	3.070	3.562	2.00	16.2	3.608	3.955
.25	22.0	2.819	2.872	1.30	12.8	3.192	3.562	2.00	19.9	3.715	3.955
.25	26.2	2.847	2.872	1.30	16.2	3.290	3.562	2.00	24.1	3.784	3.955
.25	34.5	2.868	2.872	1.30	19.9	3.372	3.562	2.00	28.2	3.834	3.955
.25	47.0	2.872	2.872	1.30	24.1	3.427	3.562	2.00	34.5	3.881	3.955
.25	59.5	2.872	2.872	1.30	28.2	3.456	3.562	2.00	42.8	3.906	3.955
.40	5.32	2.336	2.997	1.30	34.5	3.510	3.562	2.00	51.2	3.928	3.955
.40	9.48	2.575	2.997	1.30	42.8	3.527	3.562	2.00	59.5	3.955	3.955
.40	12.0	2.678	2.997	1.30	59.5	3.561	3.562	2.00	76.2	3.955	3.955
.40	14.9	2.763	2.997	1.30	76.2	3.562	3.562	2.00	92.8	3.955	3.955
.40	17.8	2.842	2.997	1.30	84.5	3.562	3.562				

See footnotes at end of table, p. A114.

TABLE 4.—*Summary of data for boundary-layer velocity distribution*—Continued

Station [2] (feet)	z^3 (feet $\times 10^3$)	u (fps)	U (fps)	Station [2] (feet)	z^3 (feet $\times 10^3$)	u (fps)	U (fps)	Station [2] (feet)	z^3 (feet $\times 10^3$)	u (fps)	U (fps)
MODEL K-1											
Test 1											
.20	1.15	.242	.774	.60	14.5	.857	.869	1.65	6.98	1.290	1.361
.20	1.98	.319	.774	.60	17.0	.860	.869	1.65	7.82	1.316	1.361
.20	2.82	.439	.774	.60	22.0	.863	.869	1.65	8.65	1.345	1.361
.20	3.65	.528	.774	.60	26.2	.869	.869	1.65	9.48	1.349	1.361
.20	4.48	.599	.774	1.10	1.98	.552	.979	1.65	10.3	1.351	1.361
.20	5.32	.650	.774	1.10	2.82	.616	.979	1.65	11.2	1.351	1.361
.20	6.15	.690	.774	1.10	3.65	.659	.979	1.65	12.8	1.351	1.361
.20	6.98	.735	.774	1.10	4.48	.721	.979	1.65	14.5	1.352	1.361
.20	7.82	.750	.774	1.10	5.32	.784	.979	1.65	17.8	1.357	1.361
.20	8.65	.756	.774	1.10	6.15	.850	.979	1.65	22.0	1.359	1.361
.20	9.48	.756	.774	1.10	6.98	.878	.979	1.65	26.2	1.361	1.361
.20	10.3	.764	.774	1.10	7.82	.902	.979	1.80	1.15	.663	1.516
.20	12.8	.767	.774	1.10	8.65	.926	.979	1.80	2.40	.971	1.516
.20	17.0	.774	.774	1.10	9.48	.951	.979	1.80	3.65	1.200	1.516
.60	1.15	.254	.869	1.10	10.3	.960	.979	1.80	4.90	1.376	1.516
.60	1.98	.351	.869	1.10	11.2	.960	.979	1.80	6.15	1.416	1.516
.60	2.82	.451	.869	1.10	12.0	.965	.979	1.80	6.98	1.452	1.516
60	3.65	.528	.869	1.10	12.8	.968	.979	1.80	7.82	1.465	1.516
.60	4.48	.585	.869	1.10	14.5	.968	.979	1.80	8.65	1.481	1.516
.60	5.32	.642	.869	1.10	17.8	.976	.979	1.80	9.48	1.499	1.516
.60	6.15	.702	.869	1.10	22.0	.976	.979	1.80	10.3	1.507	1.516
.60	6.98	.757	.869	1.10	26.2	.979	.979	1.80	11.2	1.507	1.516
.60	7.82	.788	.869	1.65	1.15	.671	1.361	1.80	12.8	1.507	1.516
.60	8.65	.809	.869	1.65	2.40	.795	1.361	1.80	14.5	1.508	1.516
.60	9.48	.828	.869	1.65	3.65	1.034	1.361	1.80	17.8	1.511	1.516
.60	10.3	.853	.869	1.65	4.90	1.204	1.361	1.80	22.0	1.513	1.516
.60	11.2	.853	.869	1.65	6.15	1.254	1.361	1.80	26.2	1.516	1.516
.60	12.8	.857	.869								
Test 2											
.20	1.15	.401	1.347	1.10	9.07	1.551	1.638	1.65	5.73	1.769	1.993
.20	1.98	.542	1.347	1.10	9.65	1.566	1.638	1.65	6.98	1.872	1.993
.20	2.82	.746	1.347	1.10	10.3	1.586	1.638	1.65	8.23	1.912	1.993
.20	3.65	.923	1.347	1.10	10.7	1.599	1.638	1.65	9.07	1.942	1.993
.20	4.48	1.060	1.347	1.10	11.2	1.598	1.638	1.65	9.90	1.958	1.993
.20	5.32	1.174	1.347	1.10	11.6	1.602	1.638	1.65	10.3	1.962	1.993
.20	6.15	1.250	1.347	1.10	12.0	1.602	1.638	1.65	10.7	1.965	1.993
.20	6.98	1.302	1.347	1.10	12.7	1.620	1.638	1.65	11.2	1.965	1.993
.20	7.82	1.336	1.347	1.10	13.2	1.607	1.638	1.65	11.6	1.971	1.993
.20	8.65	1.341	1.347	1.10	13.8	1.620	1.638	1.65	12.0	1.976	1.993
.20	9.48	1.341	1.347	1.10	14.5	1.635	1.638	1.65	12.8	1.979	1.993
.20	13.7	1.349	1.347	1.10	15.3	1.628	1.638	1.65	14.9	1.980	1.993
.20	17.8	1.347	1.347	1.10	16.2	1.635	1.638	1.65	17.0	1.985	1.993
.20	26.2	1.347	1.347	1.10	17.8	1.638	1.638	1.65	19.5	1.985	1.993
.60	1.15	.401	1.444	1.10	22.0	1.638	1.638	1.65	22.0	1.993	1.993
.60	1.98	.552	1.444	1.10	26.2	1.638	1.638	1.65	26.2	1.992	1.993
.60	2.82	.778	1.444	1.40	1.15	.774	1.756	1.65	30.3	1.993	1.993
.60	3.65	.926	1.444	1.40	1.98	.968	1.756	1.80	1.15	.929	2.095
.60	4.48	1.054	1.444	1.40	2.82	1.114	1.756	1.80	1.98	1.165	2.095
.60	5.32	1.156	1.444	1.40	3.65	1.304	1.756	1.80	2.82	1.428	2.095
.60	6.57	1.269	1.444	1.40	4.48	1.411	1.756	1.80	3.65	1.618	2.095
.60	7.82	1.358	1.444	1.40	5.32	1.495	1.756	1.80	4.48	1.774	2.095
.60	9.48	1.414	1.444	1.40	6.15	1.574	1.756	1.80	5.32	1.882	2.095
.60	10.3	1.437	1.444	1.40	6.98	1.630	1.756	1.80	6.15	1.938	2.095
.60	11.2	1.437	1.444	1.40	7.82	1.674	1.756	1.80	6.98	1.994	2.095
.60	12.8	1.437	1.444	1.40	8.65	1.706	1.756	1.80	7.82	2.024	2.095
.60	14.9	1.437	1.444	1.40	9.48	1.732	1.756	1.80	8.65	2.045	2.095
.60	17.8	1.441	1.444	1.40	10.3	1.750	1.756	1.80	9.48	2.068	2.095
.60	22.0	1.442	1.444	1.40	11.2	1.750	1.756	1.80	10.3	2.067	2.905
.60	26.2	1.444	1.444	1.40	12.8	1.750	1.756	1.80	11.2	2.081	2.095
1.10	1.15	.603	1.638	1.40	14.5	1.752	1.756	1.80	12.0	2.089	2.095
1.10	1.98	.702	1.638	1.40	17.0	1.753	1.756	1.80	12.8	2.089	2.095
1.10	3.23	.976	1.638	1.40	21.2	1.755	1.756	1.80	14.5	2.093	2.095
1.10	5.32	1.287	1.638	1.40	26.2	1.756	1.759	1.80	16.2	2.093	2.095
1.10	6.57	1.408	1.638	1.65	1.15	.937	1.993	1.80	17.8	2.093	2.095
1.10	7.15	1.448	1.638	1.65	3.23	1.409	1.993	1.80	22.0	2.095	2.095
1.10	7.82	1.490	1.638	1.65	4.48	1.644	1.993	1.80	26.2	2.095	2.095
1.10	8.40	1.526	1.638								

See footnotes at end of table, p. A114.

TABLE 4.—*Summary of data for boundary-layer velocity distribution*—Continued

Station [2] (feet)	z^3 (feet $\times 10^3$)	u (fps)	U (fps)	Station [2] (feet)	z^3 (feet $\times 10^3$)	u (fps)	U (fps)	Station [2] (feet)	z^3 (feet $\times 10^3$)	u (fps)	U (fps)
MODEL K-1—Continued											
Test 3											
.20	1.15	.501	1.962	1.10	2.82	1.562	2.221	1.65	18.7	2.502	2.524
.20	2.82	1.110	1.962	1.10	4.48	1.789	2.221	1.65	20.3	2.511	2.524
.20	3.65	1.503	1.962	1.10	6.15	1.956	2.221	1.65	22.0	2.520	2.524
.20	4.48	1.642	1.962	1.10	7.82	2.040	2.221	1.65	24.1	2.522	2.524
.20	5.32	1.825	1.962	1.10	9.48	2.120	2.221	1.65	26.2	2.523	2.524
.20	6.15	1.837	1.962	1.10	11.2	2.135	2.221	1.65	30.3	2.524	2.524
.20	7.82	1.892	1.962	1.10	12.8	2.145	2.221	1.65	34.5	2.524	2.524
.20	9.48	1.927	1.962	1.10	14.5	2.174	2.221	1.80	1.15	1.531	2.583
.20	11.2	1.935	1.962	1.10	16.2	2.193	2.221	1.80	2.82	1.942	2.583
.20	13.7	1.962	1.962	1.10	17.8	2.205	2.221	1.80	4.90	2.152	2.583
.20	17.8	1.962	1.962	1.10	19.9	2.213	2.221	1.80	6.98	2.270	2.583
.20	22.0	1.962	1.962	1.10	22.0	2.220	2.221	1.80	8.65	2.356	2.583
.60	1.15	.571	1.977	1.10	26.2	2.221	2.221	1.80	11.2	2.419	2.583
.60	2.82	1.153	1.977	1.10	30.3	2.221	2.221	1.80	12.8	2.455	2.583
.60	4.48	1.450	1.977	1.10	34.5	2.221	2.221	1.80	14.5	2.490	2.583
.60	6.15	1.707	1.977	1.65	1.15	1.368	2.524	1.80	16.2	2.514	2.583
.60	7.82	1.804	1.977	1.65	2.82	1.905	2.524	1.80	17.8	2.523	2.583
.60	9.48	1.890	1.977	1.65	4.90	2.130	2.524	1.80	19.9	2.545	2.583
.60	11.2	1.935	1.977	1.65	6.98	2.253	2.524	1.80	22.0	2.562	2.583
.60	12.8	1.949	1.977	1.65	8.65	2.305	2.524	1.80	24.1	2.568	2.583
.60	14.5	1.955	1.977	1.65	10.3	2.352	2.524	1.80	26.2	2.574	2.583
.60	17.8	1.970	1.977	1.65	12.0	2.390	2.524	1.80	30.3	2.580	2.583
.60	22.0	1.976	1.977	1.65	13.7	2.416	2.524	1.80	34.5	2.582	2.583
.60	26.2	1.976	1.977	1.65	15.3	2.448	2.524	1.80	38.7	2.583	2.583
.60	34.5	1.977	1.977	1.65	17.0	2.476	2.524	1.80	42.8	2.583	2.583
1.10	1.15	1.117	2.221								
Test 4											
.20	1.15	1.736	2.640	.60	24.1	2.830	2.840	1.40	36.2	2.962	2.975
.20	1.98	1.814	2.640	.60	26.2	2.835	3.840	1.40	38.7	2.970	2.975
.20	2.82	1.998	2.640	.60	30.3	2.836	2.840	1.40	40.7	2.970	2.975
.20	3.65	2.130	2.640	.60	32.4	2.838	2.840	1.40	42.8	2.973	2.975
.20	4.48	2.225	2.640	.60	34.5	2.840	2.840	1.40	51.2	2.973	2.975
.20	5.32	2.280	2.640	1.10	1.15	1.694	2.900	1.40	59.5	2.975	2.975
.20	6.15	2.345	2.640	1.10	3.23	2.032	2.900	1.65	1.15	1.842	3.103
.20	6.98	2.400	2.640	1.10	5.32	2.182	2.900	1.65	5.32	2.376	3.103
.20	7.82	2.453	2.640	1.10	7.40	2.300	2.900	1.65	9.48	2.573	3.103
.20	8.65	2.500	2.640	1.10	9.48	2.416	2.900	1.65	13.7	2.723	3.103
.20	9.48	2.524	2.640	1.10	11.6	2.484	2.900	1.65	17.8	2.840	3.103
.20	10.3	2.540	2.640	1.10	13.7	2.580	2.900	1.65	22.0	2.934	3.103
.20	11.2	2.560	2.640	1.10	15.7	2.655	2.900	1.65	26.2	3.002	3.103
.20	12.8	2.600	2.640	1.10	17.8	2.704	2.900	1.65	29.5	3.036	3.103
.20	14.5	2.616	2.640	1.10	19.9	2.744	2.900	1.65	32.8	3.062	3.103
.20	16.2	2.626	2.640	1.10	22.0	2.795	2.900	1.65	36.2	3.080	3.103
.20	17.8	2.640	2.640	1.10	24.1	2.835	2.900	1.65	38.7	3.086	3.103
.20	22.0	2.640	2.640	1.10	26.2	2.860	2.900	1.65	41.2	3.093	3.103
.20	26.2	2.640	2.640	1.10	28.2	2.885	2.900	1.65	44.5	3.098	3.103
.20	34.5	2.640	2.640	1.10	30.3	2.897	2.900	1.65	51.2	3.102	3.103
.60	1.15	1.743	2.840	1.10	34.5	2.898	2.900	1.65	59.5	3.103	3.103
.60	1.98	1.980	2.840	1.10	42.8	2.900	2 900	1.80	1.15	2.302	3.193
.60	3.23	2.184	2.840	1.40	1.15	1.737	2.975	1.80	3.23	2.573	3.193
.60	5.32	2.336	2.840	1.40	5.32	2.245	2.975	1.80	5.32	2.684	3.193
.60	7.40	2.442	2.840	1.40	9.48	2.405	2.975	1.80	11.6	2.850	3.193
.60	9.48	2.537	2.840	1.40	13.7	2.585	2.975	1.80	17.8	3.010	3.193
.60	11.6	2.624	2.840	1.40	17.8	2.694	2.975	1.80	24.1	3.120	3.193
.60	13.7	2.690	2.840	1.40	21.2	2.973	2.975	1.80	30.3	3.170	3.193
.60	15.7	2.744	2.840	1.40	24.5	2.842	2.975	1.80	34.5	3.190	3.193
.60	17.8	2.768	2.840	1.40	27.8	2.893	2.975	1.80	42.8	3.192	3.193
.60	19.9	2.802	2.840	1.40	31.2	2.940	2.975	1.80	51.2	3.193	3.193
.60	22.0	2.824	2.840	1.40	33.7	2.955	2.975				

See footnotes at end of table, p. A114.

TABLE 4.—*Summary of data for boundary-layer velocity distribution*—Continued

Station [2] (feet)	z^3 (feet $\times 10^3$)	u (fps)	U (fps)	Station [2] (feet)	z^3 (feet $\times 10^3$)	u (fps)	U (fps)	Station [2] (feet)	z^3 (feet $\times 10^3$)	u (fps)	U (fps)
MODEL K-1—Continued											
Test 5											
.20	1.15	2.200	3.060	1.10	3.65	2.722	3.562	1.65	3.65	2.900	3.893
.20	2.82	2.503	3.060	1.10	7.40	2.987	3.562	1.65	7.40	3.222	3.893
.20	4.48	2.643	3.060	1.10	11.2	3.194	3.562	1.65	13.7	3.526	3.893
.20	6.15	2.736	3.060	1.10	15.7	3.338	3.562	1.65	19.9	3.700	3.893
.20	6.98	2.786	3.060	1.10	19.9	3.416	3.562	1.65	26.2	3.795	3.893
.20	7.82	2.826	3.060	1.10	24.1	3.475	3.562	1.65	32.4	3.840	3.893
.20	9.48	2.903	3.060	1.10	28.2	3.512	3.562	1.65	38.7	3.876	3.893
.20	11.2	2.960	3.060	1.10	32.4	3.530	3.562	1.65	44.9	3.886	3.893
.20	14.5	3.036	3.060	1.10	36.6	3.548	3.562	1.65	51.2	3.890	3.893
.20	17.0	3.054	3.060	1.10	42.8	3.560	3.562	1.65	59.5	3.893	3.893
.20	17.8	3.057	3.060	1.10	51.2	3.562	3.562	1.65	67.8	3.893	3.893
.20	22.0	3.060	3.060	1.10	59.5	3.562	3.562	1.80	1.15	2.383	3.923
.20	26.2	3.060	3.060	1.40	1.15	2.342	3.747	1.80	3.65	2.855	3.923
.60	1.15	2.345	3.269	1.40	3.65	2.825	3.747	1.80	7.40	3.183	3.923
.60	3.23	2.662	3.269	1.40	7.40	3.113	3.747	1.80	13.7	3.533	3.923
.60	5.32	2.803	3.269	1.40	13.7	3.402	3.747	1.80	20.3	3.713	3.923
.60	8.65	2.964	3.269	1.40	19.9	3.562	3.747	1.80	27.0	3.818	3.923
.60	12.0	3.080	3.269	1.40	26.2	3.643	3.747	1.80	33.7	3.862	3.923
.60	15.3	3.165	3.269	1.40	32.4	3.698	3.747	1.80	40.3	3.892	3.923
.60	18.7	3.216	3.269	1.40	38.7	3.722	3.747	1.80	47.0	3.918	3.923
.60	22.0	3.256	3.269	1.40	42.8	3.743	3.747	1.80	53.7	3.920	3.923
.60	25.3	3.265	3.269	1.40	47.0	3.747	3.747	1.80	60.3	3.922	3.923
.60	28.7	3.265	3.269	1.40	51.2	3.747	3.747	1.80	67.0	3.922	3.923
.60	34.5	3.269	3.269	1.40	59.5	3.747	3.747	1.80	73.7	3.923	3.923
.60	42.8	3.269	3.269	1.40	67.8	3.747	3.747	1.80	80.3	3.923	3.923
1.10	1.15	2.228	3.562	1.65	1.15	2.507	3.893				
MODEL AA-1											
Test 1											
.006	1.15	−.728	1.091	.40	34.5	1.242	1.242	1.65	1.15	.990	1.942
.006	1.98	.841	1.091	.40	42.8	1.242	1.242	1.65	1.98	1.140	1.942
.006	2.82	.940	1.091	.40	51.2	1.242	1.242	1.65	3.65	1.299	1.942
.006	3.65	.974	1.091	.65	1.15	.775	1.416	1.65	5.32	1.384	1.942
.006	4.48	1.003	1.091	.65	1.98	.878	1.416	1.65	7.40	1.475	1.942
.006	5.32	1.026	1.091	.65	3.65	1.037	1.416	1.65	9.48	1.549	1.942
.096	6.57	1.091	1.091	.65	5.32	1.124	1.416	1.65	13.7	1.660	1.942
.006	9.48	1.091	1.091	.65	7.40	1.168	1.416	1.65	17.8	1.756	1.942
.006	17.8	1.092	1.091	.65	9.48	1.233	1.416	1.65	26.2	1.872	1.942
.006	26.2	1.089	1.091	.65	13.7	1.303	1.416	1.65	34.5	1.926	1.942
.10	1.15	.713	1.142	.65	17.8	1.342	1.416	1.65	42.8	1.942	1.942
.10	1.98	.794	1.142	.65	26.2	1.375	1.416	1.65	51.2	1.942	1.942
.10	2.82	.828	1.142	.65	34.5	1.415	1.416	1.65	59.5	1.942	1.942
.10	3.65	.847	1.142	.65	42.8	1.416	1.416	1.85	1.15	1.068	2.108
.10	4.48	.866	1.142	.65	51.2	1.416	1.416	1.85	1.98	1.156	2.108
.10	5.32	.885	1.142	1.00	1.15	.625	1.509	1.85	3.65	1.352	2.108
.10	6.57	.979	1.142	1.00	1.98	.690	1.509	1.85	5.32	1.569	2.108
.10	9.48	1.030	1.142	1.00	3.65	.835	1.509	1.85	7.40	1.582	2.108
.10	17.8	1.142	1.142	1.00	5.32	.960	1.509	1.85	9.48	1.682	2.108
.10	26.2	1.142	1.142	1.00	7.40	1.029	1.509	1.85	13.7	1.818	2.108
.25	1.15	.702	1.180	1.00	9.48	1.150	1.509	1.85	17.8	1.916	2.108
.25	1.98	.735	1.180	1.00	13.7	1.278	1.509	1.85	26.2	2.040	2.108
.25	3.65	.818	1.180	1.00	17.8	1.384	1.509	1.85	34.5	2.088	2.108
.25	5.32	.897	1.180	1.00	26.2	1.454	1.509	1.85	42.8	2.10	2.108
.25	7.40	.946	1.180	1.00	34.5	1.509	1.509	1.85	51.2	2.107	2.108
.25	9.48	.985	1.180	1.00	42.8	1.509	1.509	1.85	59.5	2.108	2.108
.25	13.7	1.080	1.180	1.00	51.2	1.509	1.509	2.00	1.15	1.163	2.260
.25	17.8	1.133	1.180	1.30	1.15	.753	1.654	2.00	1.98	1.292	2.260
.25	26.2	1.180	1.180	1.30	1.98	.854	1.654	2.00	3.65	1.412	2.260
.25	34.5	1.180	1.180	1.30	3.65	1.019	1.654	2.00	5.32	1.459	2.260
.25	42.8	1.180	1.180	1.30	5.32	1.116	1.654	2.00	7.40	1.654	2.260
.40	1.15	.666	1.242	1.30	7.40	1.204	1.654	2.00	9.48	1.779	2.260
.40	1.98	.746	1.242	1.30	9.48	1.254	1.654	2.00	13.7	1.936	2.260
.40	3.65	.828	1.242	1.30	13.7	1.371	1.654	2.00	17.8	2.052	2.260
.40	5.32	.943	1.242	1.30	17.8	1.467	1.654	2.00	26.2	2.179	2.260
.40	7.40	1.011	1.242	1.30	26.2	1.585	1.654	2.00	34.5	2.234	2.260
.40	9.48	1.032	1.242	1.30	34.5	1.654	1.654	2.00	42.8	2.260	2.260
.40	13.7	1.118	1.242	1.30	42.8	1.654	1.654	2.00	51.2	2.260	2.260
.40	17.8	1.147	1.242	1.30	51.2	1.654	1.654	2.00	59.5	2.259	2.260
.40	26.2	1.211	1.242								

See footnotes at end of table, p. A114.

TABLE 4.—*Summary of data for boundary-layer velocity distribution*—Continued

Station [2] (feet)	z^3 (feet $\times 10^3$)	u (fps)	U (fps)	Station [2] (feet)	z^3 (feet $\times 10^3$)	u (fps)	U (fps)	Station [2] (feet)	z^3 (feet $\times 10^3$)	u (fps)	U (fps)
MODEL AA-1—Continued											
Test 2											
.006	1.15	1.411	2.437	.40	5.32	1.645	2.524	1.30	9.48	2.160	2.976
.006	1.98	1.581	2.437	.40	7.40	1.770	2.524	1.30	13.7	2.362	2.976
.006	2.82	1.722	2.437	.40	9.48	1.867	2.524	1.30	17.8	2.510	2.976
.006	3.65	1.834	2.437	.40	11.6	1.964	2.524	1.30	22.0	2.652	2.976
.006	4.48	1.935	2.437	.40	13.7	2.054	2.524	1.30	26.2	2.776	2.976
.006	5.32	2.028	2.437	.40	15.7	2.136	2.524	1.30	30.3	2.842	2.976
.006	6.57	2.119	2.437	.40	17.8	2.220	2.524	1.30	34.5	2.890	2.976
.006	7.82	2.236	2.437	.40	22.0	2.343	2.524	1.30	38.7	2.936	2.976
.006	9.48	2.290	2.437	.40	26.2	2.450	2.524	1.30	42.8	2.962	2.976
.006	11.6	2.343	2.437	.40	34.5	2.508	2.524	1.30	51.2	2.976	2.976
.006	13.7	2.388	2.437	.40	42.8	2.524	2.524	1.30	59.5	2.976	2.976
.006	17.8	2.430	2.437	.40	51.2	2.525	2.524	1.65	1.15	1.490	3.163
.006	26.2	2.437	2.437	.40	59.5	2.524	2.524	1.65	5.32	1.983	3.163
.006	38.7	2.437	2.437	.65	1.15	1.362	2.714	1.65	11.6	2.352	3.163
.10	1.15	.850	2.393	.65	4.48	1.756	2.714	1.65	17.8	2.360	3.163
.10	1.98	.960	2.393	.65	8.65	2.030	2.714	1.65	22.0	2.768	3.163
.10	2.82	1.052	2.393	.65	11.6	2.164	2.714	1.65	26.2	2.888	3.163
.10	3.65	1.128	2.393	.65	13.7	2.257	2.714	1.65	30.3	2.980	3.163
.10	4.48	1.216	2.393	.65	15.7	2.330	2.714	1.65	34.5	3.060	3.163
.10	5.32	1.322	2.393	.65	17.8	2.397	2.714	1.65	38.7	3.110	3.163
.10	6.57	1.433	2.393	.65	22.0	2.525	2.714	1.65	42.8	3.135	3.163
.10	7.40	1.545	2.393	.65	26.2	2.618	2.714	1.65	51.2	3.162	3.163
.10	9.48	1.772	2.393	.65	30.3	2.665	2.714	1.65	59.5	3.163	3.163
.10	11.6	2.016	2.393	.65	34.5	2.698	2.714	1.65	76.2	3.163	3.163
.10	13.7	2.196	2.393	.65	38.7	2.714	2.714	1.85	1.15	1.459	3.277
.10	17.8	2.325	2.393	.65	42.8	2.714	2.714	1.85	5.32	2.011	3.277
.10	26.2	2.393	2.393	.65	51.2	2.714	2.714	1.85	11.6	2.421	3.277
.10	34.5	2.393	2.393	.65	59.5	2.714	2.714	1.85	17.8	2.701	3.277
.10	42.8	2.393	2.393	1.00	1.15	1.193	2.788	1.85	24.1	2.877	3.277
.25	1.15	1.075	2.395	1.00	5.32	1.665	2.788	1.85	30.3	3.045	3.277
.25	2.82	1.252	2.395	1.00	9.48	1.964	2.788	1.85	34.5	3.133	3.277
.25	4.48	1.412	2.395	1.00	13.7	2.210	2.788	1.85	38.7	3.180	3.277
.25	6.15	1.472	2.395	1.00	17.8	2.360	2.788	1.85	42.8	3.240	3.277
.25	7.82	1.568	2.395	1.00	22.0	2.502	2.788	1.85	47.0	3.256	3.277
.25	9.48	1.676	2.395	1.00	26.2	2.630	2.788	1.85	51.2	3.272	3.277
.25	11.6	1.814	2.395	1.00	30.3	2.680	2.788	1.85	59.5	3.277	3.277
.25	13.7	1.935	2.395	1.00	34.5	2.730	2.788	1.85	76.2	3.277	3.277
.25	15.7	2.060	2.395	1.00	38.7	2.745	2.788	2.00	1.15	1.573	3.368
.25	17.8	2.160	2.395	1.00	42.8	2.788	2.788	2.00	5.32	2.061	3.368
.25	26.2	2.380	2.395	1.00	51.2	2.788	2.788	2.00	11.6	2.462	3.368
.25	34.5	2.395	2.395	1.00	59.5	2.788	2.788	2.00	17.8	2.765	3.368
.25	51.2	2.395	2.395	1.30	1.15	1.470	2.976	2.00	24.1	2.977	3.368
.40	1.15	1.322	2.524	1.30	5.32	1.916	2.976	2.00	30.3	3.138	3.368
.40	2.82	1.452	2.524								
MODEL KA											
Test 1											
.20	1.15	.872	1.323	1.10	5.32	1.109	1.562	1.65	3.23	1.416	1.954
.20	2.82	1.013	1.323	1.10	8.65	1.228	1.562	1.65	5.32	1.531	1.954
.20	4.48	1.102	1.323	1.10	12.0	1.308	1.562	1.65	8.65	1.650	1.954
.20	6.15	1.172	1.323	1.10	15.3	1.376	1.562	1.65	12.8	1.756	1.954
.20	7.82	1.234	1.323	1.10	18.7	1.448	1.562	1.65	17.8	1.842	1.954
.20	9.48	1.282	1.323	1.10	22.0	1.492	1.562	1.65	22.8	1.886	1.954
.20	11.2	1.298	1.323	1.10	25.3	1.518	1.562	1.65	27.8	1.924	1.954
.20	12.8	1.312	1.323	1.10	28.7	1.540	1.562	1.65	32.8	1.942	1.954
.20	14.5	1.323	1.323	1.10	32.0	1.555	1.562	1.65	37.8	1.950	1.954
.20	16.2	1.323	1.323	1.10	35.3	1.562	1.562	1.65	42.8	1.954	1.954
.20	17.8	1.323	1.323	1.10	38.7	1.562	1.562	1.65	47.0	1.954	1.954
.20	26.2	1.323	1.323	1.10	42.8	1.562	1.562	1.65	55.3	1.954	1.954
.20	34.5	1.323	1.323	1.40	1.15	.899	1.733	1.65	63.7	1.954	1.954
.60	1.15	.638	1.451	1.40	3.23	1.127	1.733	1.65	76.2	1.954	1.954
.60	2.82	.937	1.451	1.40	5.32	1.253	1.733	1.80	1.15	1.246	2.094
.60	4.90	1.082	1.451	1.40	8.65	1.378	1.733	1.80	3.23	1.464	2.094
.60	6.98	1.145	1.451	1.40	10.7	1.439	1.733	1.80	5.32	1.620	2.094
.60	9.07	1.186	1.451	1.40	12.8	1.480	1.733	1.80	8.65	1.760	2.094
.60	11.2	1.228	1.451	1.40	15.7	1.541	1.733	1.80	12.8	1.879	2.094
.60	13.2	1.262	1.451	1.40	17.8	1.574	1.733	1.80	17.8	1.948	2.094
.60	15.3	1.302	1.451	1.40	22.8	1.636	1.733	1.80	22.8	2.002	2.094
.60	17.4	1.341	1.451	1.40	27.8	1.678	1.733	1.80	28.7	2.047	2.094
.60	19.5	1.377	1.451	1.40	32.8	1.708	1.733	1.80	34.5	2.080	2.094
.60	22.0	1.409	1.451	1.40	37.8	1.723	1.733	1.80	40.3	2.093	2.094
.60	26.2	1.440	1.451	1.40	42.8	1.733	1.733	1.80	46.2	2.093	2.094
.60	34.5	1.450	1.451	1.40	51.2	1.733	1.733	1.80	52.0	2.093	2.094
.60	42.8	1.451	1.451	1.40	59.5	1.733	1.733	1.80	59.5	2.093	2.094
1.10	1.15	.815	1.562	1.40	76.2	1.733	1.733	1.80	67.8	2.094	2.094
1.10	3.23	1.008	1.562	1.65	1.15	1.168	1.954	1.80	80.3	2.094	2.094

See footnotes at end of table, p. A114.

TABLE 4.—*Summary of data for boundary-layer velocity distribution*—Continued

Station [2] (feet)	z^3 (feet $\times 10^3$)	u (fps)	U (fps)	Station [2] (feet)	z^3 (feet $\times 10^3$)	u (fps)	U (fps)	Station [2] (feet)	z^3 (feet $\times 10^3$)	u (fps)	U (fps)
MODEL KA—Continued											
Test 2											
.20	1.15	1.021	2.566	.60	67.8	2.713	2.713	1.40	80.3	2.875	2.875
.20	2.82	1.234	2.566	1.10	1.15	1.018	2.774	1.65	1.15	1.495	3.042
.20	4.48	1.380	2.566	1.10	3.23	1.279	2.774	1.65	5.32	1.972	3.042
.20	6.15	1.519	2.566	1.10	7.40	1.604	2.774	1.65	9.48	2.200	3.042
.20	7.82	1.630	2.566	1.10	13.7	1.970	2.774	1.65	15.7	2.452	3.042
.20	9.48	1.754	2.566	1.10	19.9	2.195	2.774	1.65	22.0	2.604	3.042
.20	11.6	1.903	2.566	1.10	26.2	2.368	2.774	1.65	30.3	2.762	3.042
.20	15.7	2.166	2.566	1.10	32.4	2.502	2.774	1.65	38.7	2.912	3.042
.20	19.1	2.318	2.566	1.10	38.7	2.642	2.774	1.65	47.0	2.982	3.042
.20	22.0	2.435	2.566	1.10	44.9	2.710	2.774	1.65	55.3	3.006	3.042
.20	28.2	2.522	2.566	1.10	51.2	2.743	2.774	1.65	63.7	3.024	3.042
.20	34.5	2.563	2.566	1.10	59.5	2.766	2.774	1.65	72.0	3.040	3.042
.20	40.7	2.566	2.566	1.10	67.8	2.774	2.774	1.65	80.3	3.042	3.042
.20	47.0	2.566	2.566	1.10	76.2	2.774	2.774	1.65	88.7	3.042	3.042
.20	55.3	2.566	2.566	1.10	84.5	2.774	2.774	1.80	1.15	1.412	3.143
.60	1.15	1.360	2.713	1.40	1.15	1.302	2.875	1.80	5.32	1.933	3.143
.60	3.23	1.615	2.713	1.40	4.48	1.667	2.875	1.80	9.48	2.203	3.143
.60	7.40	1.896	2.713	1.40	9.48	1.951	2.875	1.80	17.8	2.543	3.143
.60	13.7	2.177	2.713	1.40	15.7	2.190	2.875	1.80	26.2	2.756	3.143
.60	19.9	2.404	2.713	1.40	22.0	2.378	2.875	1.80	38.7	2.968	3.143
.60	26.2	2.563	2.713	1.40	30.3	2.568	2.875	1.80	51.2	3.076	3.143
.60	32.4	2.648	2.713	1.40	38.7	2.688	2.875	1.80	63.7	3.123	3.143
.60	38.7	2.685	2.713	1.40	47.0	2.782	2.875	1.80	72.0	3.140	3.143
.60	44.9	2.708	2.713	1.40	55.3	2.857	2.875	1.80	80.3	3.143	3.143
.60	51.2	2.712	2.713	1.40	63.7	2.875	2.875	1.80	88.7	3.143	3.143
.60	59.5	2.712	2.713	1.40	72.0	2.875	2.875	1.80	101.2	3.143	3.143

[1] See table 2 for values of head (h) and discharge (q).
[2] Distance in feet (model) from upstream edge of upstream shoulder. Crown line is at station 1.67 feet for all models.
[3] Distance measured perpendicularly from roadway surface to position of pitot tube.

☆U.S. GOVERNMENT PRINTING OFFICE: 1964 O—690-195